AD-A174 602 DYNAMIC ANALYSES OF TWO-DIMENSIONAL LATTICES(U) WEA ` 1/2
CAMBRIDGE MA J H WILLIAMS ET AL 01 AUG 84
AFOSR-TR-86-2070 F49620-83-C-0092

UNCLASSIFIED F/G 22/2 NL

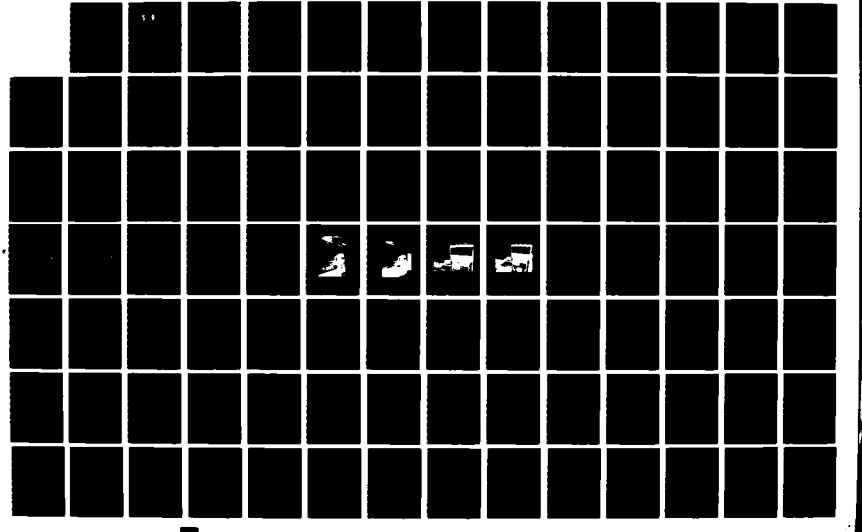

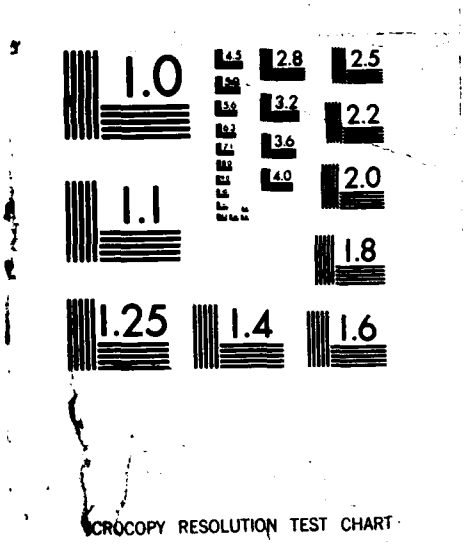
1.0
1.1
1.25
1.4
1.6
2.8
3.2
3.6
4.0
2.5
2.2
2.0
1.8
CROCOPY RESOLUTION TEST CHART

AD-A174 602

(2)

UNCLASSIFIED

SECURITY CLASSIFICATION OF THIS PAGE

REPORT DOCUMENTATION PAGE

1a. REPORT SECURITY CLASSIFICATION Unclassified	1b. RESTRICTIVE MARKINGS
2a. SECURITY CLASSIFICATION AUTHORITY	3. DISTRIBUTION/AVAILABILITY OF REPORT Approved for Public Release; Distribution Unlimited.
2b. DECLASSIFICATION/DOWNGRADING SCHEDULE	
4. PERFORMING ORGANIZATION REPORT NUMBER(S)	5. MONITORING ORGANIZATION REPORT NUMBER(S) AFOSR-TR- 86-2070
6a. NAME OF PERFORMING ORGANIZATION WEA	6b. OFFICE SYMBOL (If applicable)
6c. ADDRESS (City, State and ZIP Code) P.O. Box 260, MIT Branch Cambridge, MA 02139	7a. NAME OF MONITORING ORGANIZATION AFOSR/NA 7b. ADDRESS (City, State and ZIP Code) Bolling AFB DC 20332-6448
8a. NAME OF FUNDING/SPONSORING ORGANIZATION Office of Scientific Research	8b. OFFICE SYMBOL (If applicable) AFOSR/NA
8c. ADDRESS (City, State and ZIP Code) BA 410 Bolling AFB, DC 20332	9. PROCUREMENT INSTRUMENT IDENTIFICATION NUMBER F49620-83-C-0092
11. TITLE (Include Security Classification) DYNAMIC ANALYSES OF TWO-DIMENSIONAL LATTICES	10. SOURCE OF FUNDING NOS. PROGRAM ELEMENT NO.: 61102F; PROJECT NO.: 2307; TASK NO.: B1; WORK UNIT NO.:

DTIC SELECTE NOV 25 1986 S D

12. PERSONAL AUTHOR(S)
James H. Williams, Jr., Robert A. Schroeder and Samson S. Lee

13a. TYPE OF REPORT	13b. TIME COVERED	14. DATE OF REPORT (Yr., Mo., Day)	15. PAGE COUNT
Technical	FROM 1 Apr 83 TO 1 Aug84	84 Aug 01	138

16. SUPPLEMENTARY NOTATION

17. COSATI CODES			18. SUBJECT TERMS (Continue on reverse if necessary and identify by block number)
FIELD	GROUP	SUB. GR.	EXPERIMENTAL DYNAMIC MODES; LARGE SPACE STRUCTURES; LATTICE STRUCTURES

19. ABSTRACT (Continue on reverse if necessary and identify by block number)

The dynamic properties of two two-dimensional lattice structures for large space structures were investigated both analytically, using the COSMIC NASTRAN finite element code, and experimentally, using an HP5451C Fourier analyzer, its accompanying modal analysis software, and a procedure called experimental modal analysis. One of the lattices was composed of five identical repeating substructures (5-bay beam). The other lattice was composed of twenty-two identical repeating substructures (22-bay beam).

For a frequency range extending from 0 Hz to 20 kHz, the NASTRAN analyses identified approximately 180 natural frequencies and mode shapes for each of the structures. The experimental modal analyses (limited by the frequency content of the impact excitation force) identified 34 mode shapes and natural frequencies of the 5-bay beam, and 18 mode shapes and 30 natural frequencies of the 22-bay beam.

86 11 25 282

20. DISTRIBUTION/AVAILABILITY OF ABSTRACT	21. ABSTRACT SECURITY CLASSIFICATION
UNCLASSIFIED/UNLIMITED ☒ SAME AS RPT. ☐ DTIC USERS ☐	UNCLASSIFIED

22a. NAME OF RESPONSIBLE INDIVIDUAL	22b. TELEPHONE NUMBER (Include Area Code)	22c. OFFICE SYMBOL
Anthony K. Amos	202/767-4935	AFOSR/NA

DD FORM 1473, 83 APR EDITION OF 1 JAN 73 IS OBSOLETE.

UNCLASSIFIED

SECURITY CLASSIFICATION OF THIS PAGE

The COSMIC NASTRAN-predicted natural frequencies and the natural frequencies measured using experimental modal analyses agreed to within seven percent. The NASTRAN frequencies were consistently lower than those measured using the Fourier analyzer, probably because of inaccuracies in the finite element modeling of the intersections of the substructures. The errors were larger for the higher frequencies and were, in general, smaller for the 5-bay beam which had fewer substructure intersections (joints).

The Fourier analyzer also generated modal parameters (natural frequencies, damping ratios, and complex residues) for the two structures. In general, these parameters can be used to predict the impulse response, h(t), of a structure. An attempt to predict the impulse response of the 5-bay structure revealed that the dominant modes of vibration of this structure occurred at frequencies above the cut-off frequency of the power spectrum of the impulse source. Thus it was not possible to accurately predict the impulse response of the 5-bay lattice structure. The 22-bay beam was not suitable for impulse response investigations.

ACKNOWLEDGMENTS

The Air Force Office of Scientific Research (Project Monitor, Dr. Anthony K. Amos) is gratefully acknowledged for its support of this research.

NOTICE

This document was prepared under the sponsorship of the Air Force. Neither the US Government nor any person acting on behalf of the US Government assumes any liability resulting from the use of the information contained in this document. This notice is intended to cover WEA as well.

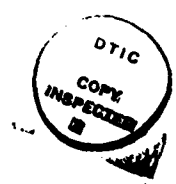

TABLE OF CONTENTS

LIST OF TABLES

LIST OF FIGURES

INTRODUCTION

BACKGROUND

A lattice structure can be thought of as a structure consisting of identical substructures coupled together in identical ways to form a complete system. These substructures are typically formed by joining together bars or trusses in a relatively simple configuration.

Lattice structures are currently used to reduce weight, cost and production time. Power line support towers, off-shore oil wells and crane booms are typical examples of lattice structures.

Because of their low weight, ease of transportation and ease of assembly, lattice structures appear to be particularly well suited for outer space constructions. Research is presently being conducted to assess the viability of these structures in the outer space environment and to develop analytical models to describe their behavior. One approach involves replacing the lattice structure with an equivalent continuum model.

SCOPE OF THE PRESENT WORK

As with any analysis, it is best to begin with a relatively simple model of the actual structure, and then to increase the complexity of the model as the need arises. The structures to be analyzed in this report are relatively simple two-dimensional lattice structures.

Of particular importance in the absence of gravity are the dynamic properties of the lattice structures. The vibration properties of the

simplified two-dimensional lattices were first analyzed using the NASTRAN finite element code. These finite element predictions were then compared to experimental results obtained via an HP5451C Fourier Analyzer and its Modal Analysis software package.

Finite element procedures and programs are fairly well documented and will not be discussed in this work. Experimental modal analysis, however, is a relatively new analysis tool and will be explained in detail to give the reader a general understanding of the experimental procedures used and how the results can be interpreted.

FINITE ELEMENT PREDICTIONS

LATTICE STRUCTURE GEOMETRY

Figs. 1 and 2 show the two-dimensional lattice structures that were analyzed and tested. The structures were each machined from one piece of aluminum; that is, there were no welds or fasteners used in their construction. The structure shown in Fig. 1 will be referred to as the 5-bay beam, and the structure in Fig. 2 will be called the 22-bay beam.

FINITE ELEMENT MODEL DESCRIPTION

The two structures were modeled and analyzed using the M.I.T. Lincoln Laboratory version of COSMIC NASTRAN. Figs. 3 and 4 are computer generated drawings of the finite element models that were used to analyze the dynamic behavior of the 5 and 22-bay beams, respectively. Both models were composed solely of grid points, or nodes, connected together by BAR elements. (See [1]* for an explanation of the BAR element.) The solid lines of Figs. 3 and 4 represent connections of BAR elements. Grid points are not shown in the figures. The 5-bay beam model was composed of 411 grid points and 416 BAR elements. The 22-bay beam was modeled using 514 grid points connected together by 536 BAR elements.

The finite element models were constrained so as to simulate the free-free boundary conditions that would exist in outer space. The

*Numbers in square brackets denote references at the end of the report.

structures were not allowed to deflect in the Z-direction, nor were there allowed to be any rotations about the X-axis, thus preserving the assumption of a 2-dimensional lattice. (See Figs. 1 and 2 for a definition of the coordinate axes.) One percent structural element damping was assumed for both models [1]. Note, the natural frequencies and mode shapes did not change when the structural element damping was set equal to zero.

RESULTS OF DYNAMIC ANALYSES

Inverse power method [1] dynamic analyses of the finite element models were performed to determine all of the natural frequencies and mode shapes of the two models from 0 Hz to 20,000 Hz. In this frequency range, 172 natural frequencies and mode shapes were identified for the 5-bay beam model, while 194 natural frequenices and mode shapes were found for the 22-bay beam model. Some representative mode shapes are given in Appendix A.

Computer times required for dynamic solutions of the two models are also contained in Appendix A.

Fig. 5 is a plot of the first 35 natural frequencies of the 22-bay beam model and the first 36 natural frequencies of the 5-bay beam model.

EXPERIMENTAL MODAL ANALYSIS

INTRODUCTION

A modal analysis involves the determination of the resonance characteristics of a structure by defining its modes of vibration. Each mode has a specific natural frequency and damping factor which can be identified at almost any point of the structure. In addition, each mode is also associated with a mode shape which defines the mode spatially over the entire structure. Once the dynamic properties of a structure have been identified, its behavior can be predicted (see Appendix C). For a detailed explanation of modal analysis theory see [2] through [12].

THE FREQUENCY RESPONSE FUNCTION

The basis for an effective experimental modal analysis lies in the measurement of the frequency response function [2-6]. Considering the system of Fig. 6, the transfer function H(s) can be defined as the Laplace transform of the system output y(t) divided by the Laplace transform of the system input x(t). This can be written as

$$H(s) = \frac{Y(s)}{X(s)} \tag{1}$$

where $Y(s)$ = Laplace transform of a system output, $y(t)$

$X(s)$ = Laplace transform of system input, $x(t)$

s = Laplace variable (a complex number).

The transfer function is complex valued having both a real and an imaginary part.

Note that the Fourier transform gives the value of the transfer function along the imaginary, or frequency axis. The transfer function evaluated along the frequency axis is often referred to as the frequency response function. The frequency response function H(f), can be written as

$$H(f) = \frac{Y(f)}{X(f)} \tag{2}$$

where Y(f) is the Fourier transform of y(t)

X(f) is the Fourier transform of x(t).

The frequency response function H(f) is also a complex function and is composed of real and imaginary parts.

FREQUENCY RESPONSE FUNCTION MEASUREMENT

The implementation of the digital Fast Fourier Transform (FFT) on relatively low cost mini-computer systems has greatly facilitated the identification of the frequency spectrum of a time varying signal. These devices are called digital Fourier analyzers. Thus, a Fourier analyzer which can simultaneously measure excitation (input) signals and response (output) signals, digitize these signals, Fourier transform them, and then divide the resulting Fourier transformed response signal by the Fourier transformed excitation signal is an ideal tool for measuring frequency response functions. Since the modes of vibration of a structure can be identified from frequency response functions

[2-10], a dual channel Fourier analyzer with additional processing capabilities can be used to identify the dynamic, or modal properties of a structure.

An HP5451C Fourier analyzer was used to perform the experimental modal analyses of the lattice structures of Figs. 1 and 2. This device was capable of performing the tasks described in the previous paragraph. However, the analyzer was also capable of obtaining better results by computing the frequency response function as the ratio of the cross power spectrum between the input and the output to the auto power spectrum of the input [3-6, 11]

$$H(f) = \frac{Y(f)}{X(f)} = \frac{Y(f)}{X(f)} \cdot \frac{X(f)^*}{X(f)^*} = \frac{Gyx(f)}{Gxx(f)} \qquad (3)$$

where $X(f)^*$ = complex conjugate of $X(f)$

$Gyx(f)$ = cross power spectrum between the input and the output = $Y(f)\ X(f)^*$

$Gxx(f)$ = auto power spectrum of input $x(t)$ = $X(f)\ X(f)^*$.

Eqn. (3) is particularly useful because it allows averaging of the measurements. Averaging reduces the variance between single measurements. Eqn. (3) can be written as [4]

$$H(f) = \frac{\overline{G(f)yx}}{\overline{G(f)xx}} \qquad (4)$$

where $\overline{Gyx(f)}$ = ensemble average of cross power spectrum

$\overline{Gxx(f)}$ = ensemble average of input auto power spectrum.

Eqn. (4) was used for measuring the frequency response functions of the lattice structures.

THE IMPULSE EXCITATION TECHNIQUE

There are many techniques available for performing experimental modal analyses, such as swept sine excitation, random excitation, periodic random excitation and transient excitation [4, 12]. The impulse excitation technique, a form of transient excitation, is often the simplest and quickest method of obtaining reliable frequency response functions. The impulse excitation technique was used to perform the experimental modal analyses of the lattice structures of Figs. 1 and 2. Reference [7] contains a detailed explanation of this excitation method.

An important point to note is that frequency response functions are valid only over the band of frequencies which are contained in the input signal. Figs. 7 and 8 show the range of frequencies present in the impacts used to excite the 5-bay beam at locations 1 and 2 respectively. The structure was hit with the impact hammer (to be described later) at the 2 locations in the Y-direction (see Fig. 1 for locations and directions). The cutoff frequency (about 6 dB down from the amplitude at 0Hz) for location 1 is about 1500Hz. Using the same cutoff definition as above, impacts made at location 2 have a bandwidth extending from 0Hz to about 5000Hz. Reasons for the differences between the curves in Figs. 7 and 8 will be explained later.

EXPERIMENTAL MODAL ANALYSIS SETUP

Fig. 9 shows a schematic view of the test setup used to perform the experimental modal analyses. The impact hammer was simply a hammer with a PCB SN1377 force sensor (load cell) attached to its head. The impact hammer was equipped with an aluminum tip. (The effects of different tip materials are shown in Appendix C.) The load cell measured the force with which the structure was hit as a function of time, and converted this excitation force to an equivalent electrical signal.

Figs. 10 and 11 show the excitation time histories obtained by hitting the structure with the impact hammer in the Y-direction at locations 1 and 2, respectively. Fig. 10 shows that multiple hits occurred when the structure was impacted at location 1. Figure 11, however, indicates that the hammer came in contact with the structure only once during an impact at location 2. Note that Figs. 7 and 8 are the Fourier transforms of Figs. 10 and 11, respectively, and that the Fourier transform of the signal shown in Fig. 10 is much more erratic than that of a single impact as shown in Fig. 11.

The excitation signal traveled from the hammer through an anti-aliasing low pass filter. (See [13] for an explanation of the aliasing phenomenon.) The hammer impact signal then entered the Fourier analyzer as the input (channel A) signal which was then digitized and processed.

The lattice structures were both suspended from the ceiling by strings. The structures were oriented such that the Z-direction was parallel to the direction of gravity. This configuration closely

represented a 2-dimensional lattice structure in zero gravity.

The Endevco 2222B piezoelectric accelerometer attached to the lattice structure measured the Y-direction response acceleration due to impacts at any location on the structure. The response acceleration signal was also passed through an anti-aliasing filter before it entered the analyzer as the response (channel B) signal. The response signal was then digitized and processed.

Figs. 12 and 13 are photographs of the laboratory setups that were used in the experimental modal analyses of the 22-bay beam and 5-bay beam respectively. Figs. 14 and 15 are close-ups of the response accelerometers and the Fourier analyzer. Fig. 14 shows the 22-bay beam and Fig. 15 shows the 5-bay beam.

EXPERIMENTAL PROCEDURE

The procedures described in references [2-4, 6, 11, 12] were used in determining the dynamic characteristics of the two lattice structures. The response accelerometer was fixed at the locations shown in Figs. 14 and 15 for all of the frequency response function measurements. Different frequency response functions were obtained by impacting the structures at different locations. Some representative frequency response functions are shown in Appendix B.

In order to gain frequency resolution, many of the frequency response functions were measured using band selectable Fourier analysis (BSFA). Some frequency response functions made using BSFA are also shown in Appendix B. For an explanation of BSFA see [3, 4].

The Fourier analyzer then curve fit an analytical expression to each frequency response function [2, 3, 7]. The parameters of these analytic expressions were then used to determine the natural frequencies, damping ratios, residues and mode shapes of the structures. Appendix C contains an explanation of these parameters, commonly called modal parameters, and describes their significance.

An extension of the results of the analyses in Appendix C led to an attempt to predict the impulse responses of the two structures. These impulse response investigations are explained in Appendix D.

RESULTS

Through the use of experimental modal analysis it was possible to identify natural frequencies, damping ratios, complex residues, and mode shapes of the two lattice structures. The limited bandwidth of the impact signals determined the number of mode shapes that could accurately be identified. Thirty-four mode shapes and natural frequencies were identified for the 5-bay lattice structure, and the first 18 mode shapes and natural frequencies were found for the 22-bay lattice structure. It was, however, possible to identify the frequencies corresponding to the next 12 natural modes of vibration of the 22-bay beam. Thus, the first 30 natural frequencies of the 22-bay beam were identified.

Fig. 16 is a plot of frequency versus the mode number for the two lattice structures.

The results of the impulse response of the lattice structures (Appendix D) revealed that location 2 of the 5-bay beam was the only suitable excitation location available for this investigation. It was found that impact hammer impulses at this location did not sufficiently excite the higher natural frequency modes of vibration of the 5-bay structure. Thus, it was not possible to use modal parameters to predict the response acceleration at the response location due to an impulse at location 2 of the 5-bay beam.

COMPARISON OF RESULTS

Fig. 17 shows the frequencies versus mode numbers for the 5-bay beam as predicted by NASTRAN and as measured using experimental modal analysis and the Fourier analyzer. The analyzer was able to identify 34 of the first 36 natural modes of vibration that were predicted by NASTRAN. A comparison of mode shapes revealed that the experimental modal analyses failed to identify the 6th and 13th modes that were predicted by NASTRAN. The close correlation between the finite element-predicted natural frequencies and mode shapes, and the experimental modal analysis-measured natural frequencies and mode shapes suggests that the 6th and 13th mode shapes that were found using NASTRAN did indeed exist, however, their mode shape amplitudes may have been too small for the response accelerometer to measure.

Fig. 17 shows that for each mode, the NASTRAN-predicted natural frequencies were lower than the experimental modal analysis-measured natural frequencies. Note that the linear interpolations used in Fig. 17 cause the NASTRAN curve to lie above the HP FOURIER ANALYZER curve at the missing Fourier analyzer mode numbers 6 and 13.

There is a region in Fig. 17 where the difference in frequency between successive natural modes of vibration is much larger compared to the average frequency difference between consecutive modes. This region is the steepest sloped section of the two curves and appears to be a transition region between modes whose shapes are such that the sides of the bays deform in at most a shape similar to a half sine

wave, as in Fig. 18, and modes with shapes that have at least full sine wave shaped deformations on the sides of each bay, as in Fig. 19. Figs. 18 and 19 show the 21st and 22nd mode shapes of the 5-bay beam, respectively.

Fig. 20 is a plot of the frequencies versus mode numbers for the 22-bay beam as predicted by NASTRAN and as measured using experimental modal analyses. The 18 mode shapes that were found using experimental modal analyses were the same as the first 18 mode shapes predicted by NASTRAN. The similarity of shapes of the two curves of Fig. 20 indicate that the first 30 modes of vibration predicted by NASTRAN would have been identified by experimental modal analysis if the analyzer had been capable of accurately recording mode shapes at these higher frequencies.

The steep sloped segments of the two curves of Fig. 20 indicate a transition similar to that observed for the 5-bay beam in Fig. 17. For the 22-bay beam this region roughly defines a boundary between modes of vibration whose mode shapes represent a somewhat sinusoidal, or wave-like deflection of the entire structure as in Fig. 21, and modes whose shapes appear to behave much more independently in each of the bays as in Fig. 22. Fig. 21 shows the mode shape of mode 23, and Fig. 22 shows the mode shape of mode 25. Note, Figs. 21 and 22 show the deformed mode shape superimposed over the undeformed shape of the 22-bay beam finite element model (see Fig. 4). Also, as with the 5-bay beam, NASTRAN-predicted natural frequencies were lower than those measured using the Fourier analyzer.

For both structures the differences between NASTRAN-predicted natural frequencies and experimental modal analyses-measured natural frequencies increase with the mode numbers. These errors were larger for the 22-bay beam lattice structure than for the 5-bay beam lattice structure.

Appendix D contains a comparison between the modal parameter-predicted impulse response and the measured impulse response of the 5-bay lattice structure.

CONCLUSIONS AND RECOMMENDATIONS

CONCLUSIONS

Finite element dynamic analyses and experimental modal analyses were performed on two relatively simple two-dimensional lattice structures. The following conclusions can be drawn based on the results and comparisons of this work.

(1) Over a limited frequency range, the NASTRAN-predicted mode shapes of both structures correlate well with the mode shapes measured using a Fourier analyzer and the modal analysis software package.

(2) The first 30 NASTRAN-predicted natural frequencies of both beams are slightly lower than those measured using the Fourier analyzer. The NASTRAN and experimental model analyses results agree to within 7% for the 22-bay beam and to within 5% for the 5-bay beam.

(3) The errors between natural frequencies predicted by NASTRAN and natural frequencies measured by the Fourier analyzer increase as the mode numbers increase.

(4) The major cause for errors in the NASTRAN solutions probably arise from modeling a continuous structure as an assemblage of finite elements. The largest cause of these inaccuracies in the finite element models occurs at the intersections of adjacent substructures such as at location 2 of the 5-bay beam. The additional stiffness provided by the radius of curvatures at these intersections was not included in the

finite element models. Thus, the finite element models underestimated the stiffness of the actual lattices.

(5) The NASTRAN-predicted natural frequencies of the 5-bay structure are closer to those measured experimentally using the Fourier analyzer probably because the 5-bay structure had fewer substructure intersections. In other words, the finite element model of the 5-bay beam seems to be more accurate than the finite element model of the 22-bay beam.

(6) Experimental modal analyses are not exact because information contained in the continuous signals is lost when these signals are sampled at discrete intervals. Resolution can be improved by using band selectable Fourier analysis (BSFA).

(7) Natural frequencies measured using experimental modal analyses are probably slightly higher than what they should be because the lattice structures were not totally unconstrained.

(8) The experimental modal analyses are limited by the frequency content of the input signal. Accurate mode shapes can only be obtained for natural modes of vibration falling within the bandwidth of the input signal. Also, there is very little user control over excitation frequencies when the impact excitation technique is used.

(9) It is possible to use the modal parameters to predict the impulse response of multiple degree of freedom systems. However, this technique is not accurate when the dominant

modes of vibration of a structure lie outside the frequency range of the impact signal. This is the case for the 5-bay beam. (The 22-bay beam is not suitable for impulse response testing.)

(10) The two lattice structures have a transition frequency region below which the mode shapes have roughly similar mode shape characteristics. Mode shapes corresponding to natural frequencies above this region also have characteristics that differentiate them from those below the transition region.

RECOMMENDATIONS

The following suggestions for further investigation should alleviate some of the problems, and confirm some of the results mentioned above.

(1) The NASTRAN finite element models should be modified to more accurately represent the two lattice structures. The major modification should involve an attempt to model the intersections of the sides of 2 bays with the cross member that separates them, that is, the regions similar to location 2 of the 5-bay beam. In this work, all NASTRAN bar elements had identical cross-sectional properties, and the radius of curvature at 90 degree intersections was neglected. Including the effects of this radius in a finite element model might give a more accurate prediction of the actual behavior of the lattice structures.

(2) Modal analyses should be performed using a random noise excitation. This would give the user much more control

over the frequency content of the input excitation. The modal analyses would be limited by the characteristics of the random noise generator and the electro-mechanical transducer.

(3) A heavier, but not stronger, lattice structure should be constructed and tested. A heavier structure would have lower natural frequencies, therefore it might be possible to more accurately predict the impulse response of the structure. Also, it might be possible to measure more mode shapes of the heavier structure because more natural frequencies might fall in the frequency range of the input excitation signal.

(4) Finally, a three-dimensional lattice structure should be analyzed via the finite element method. The predictions should be compared to the results of experimental modal analyses to determine the degree of correlation between the two methods of analyses.

REFERENCES

[1] Schaeffer, H. G., MSC/NASTRAN Primer - Static and Normal Modes Analysis, Schaeffer Analysts, Inc., Mount Vernon, NH, 1979.

[2] Klosterman, A. and Zimmerman, R., "Modal Survey Activity Via Frequency Response Functions," SAE Paper Number 751068, 1975.

[3] Richardson, M., "Modal Analysis Using Digital Test Systems," Seminar on Understanding Digital Control and Analysis in Vibration Test Systems (Part 2), 1975, pp. 43-64.

[4] Ramsey, K., "Effective Measurements for Structural Dynamics Testing: Part I", Sound and Vibration, Nov. 1975, pp. 24-35.

[5] Hewlett-Packard Company, "Model Theory of Operation," Modal Analysis System Operating Manual, Section XI, 1974.

[6] Peterson, E. L. and Klosterman, A. L., "Obtaining Good Results from an Experimental Modal Survey," Journal of the Society of Environmental Engineers, March 1978, pp. 3-10.

[7] Brown, D. L., et. al., "Parameter Estimation Techniques for Modal Analysis," SAE Paper Number 790221, 1979, pp. 828-846.

[8] Ensminger, R. R. and Turner, M. J., "Structural Parameter Identification from Measured Vibration Data," AIAA Paper Number 79-0289, 1979, pp. 410-416.

[9] Richardson, M. and Potter, R., "Identification of the Modal Properties of an Elastic Structure from Measured Transfer Function Data," Instrument Society of America, ISA ASI 74250, 1974, pp. 239-246.

[10] Potter, R. W. and Richardson, W., "Mass, Stiffness, and Damping Matrices from Measured Modal Properties," Instrument Society of America, ISA-74-630, 1974.

[11] Halvorsen, W. G. and Brown D. L., "Impulse Technique for Structural Frequency Response Testing," Sound and Vibration, Nov. 1977, pp. 8-21.

[12] Ramsey, K., "Effective Measurements for Structural Dynamics Testing: Part II," Sound and Vibration, April 1976, pp. 18-31.

[13] Newland, D. E., Random Vibrations and Spectral Analysis, Longman Group Ltd., London, 1975, pp. 118-120.

[14] Formenti, D., "Analytical and Experimental Modal Analysis," Modal Analysis Seminar, University of Cincinnati, June 1979.

[15] Meriovitch, L., Elements of Vibration Analysis, McGraw-Hill, Inc., 1975.

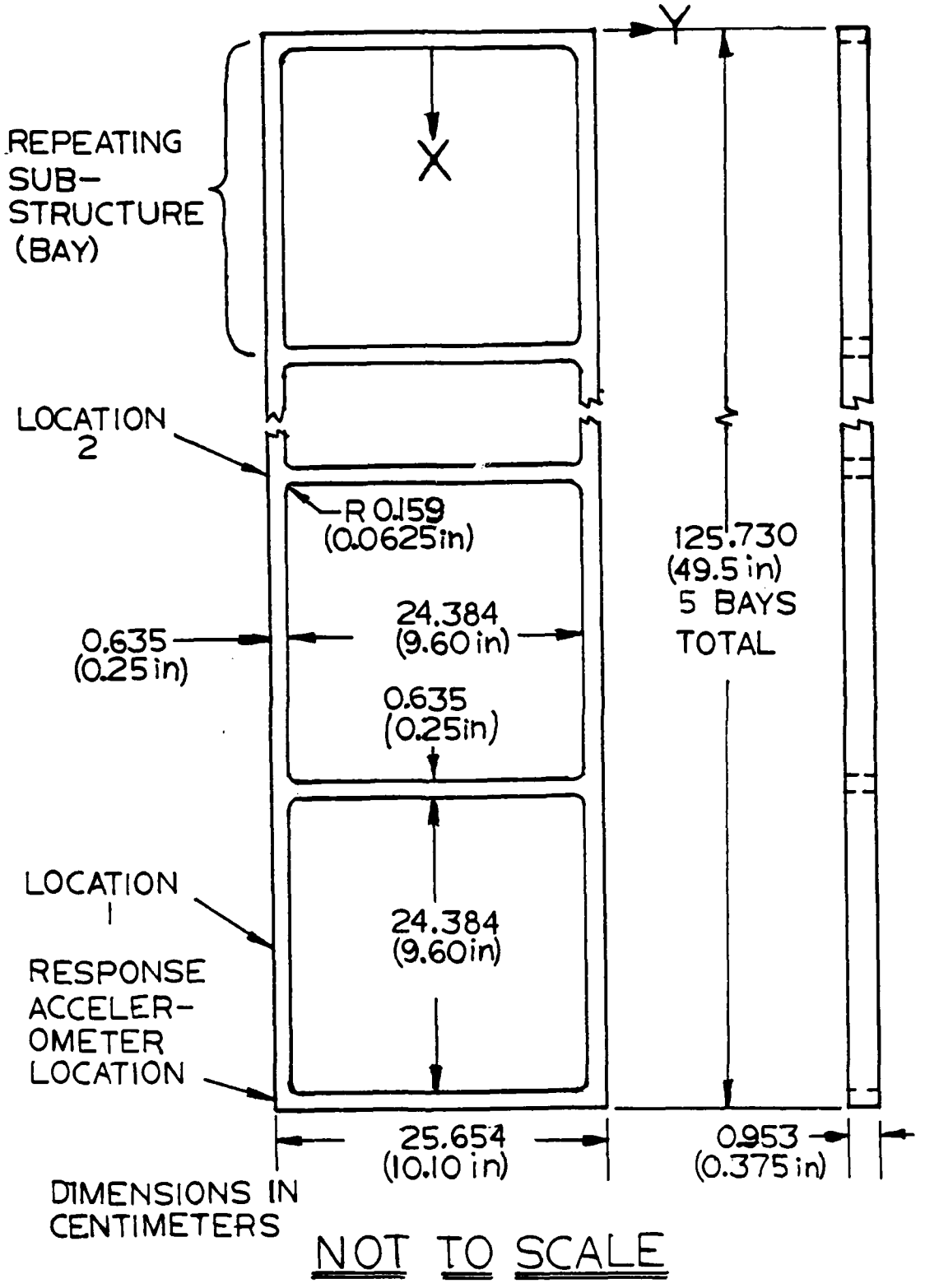

Fig. 1 5-bay lattice beam.

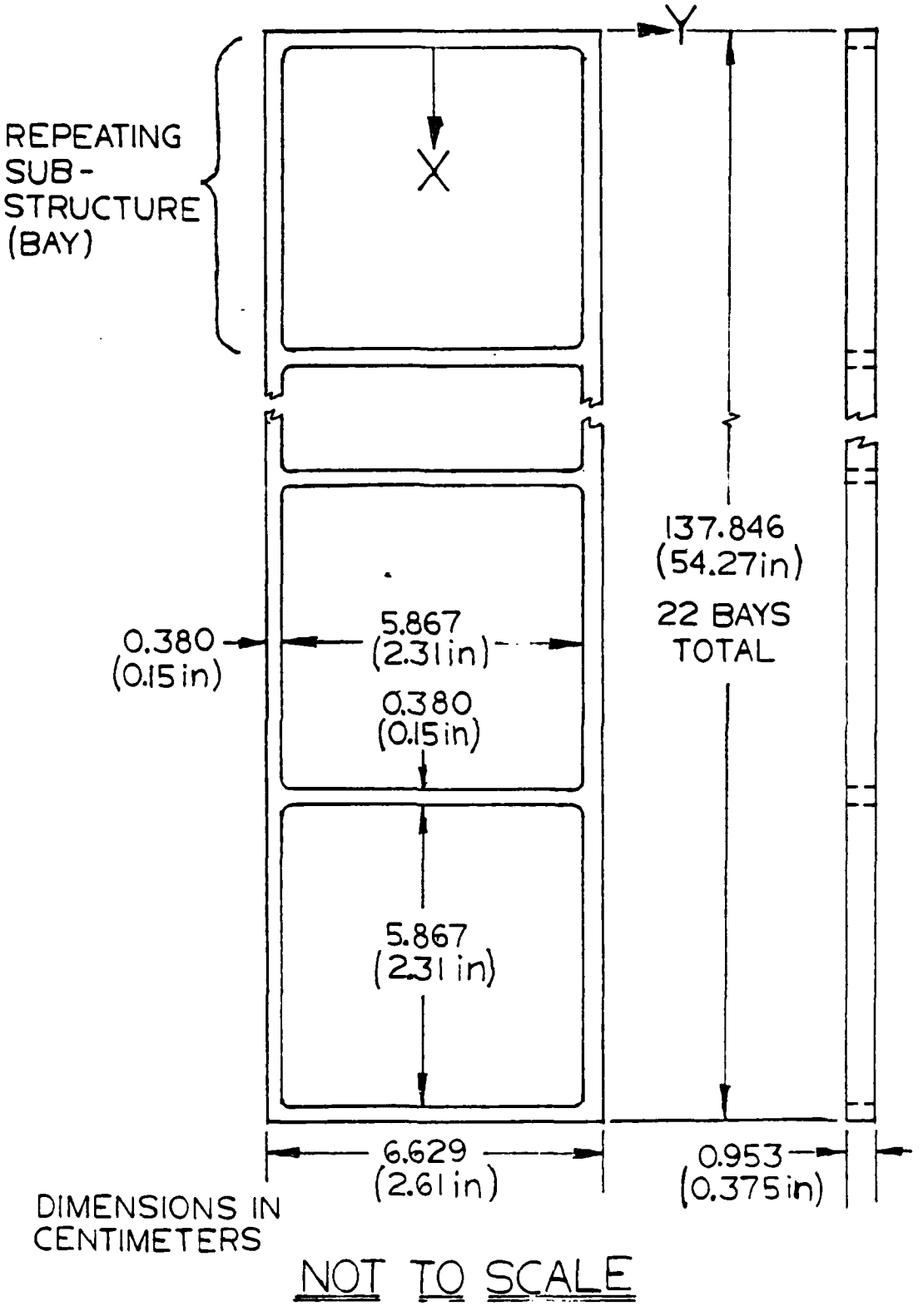

Fig. 2 22-bay lattice beam.

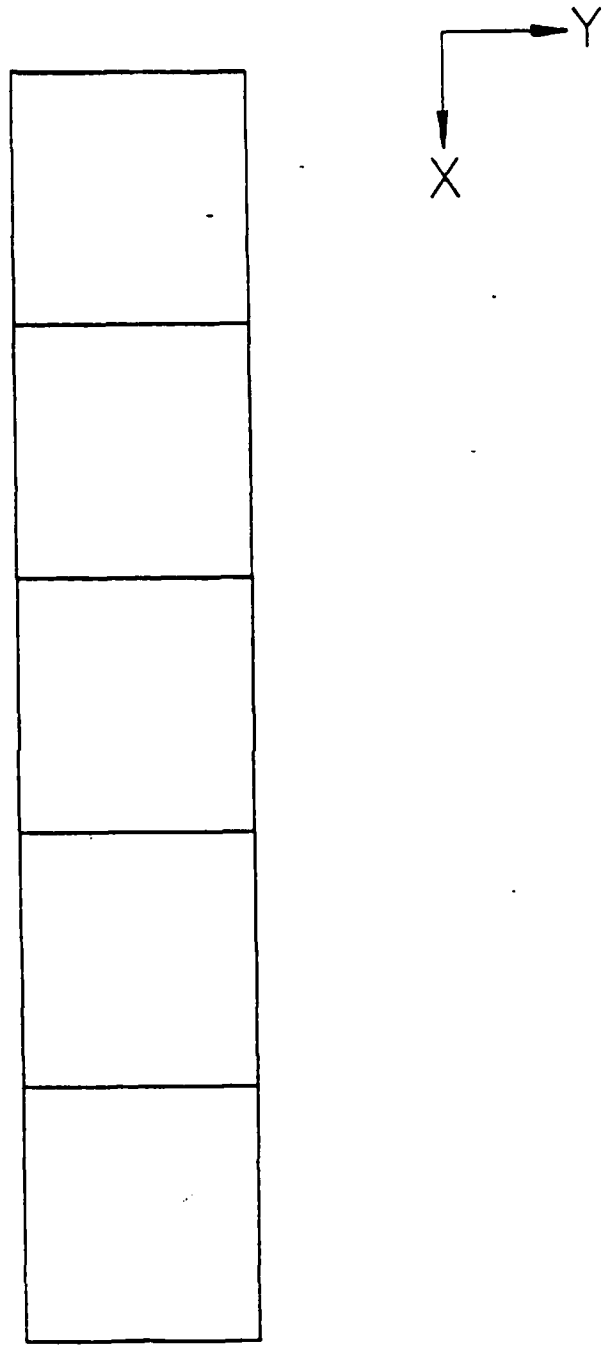

Fig. 3 Finite element model of 5-bay beam.

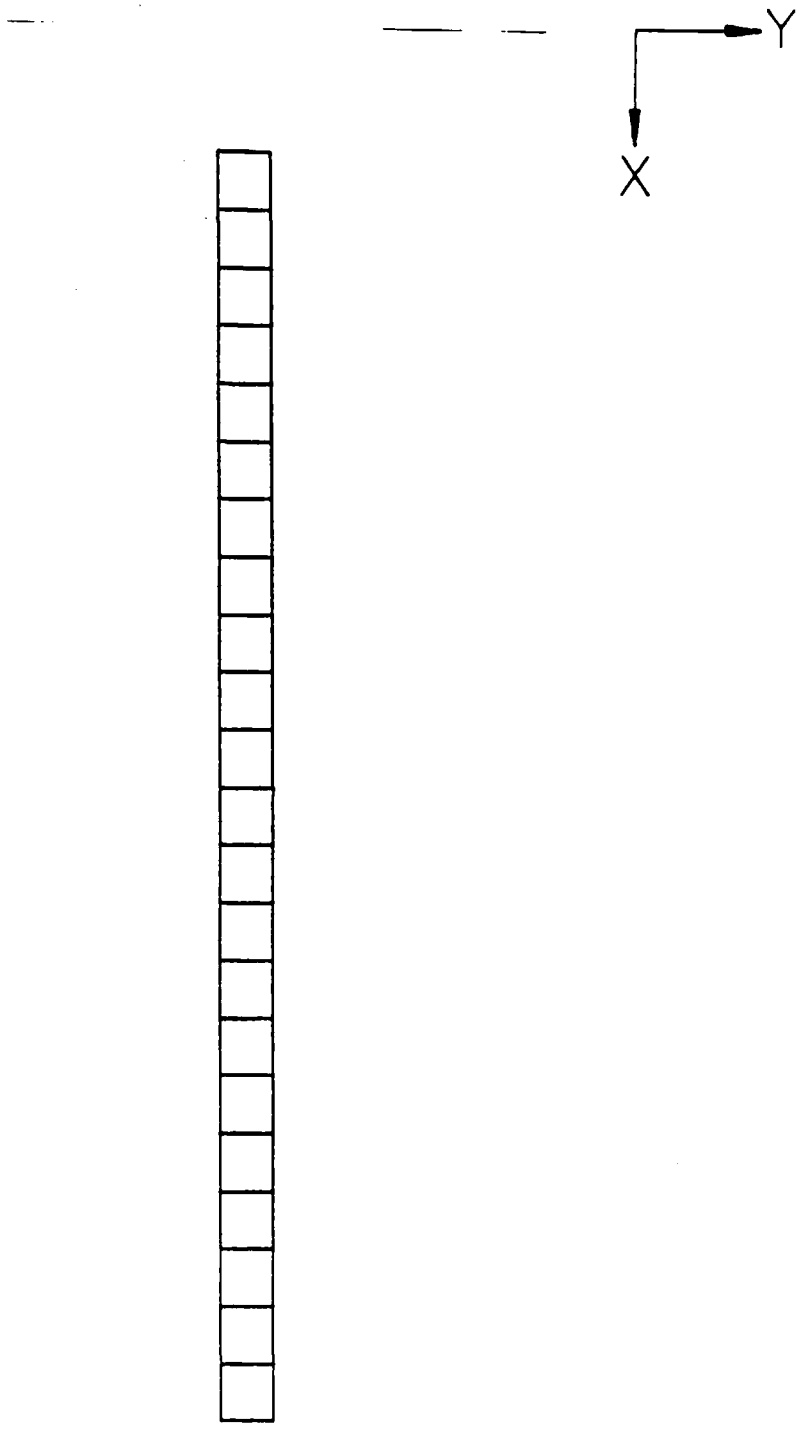

Fig. 4 Finite element model of 22-bay beam.

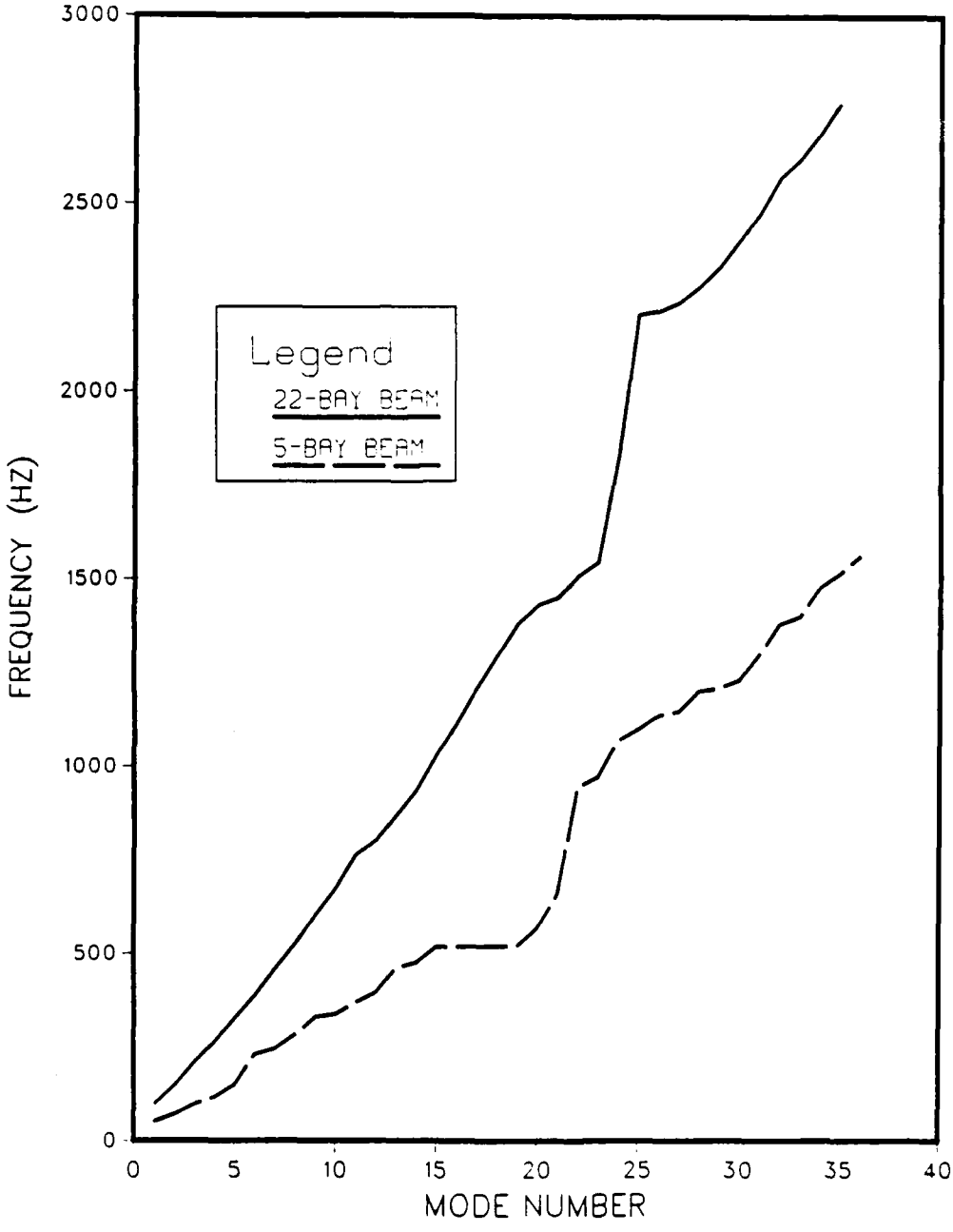

Fig. 5 First 35 natural frequencies of the 22-bay beam and the first 36 natural frequencies of the 5-bay beam as predicted by NASTRAN.

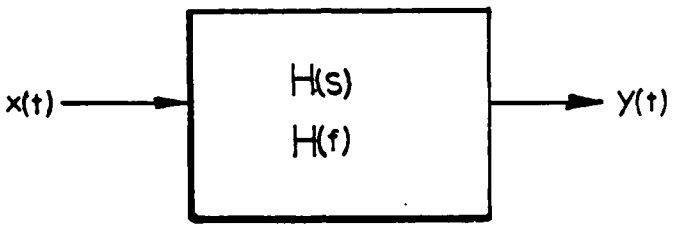

Fig. 6 Single input/single output system.

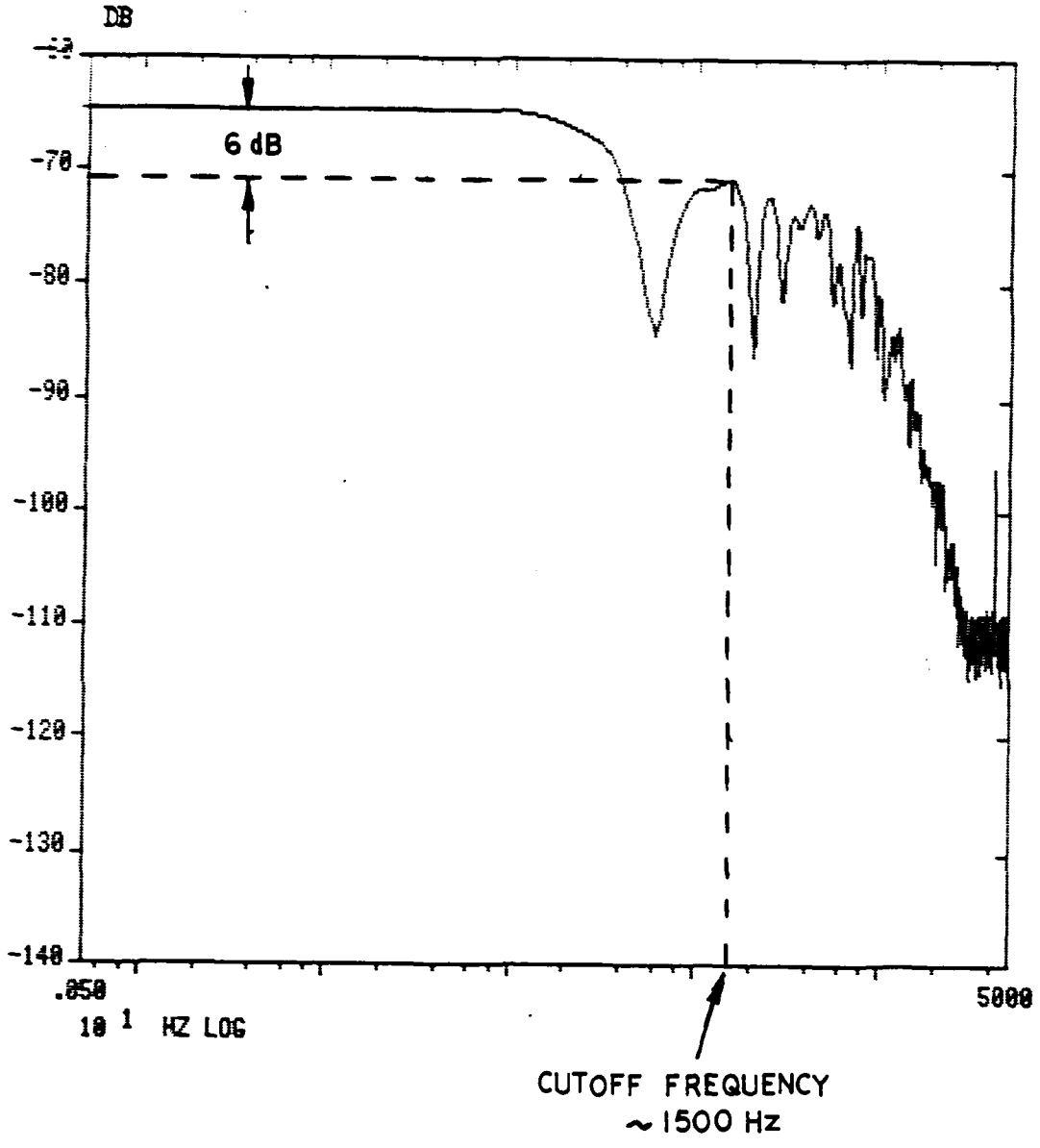

Fig. 7 Frequency spectrum of an impact at location 1 of the 5-bay beam.

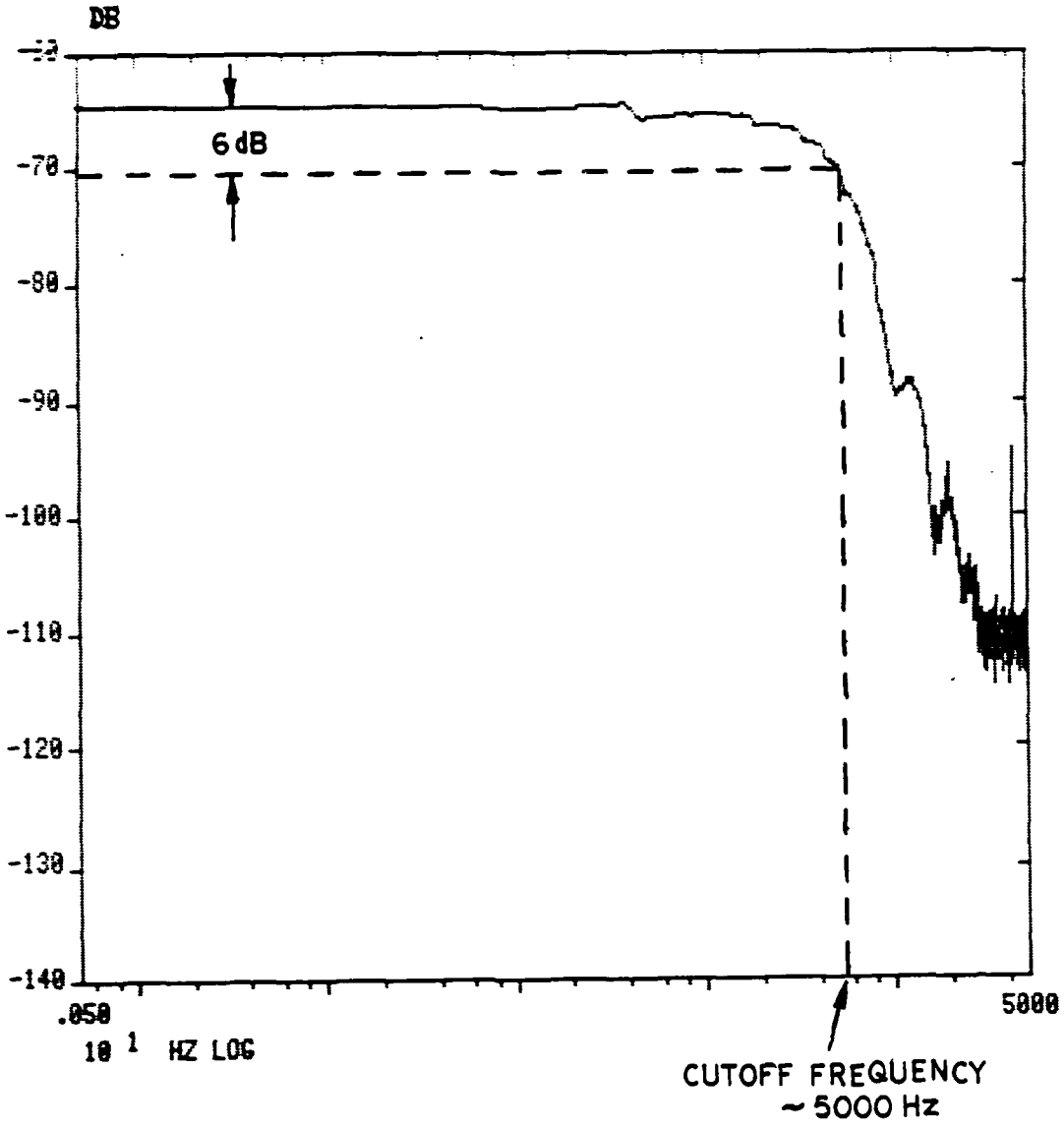

Fig. 8 Frequency spectrum of an impact at location 2 of the 5-bay beam.

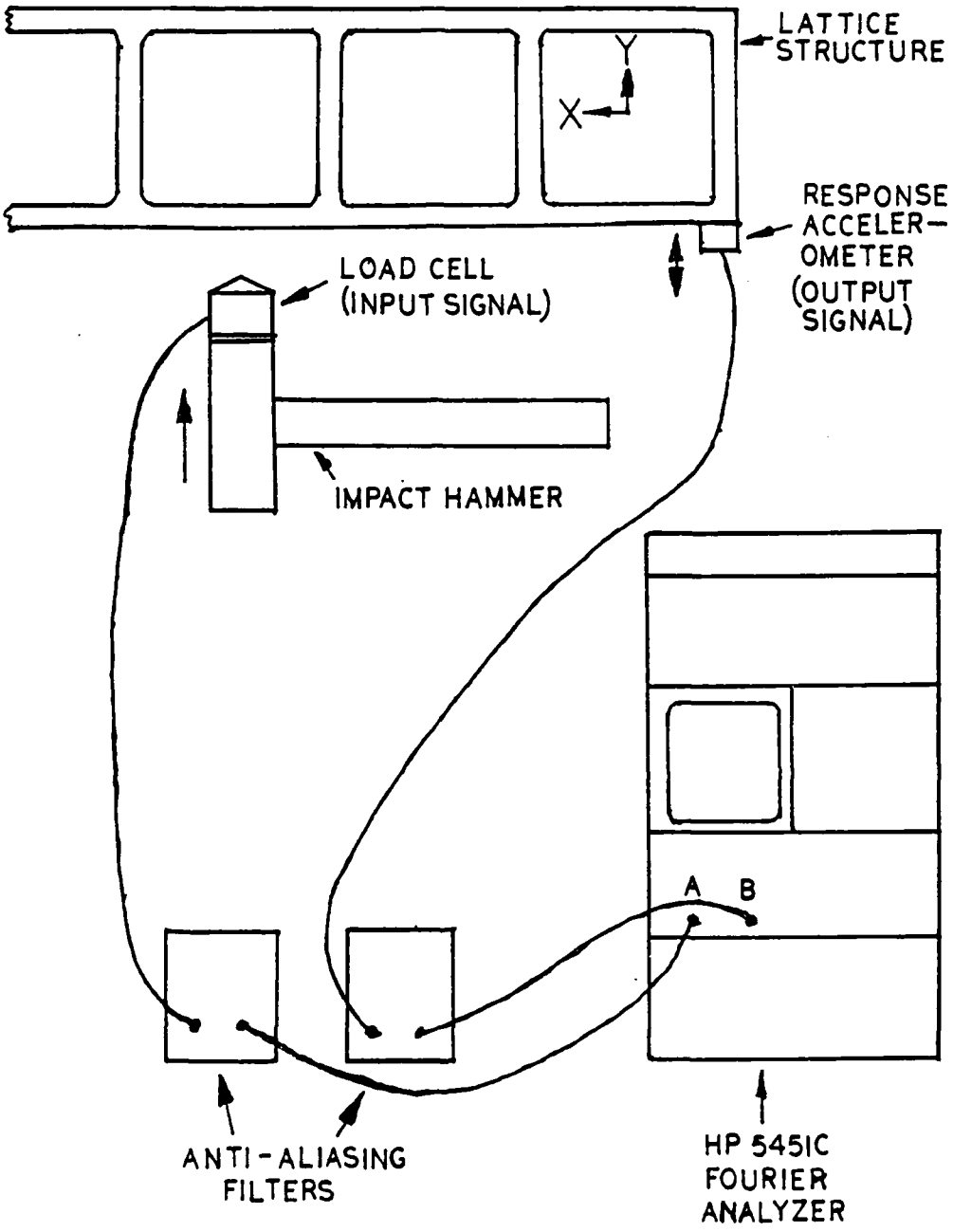

Fig. 9 Schematic representation of the experimental modal analysis setup.

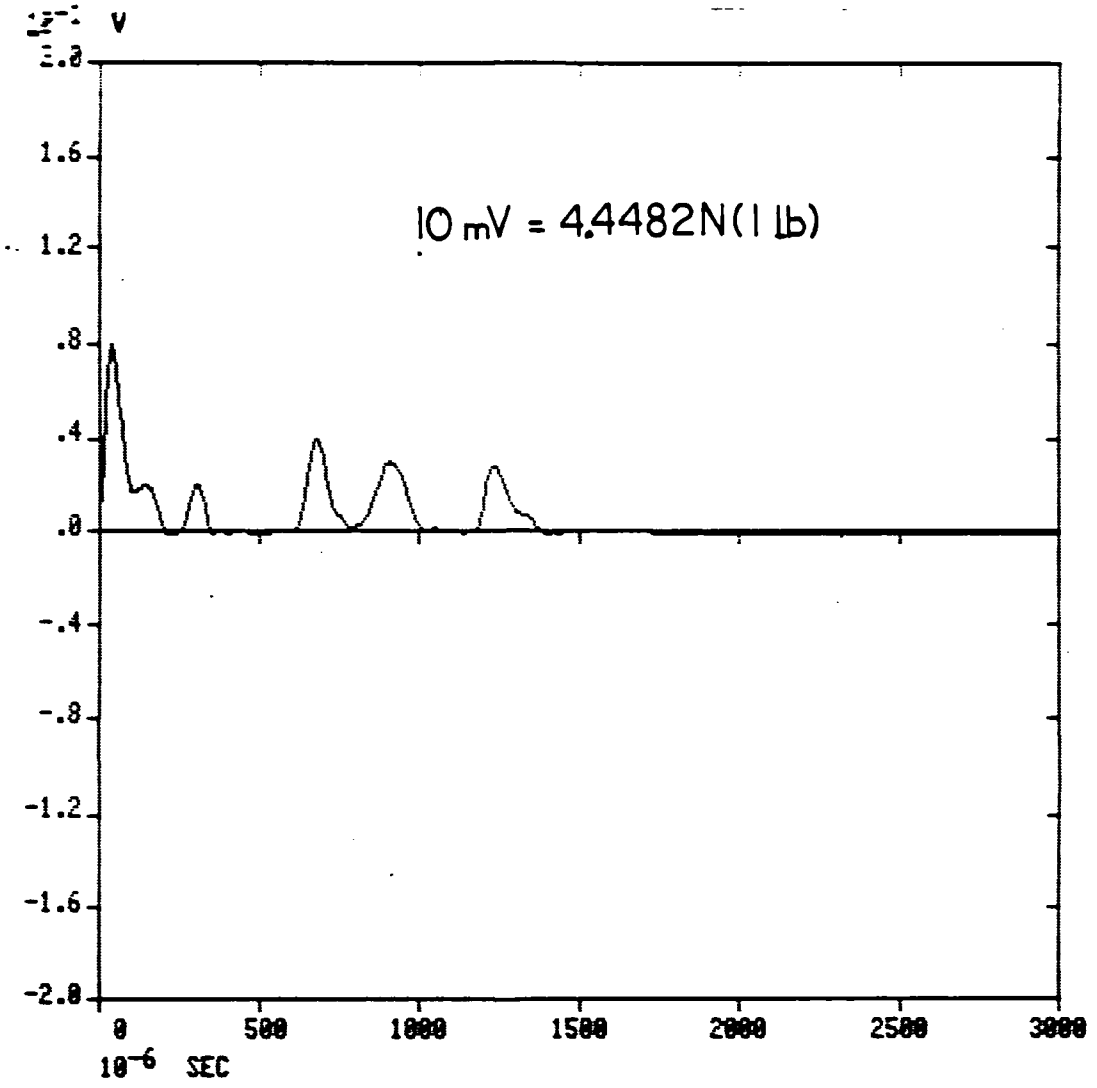

Fig. 10 Excitation hammer force versus time obtained by impacting the 5-bay beam at location 1.

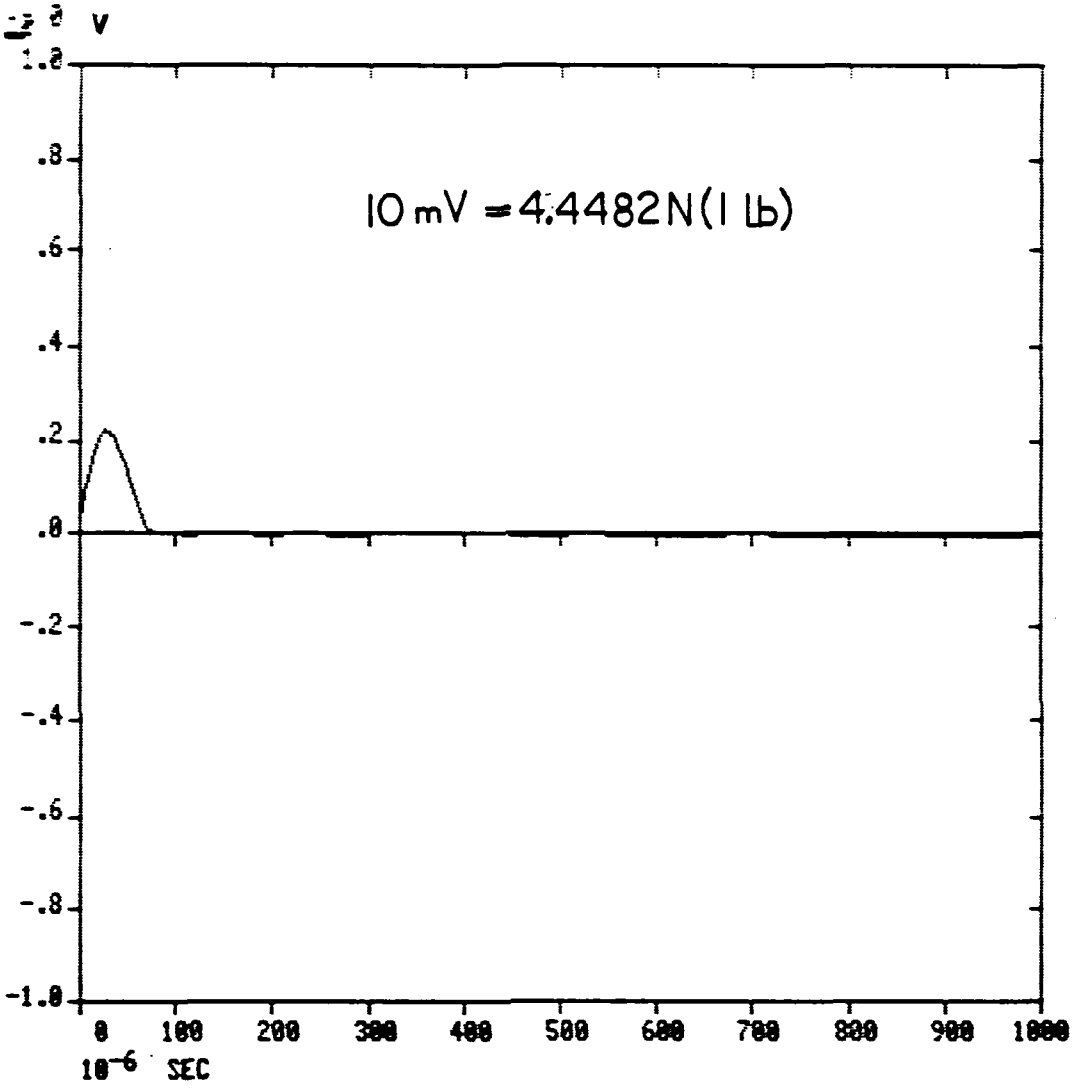

Fig. 11 Excitation hammer force versus time obtained by impacting the 5-bay beam at location 2.

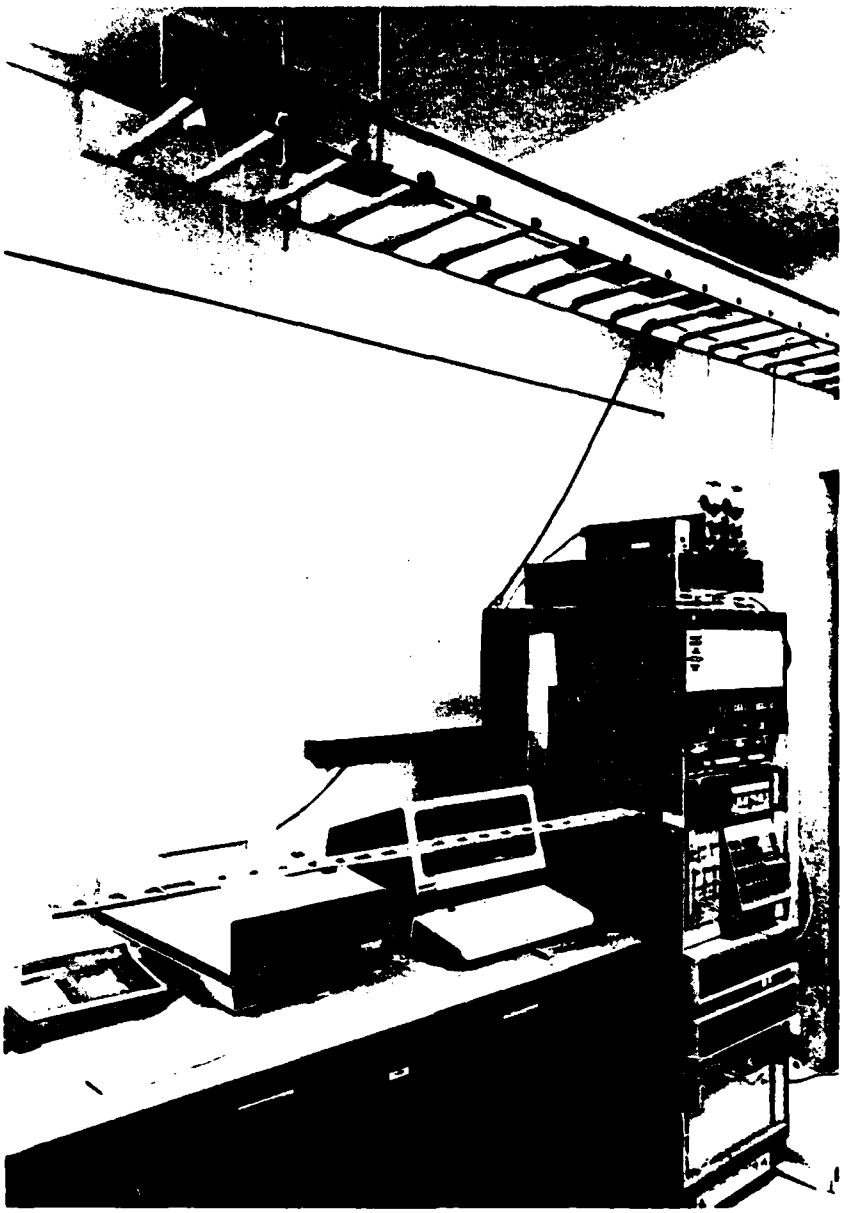

Fig. 12 Photograph of the laboratory setup used for modal analyses of the 22-bay beam.

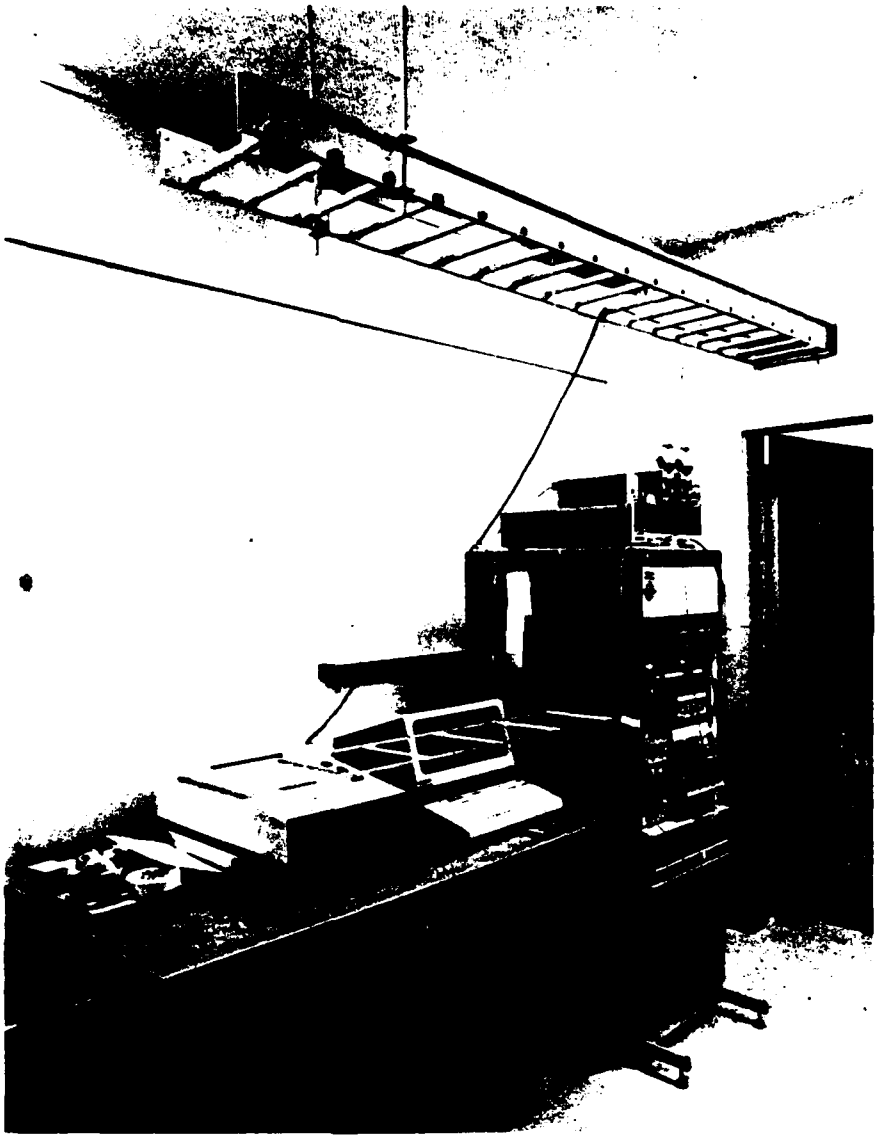

Fig. 13 Photograph of the laboratory setup used for modal analyses of the 5-bay beam.

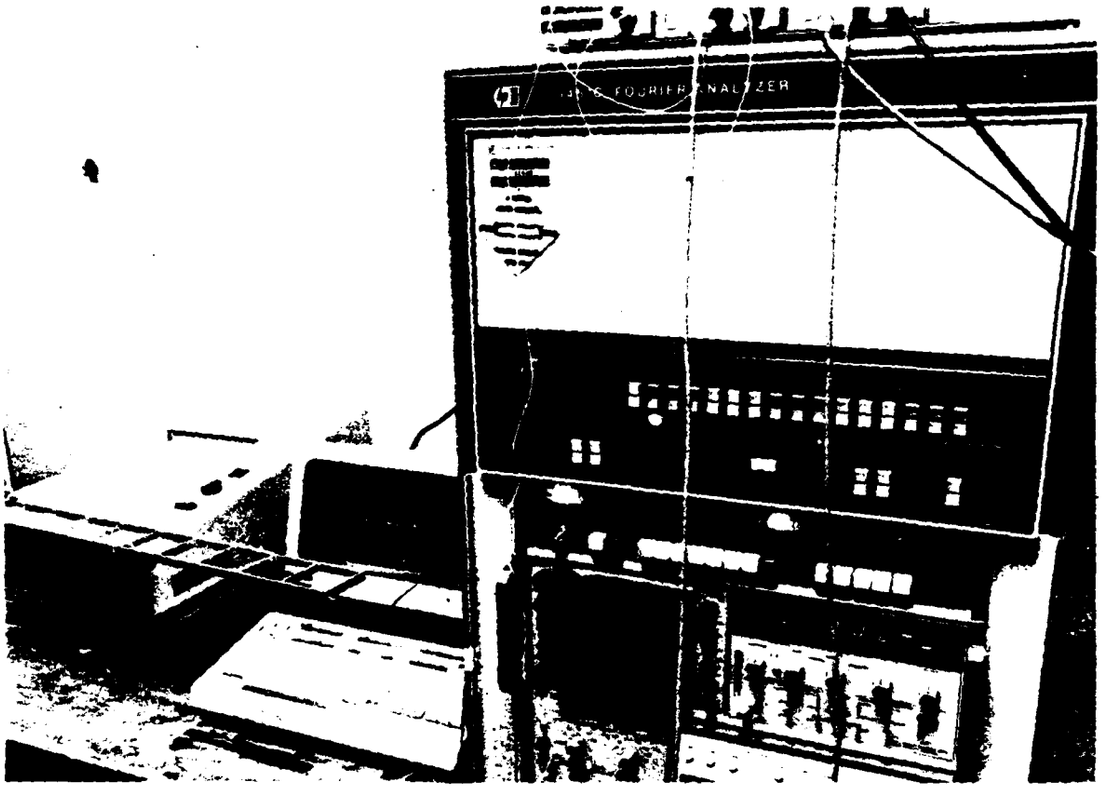

Fig. 14 Photograph of 22-bay beam experimental modal analysis setup showing response accelerometer, impact hammer and Fourier analyzer.

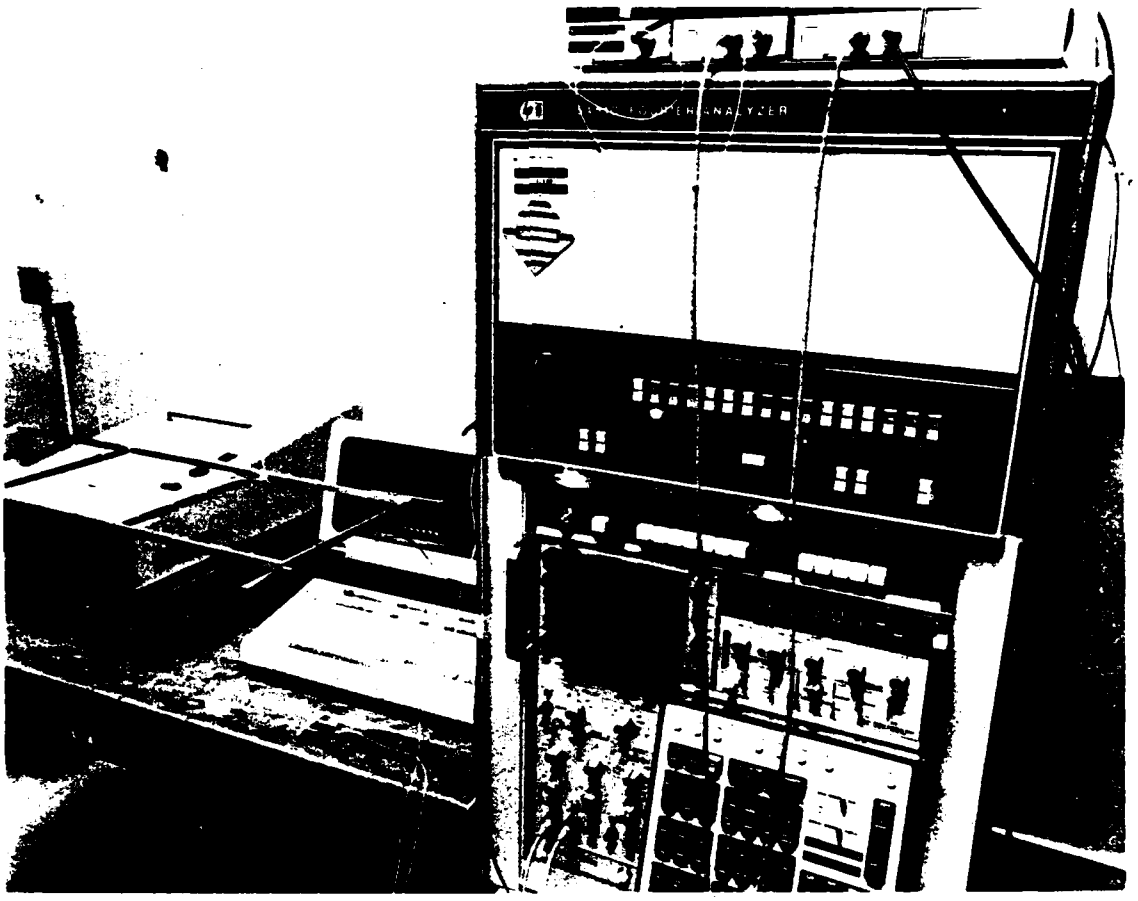

Fig. 15 Photograph of 5-bay beam experimental modal analysis setup showing response accelerometer, impact hammer and Fourier analyzer.

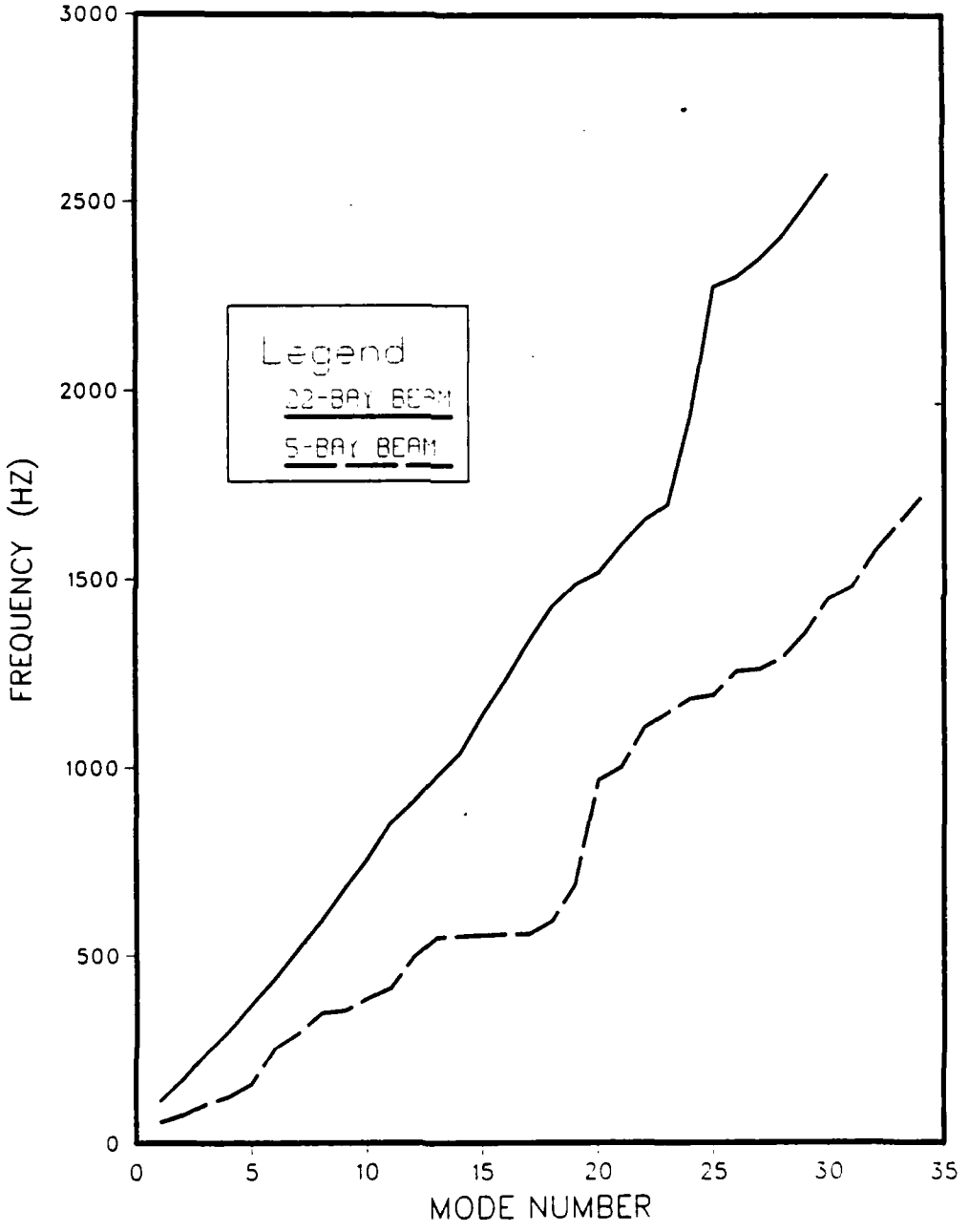

Fig. 16 Frequency versus mode number for the two lattice structures measured using experimental modal analyses.

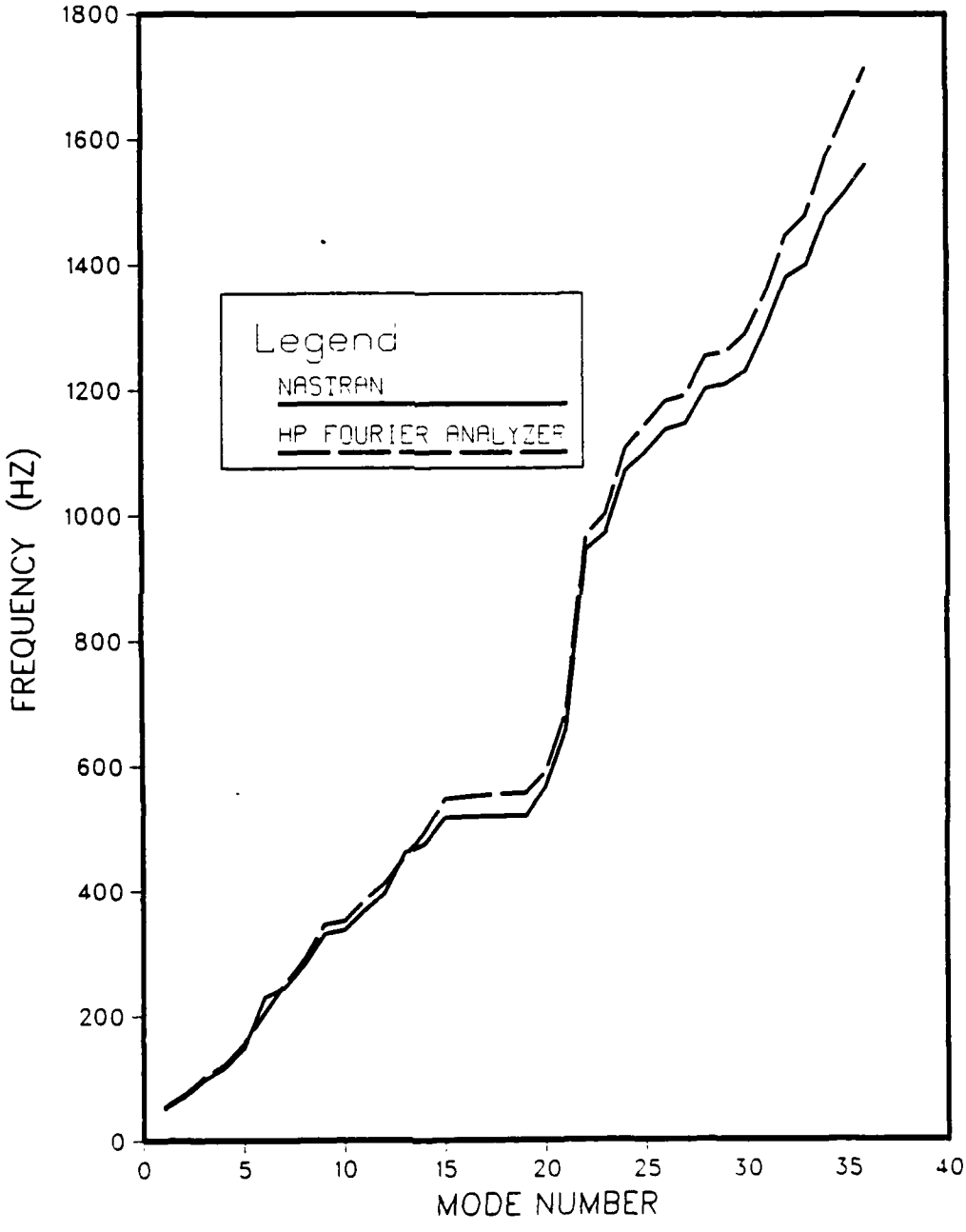

Fig. 17 Frequency versus mode number for the 5-bay beam as predicted using NASTRAN and as measured using the Fourier analyzer and modal analyses.

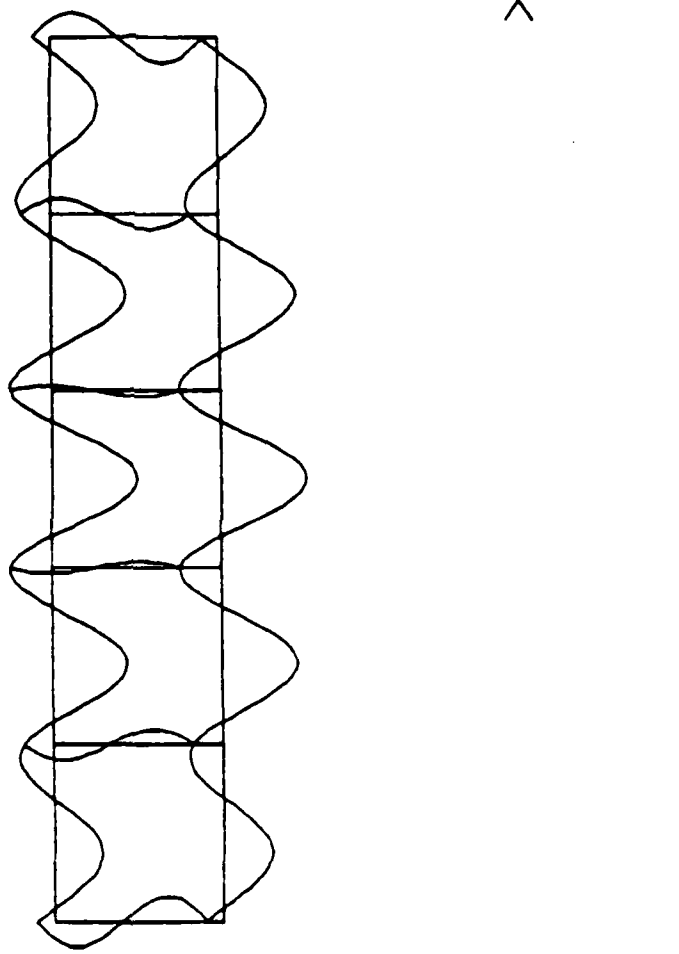

Fig. 18 Mode 21 of the 5-bay beam (frequency = 657.39 Hz).

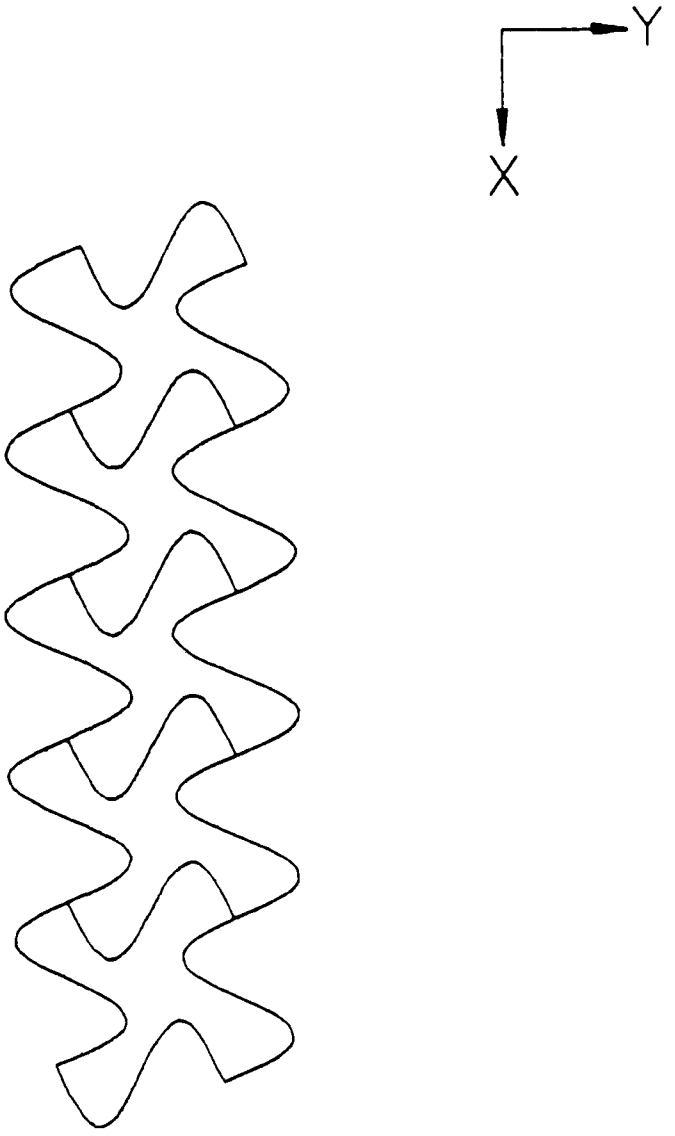

Fig. 19 Mode 22 of the 5-bay beam (frequency = 944.95 Hz).

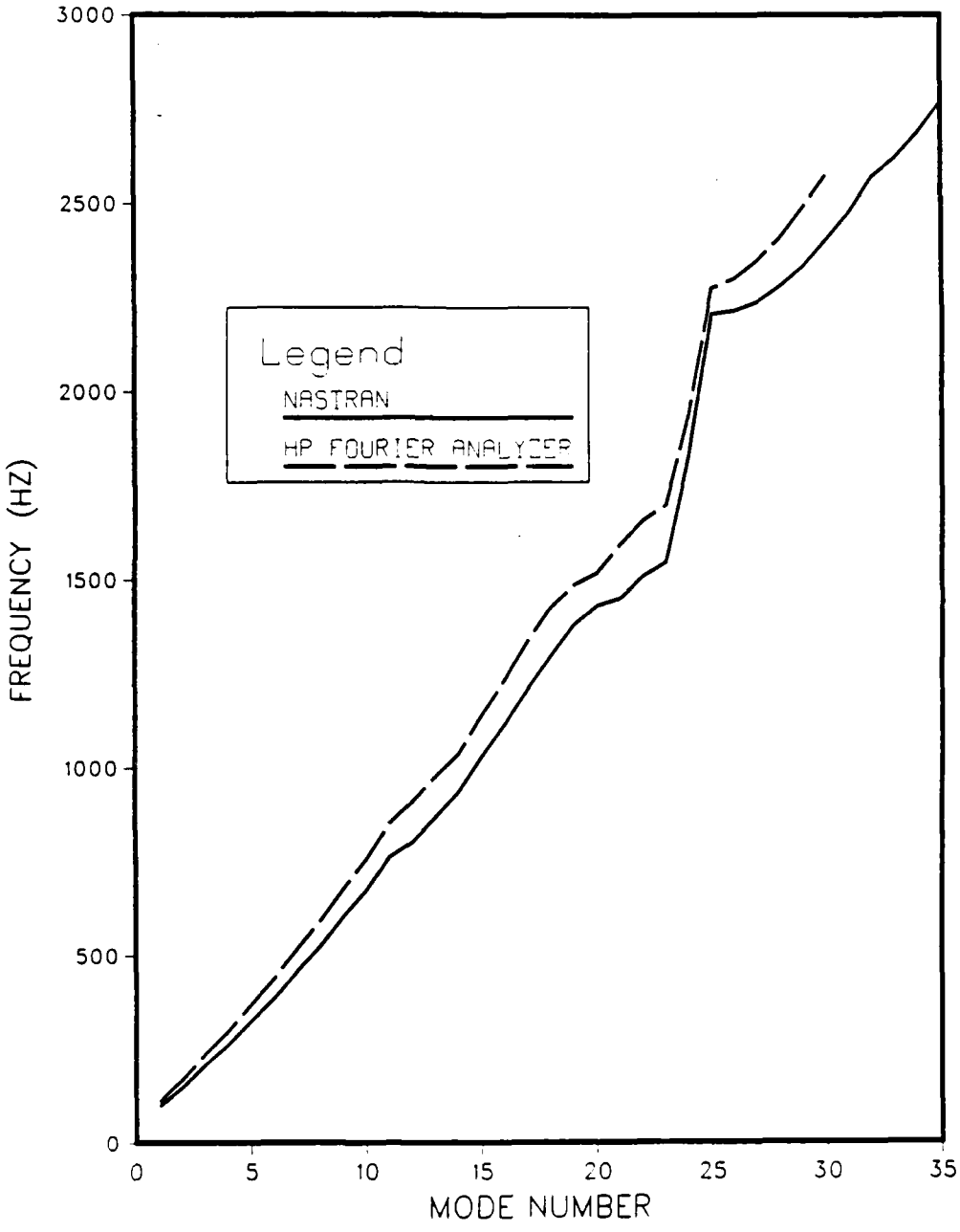

Fig. 20 Frequency versus mode number for the 22-bay beam as predicted using NASTRAN and as measured using a Fourier analyzer and modal analyses.

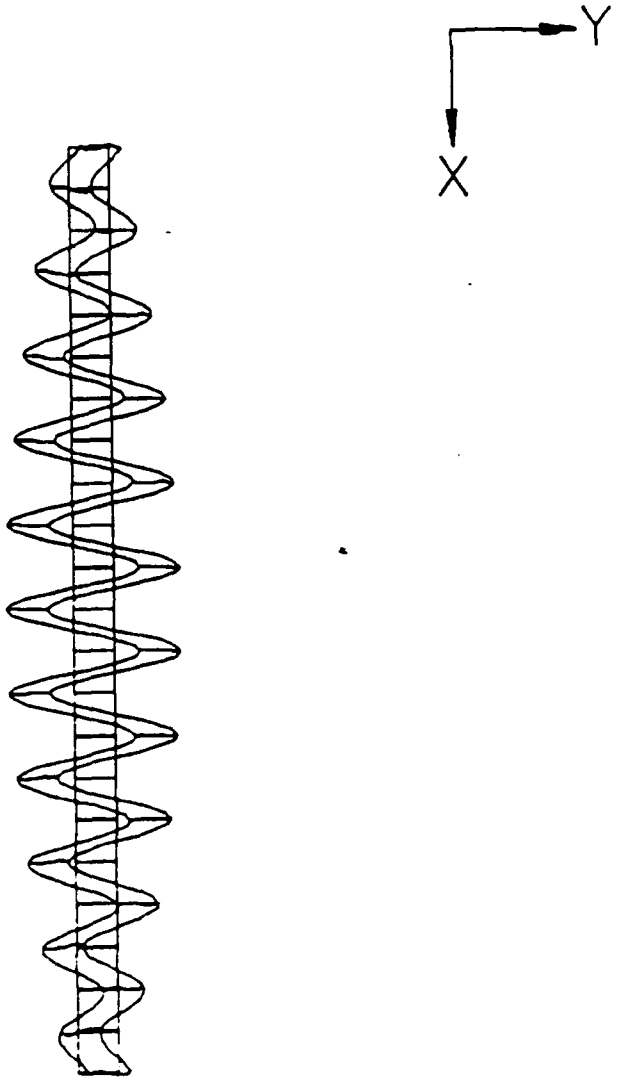

Fig. 21 Mode 23 of the 22-bay beam (frequency = 1544.77 Hz).

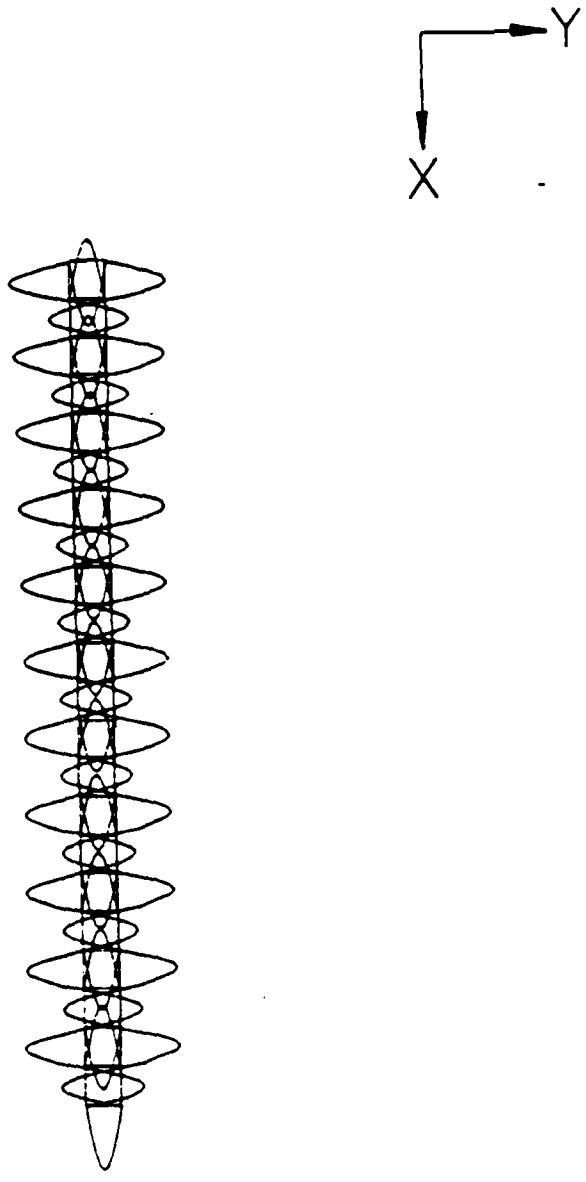

Fig. 22 Mode 25 of the 22-bay beam (frequency = 2205.80 Hz).

APPENDIX A

MODE SHAPES AND SOLUTION TIMES FOR FINITE ELEMENT DYNAMIC ANALYSES

5-Bay Beam

Figs. A1 through A19 show some of the mode shapes of the 5-bay beam that were found using NASTRAN. These 19 mode shapes are representative of some of the 172 total configurations that were identified in the NASTRAN analyses of the 5-bay beam. Figs. A1 through A8 show the mode shapes superimposed over the undeformed finite element model. Figs. A9 through A19 show only the deformed mode shapes.

The inverse power method [1] was used to determine the natural frequencies and mode shapes. The solution time (cpu-sec) was independent of the frequency range in which the natural frequencies and mode shapes were to be calculated. In other words, it took approximately the same amount of time for the computer to determine a natural frequency and associate mode shape near 20 kHz as it took to find the lowest natural frequency and associated mode shape (approximately 95 Hz). The computer required approximately 11.25 cpu-sec to determine each natural frequency/mode shape pair.

Note, the mode shapes were normalized to the mass matrix.

22-Bay Beam

Figs. A20 through A35 show some of the mode shapes of the 22-bay lattice structure that were found using NASTRAN. These 16 mode shapes were selected from the 194 total mode shapes because they represent

the variety of mode shape configurations of the 22-bay beam. Figs. A20 through A24 and figs. A27 through A31 show the mode shapes superimposed over the undeformed finite element model. The remaining figures show only the deformed modes of vibration.

As with the calculations of the natural frequencies and mode shapes of the 5-bay beam, the inverse power method solution times were independent of the magnitude of the natural frequencies being calculated. The solution of each natural frequency/mode shape pair for the 22-bay beam required about 13.95 cpu-sec.

Note, the mode shapes of the 22-bay beam were also normalized to the mass matrix.

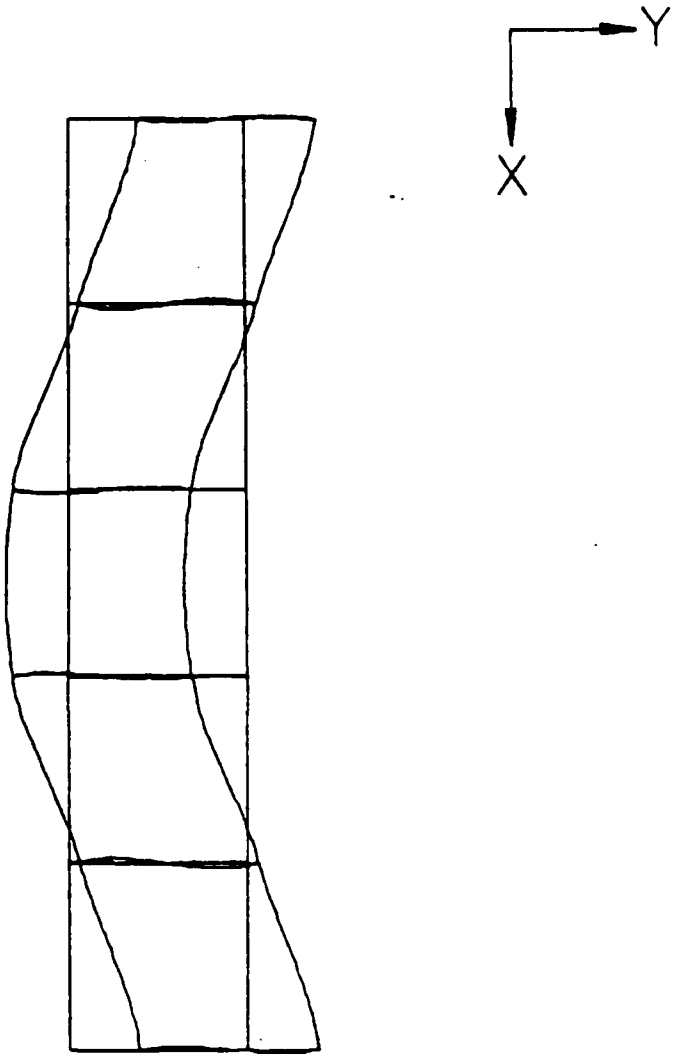

Fig. A1 Mode 1 (frequency = 49.20 Hz).

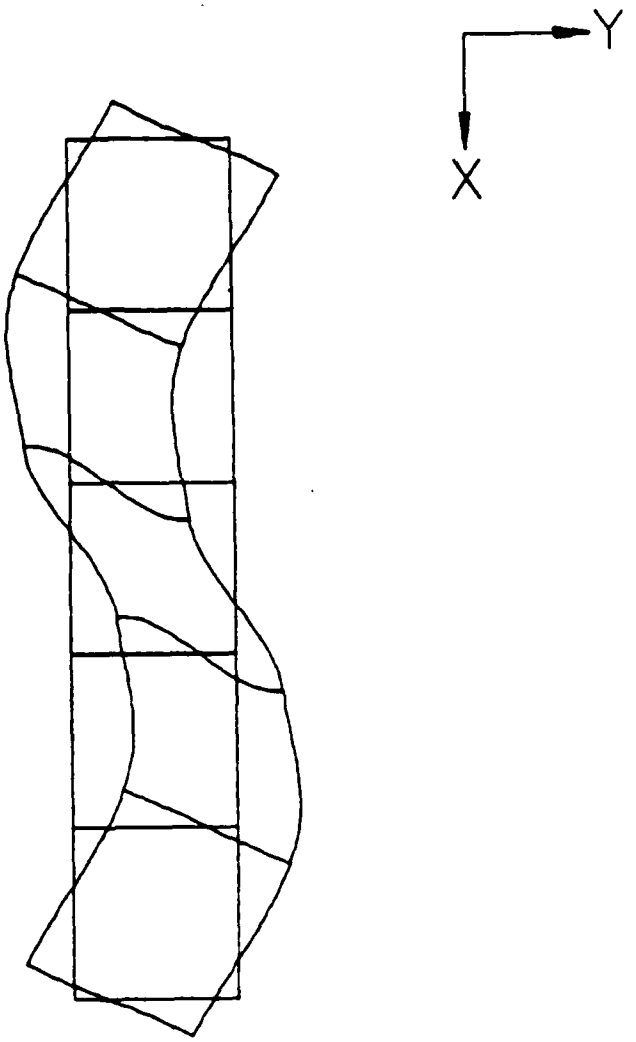

Fig. A2 Mode 2 (frequency = 69.16 Hz).

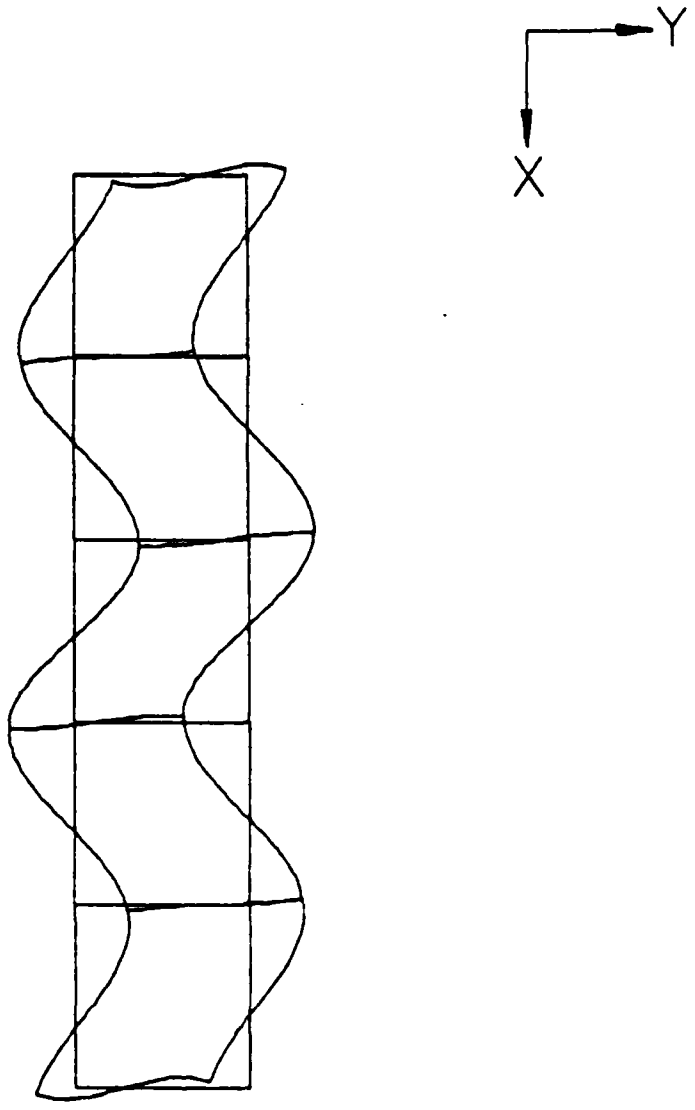

Fig. A3 Mode 5 (frequency = 148.77 Hz).

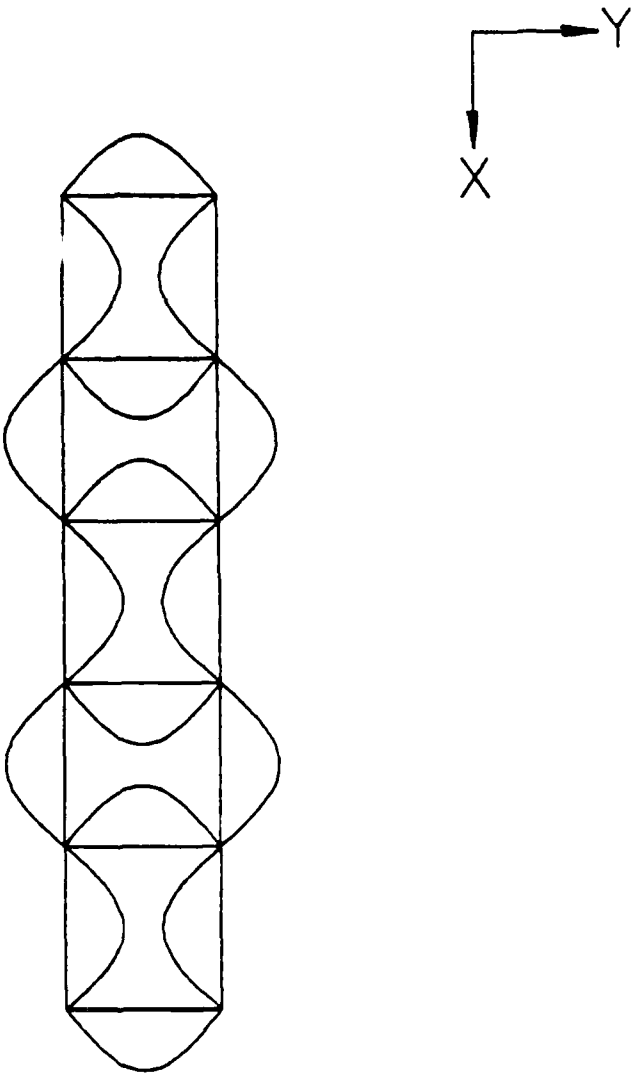

Fig. A4 Mode 6 (frequency = 229.53 Hz).

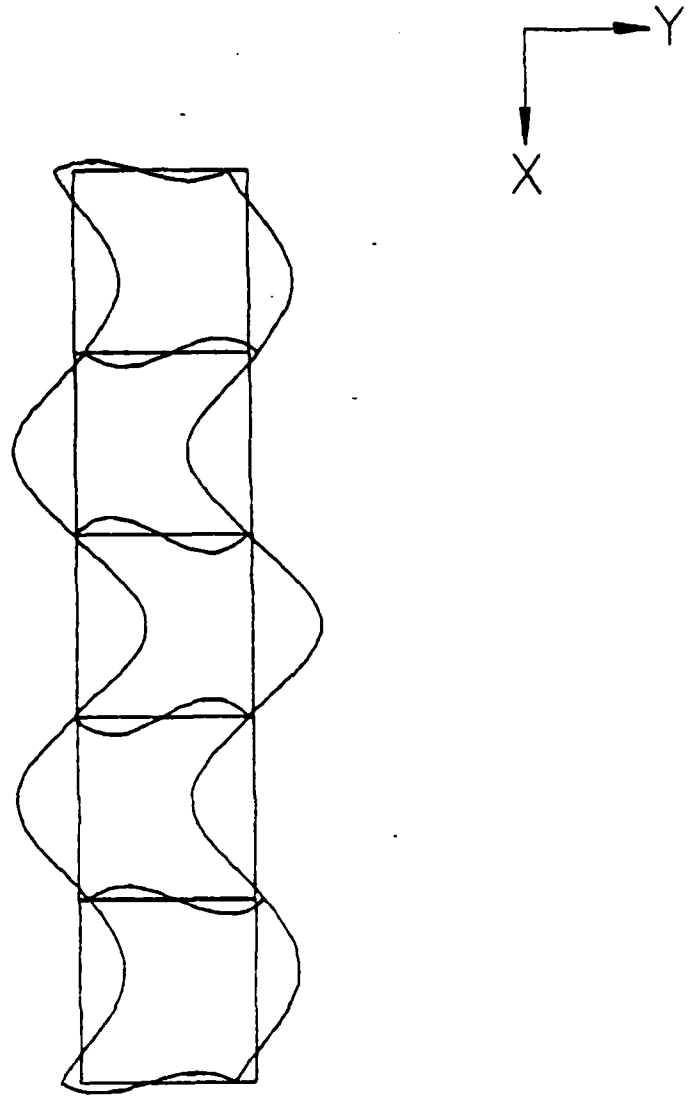

Fig. A5 Mode 10 (frequency = 337.52 Hz).

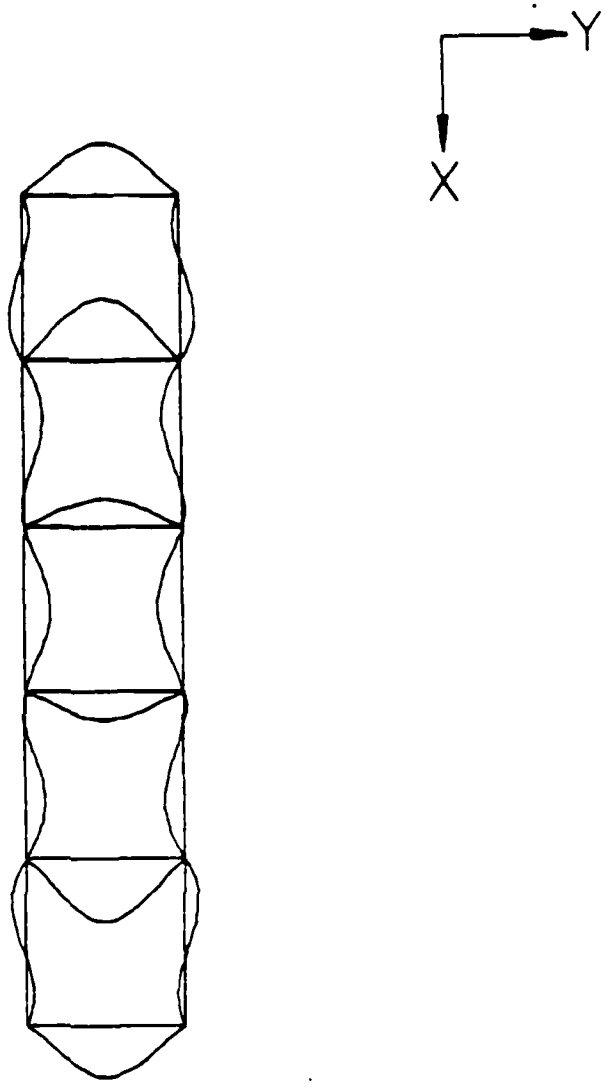

Fig. A6 Mode 11 (frequency = 368.22 Hz).

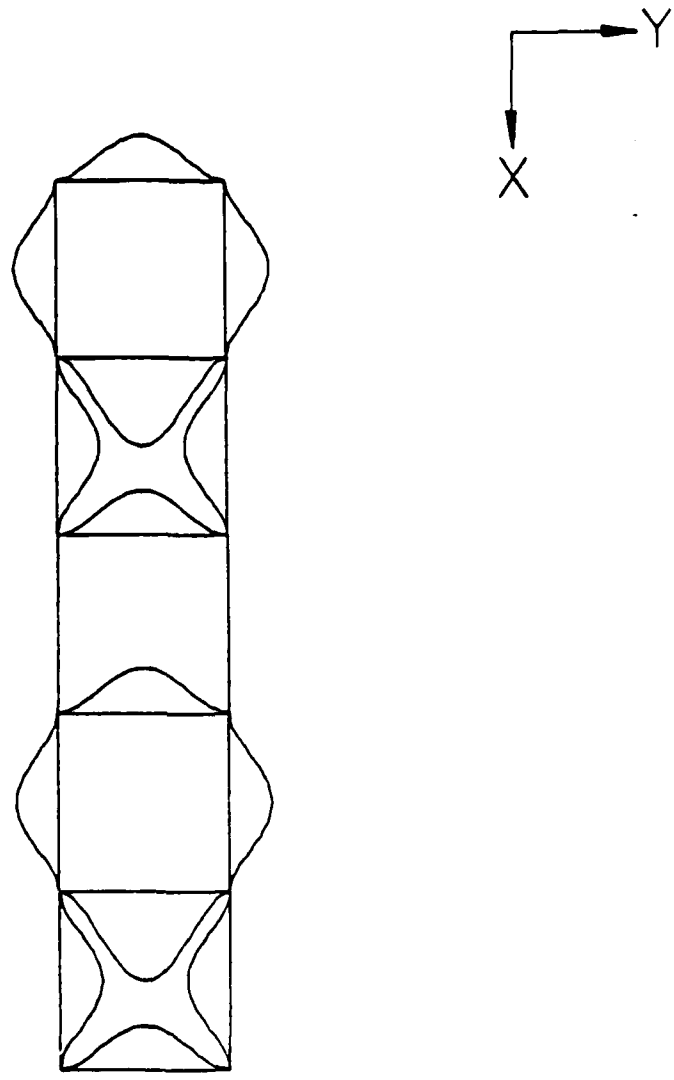

Fig. A7 Mode 18 (frequency = 519.73 Hz).

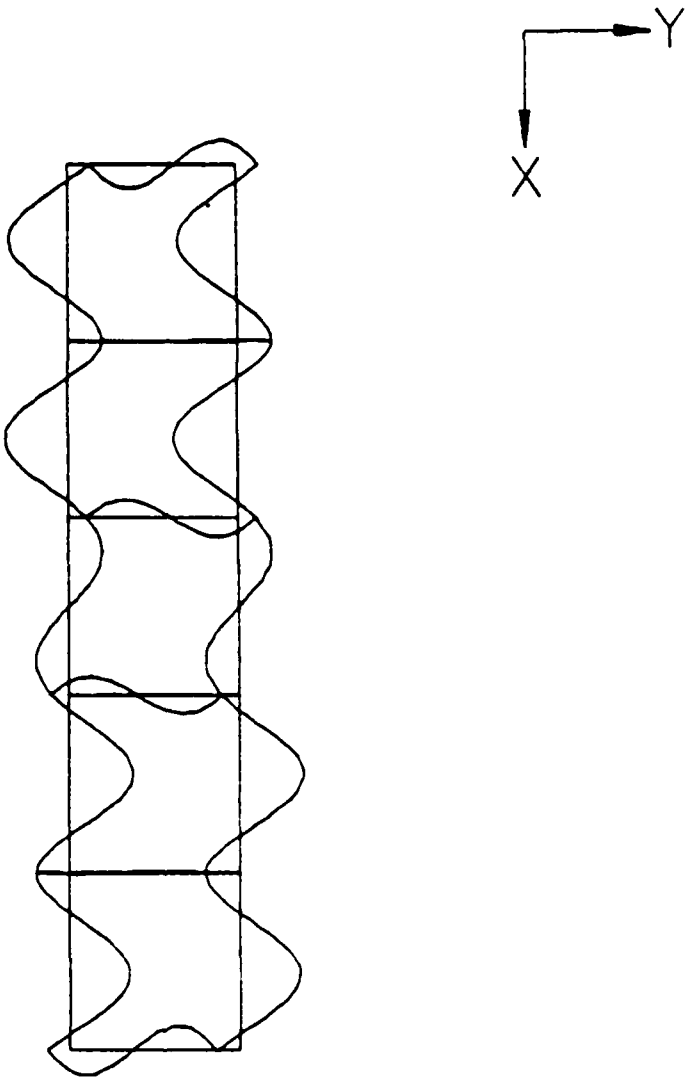

Fig. A8 Mode 20 (frequency = 568.84 Hz).

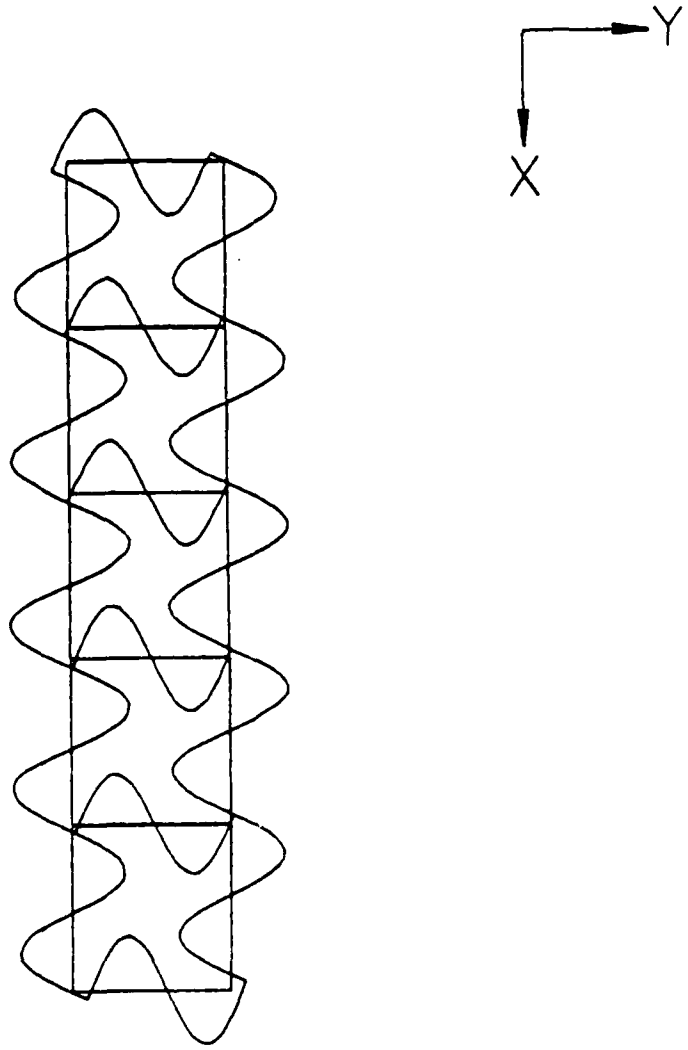

Fig. A9 Mode 22 (frequency = 944.95 Hz).

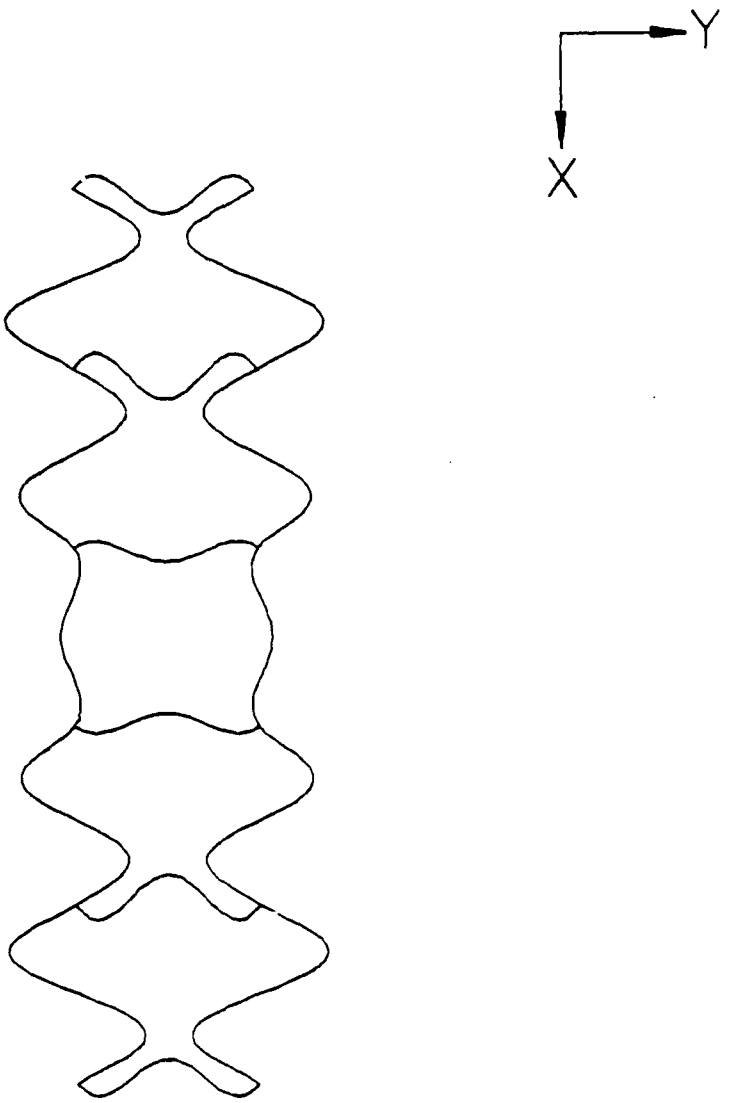

Fig. A10 Mode 26 (frequency = 1136.55 Hz).

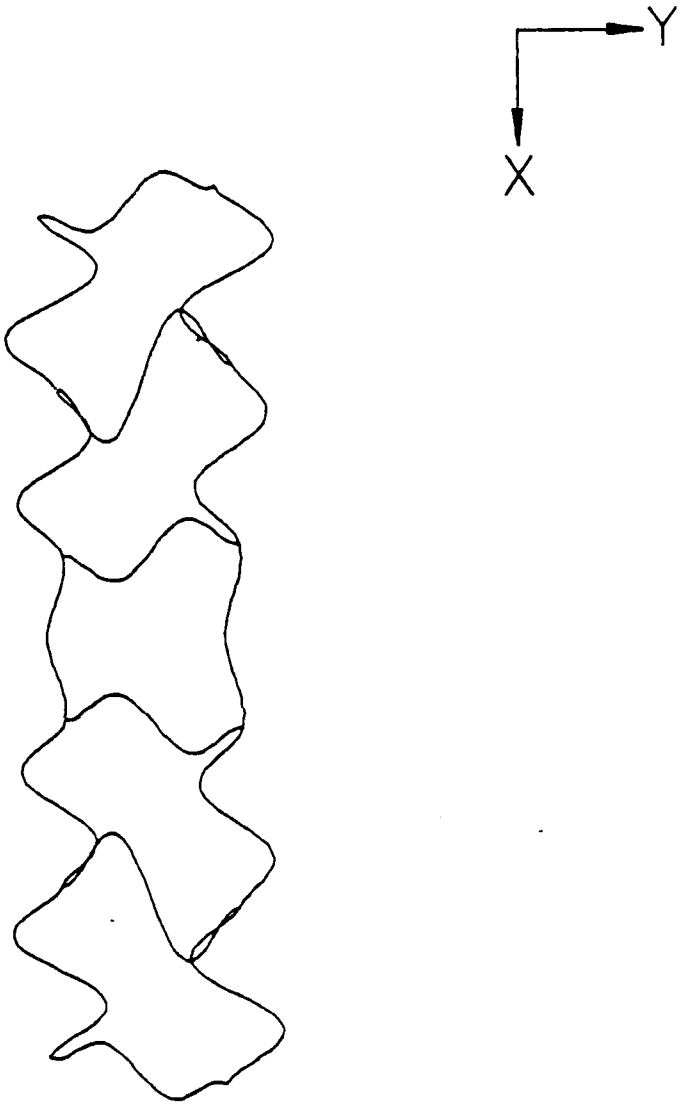

Fig. A11 Mode 36 (frequency = 1400.10 Hz).

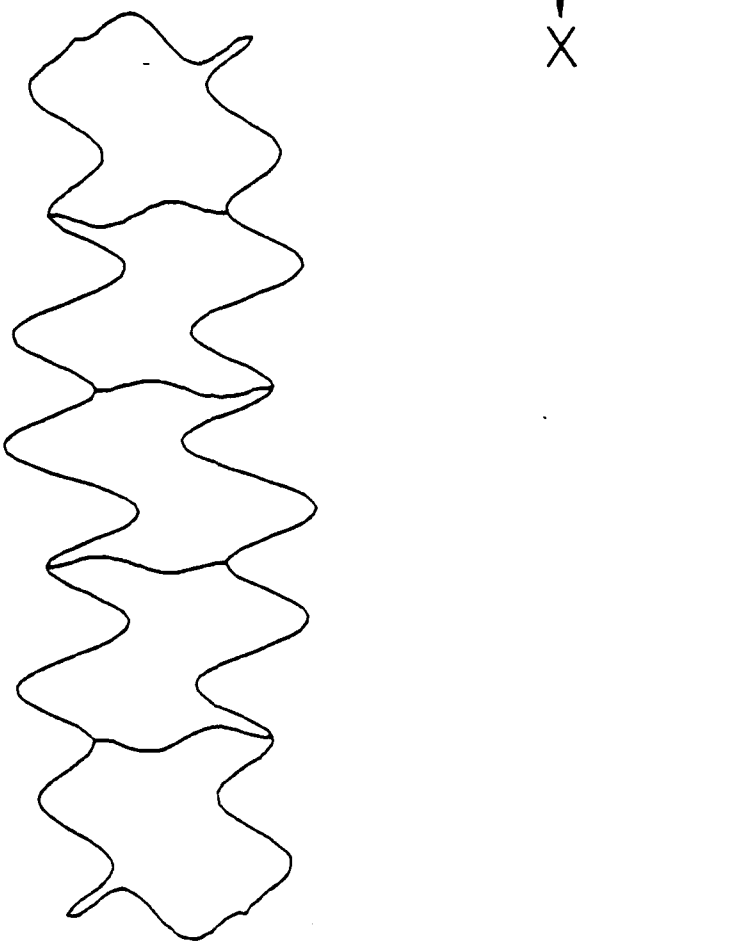

Fig. A12 Mode 37 (frequency = 1635.81 Hz).

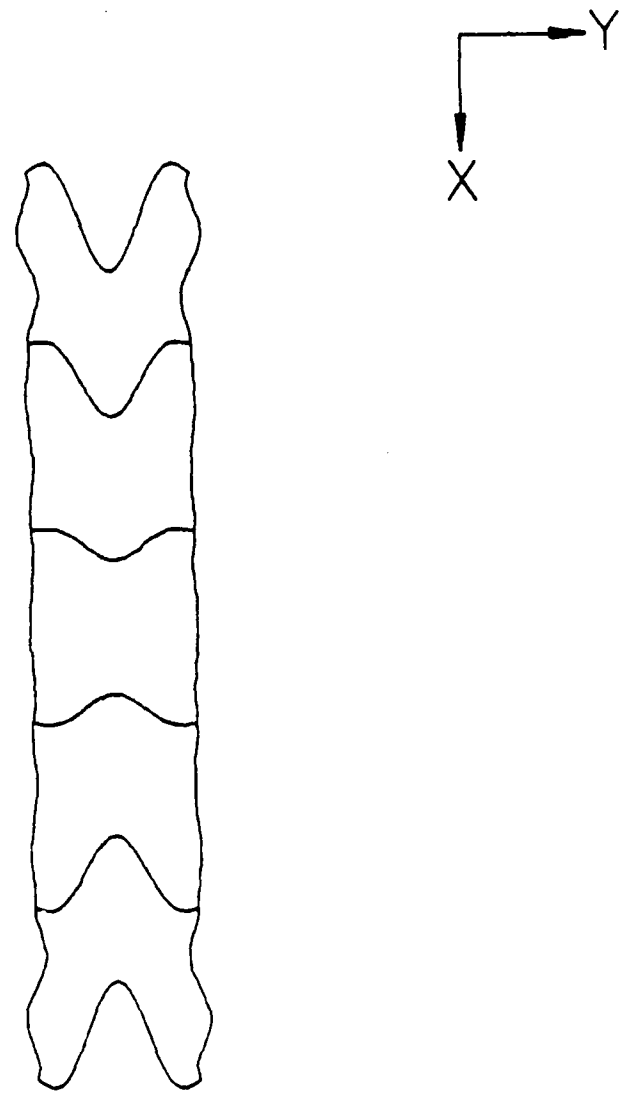

Fig. A13 Mode 28 (frequency = 1784.21 Hz).

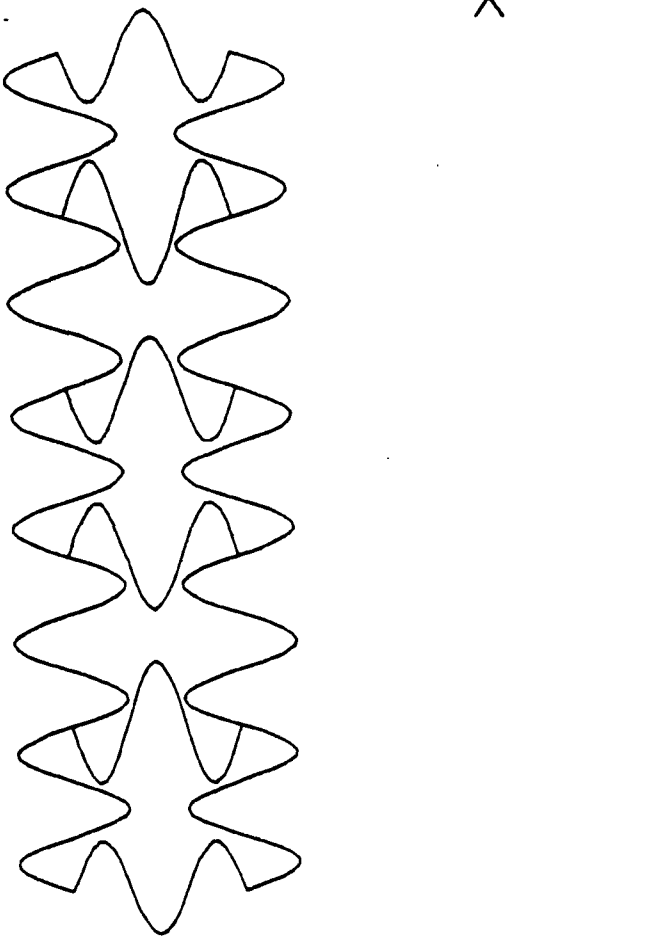

Fig. A14 Mode 40 (frequency = 2065.36 Hz).

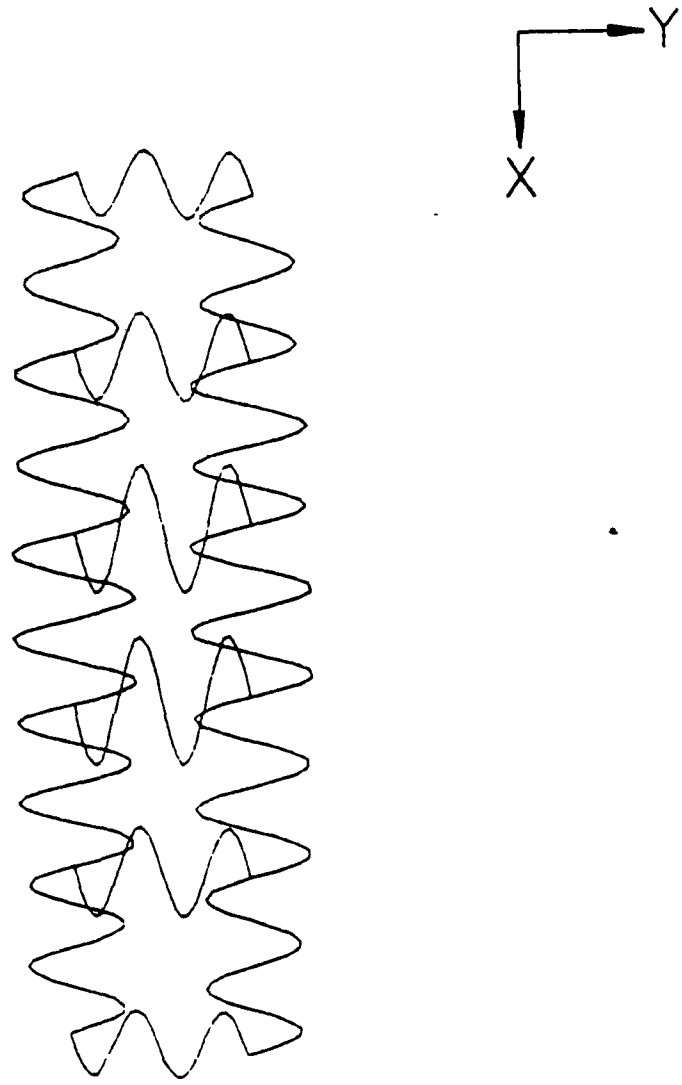

Fig. A15 Mode 58 (frequency = 3703.63 Hz).

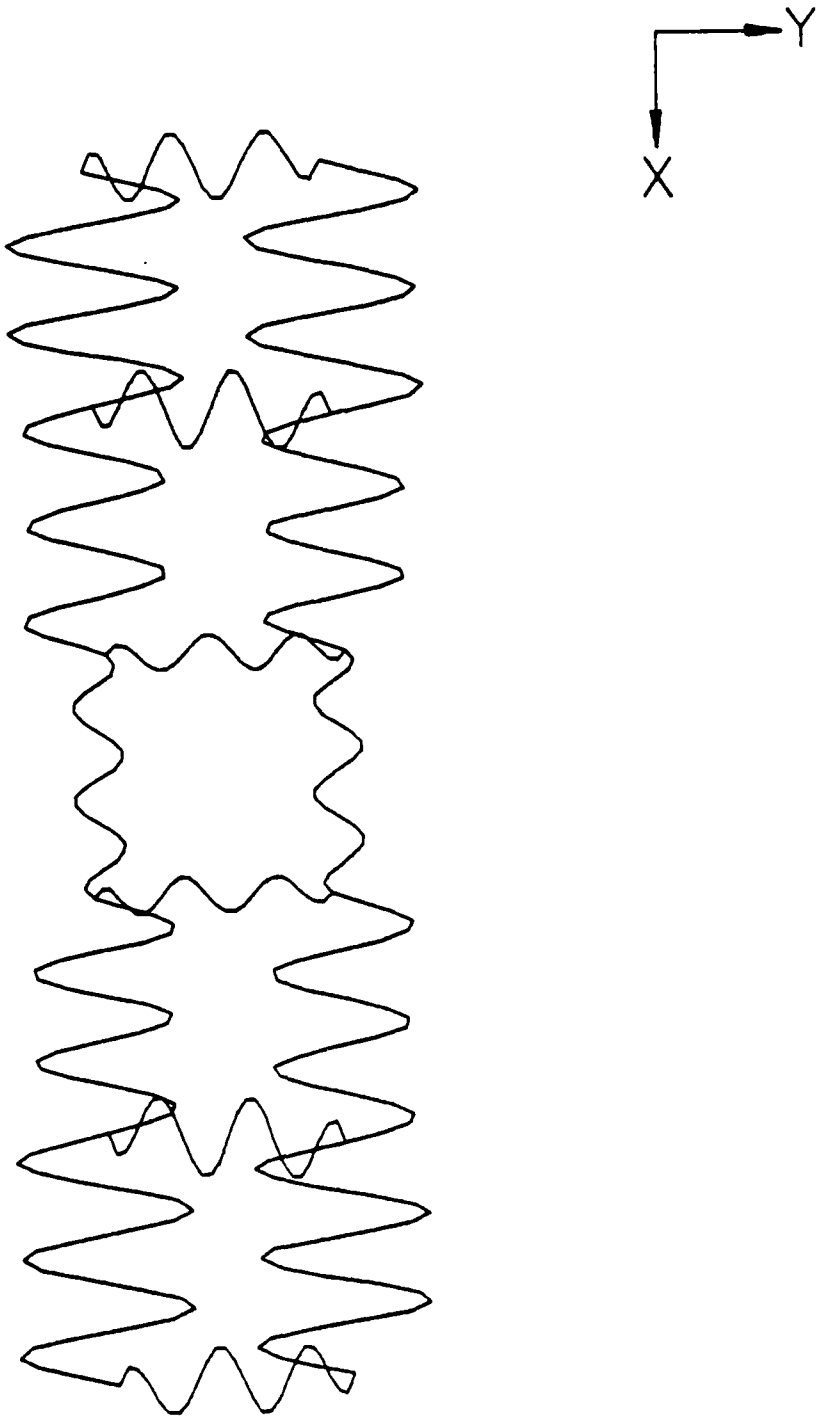

Fig. A16 Mode 82 (frequency = 6317.29 Hz).

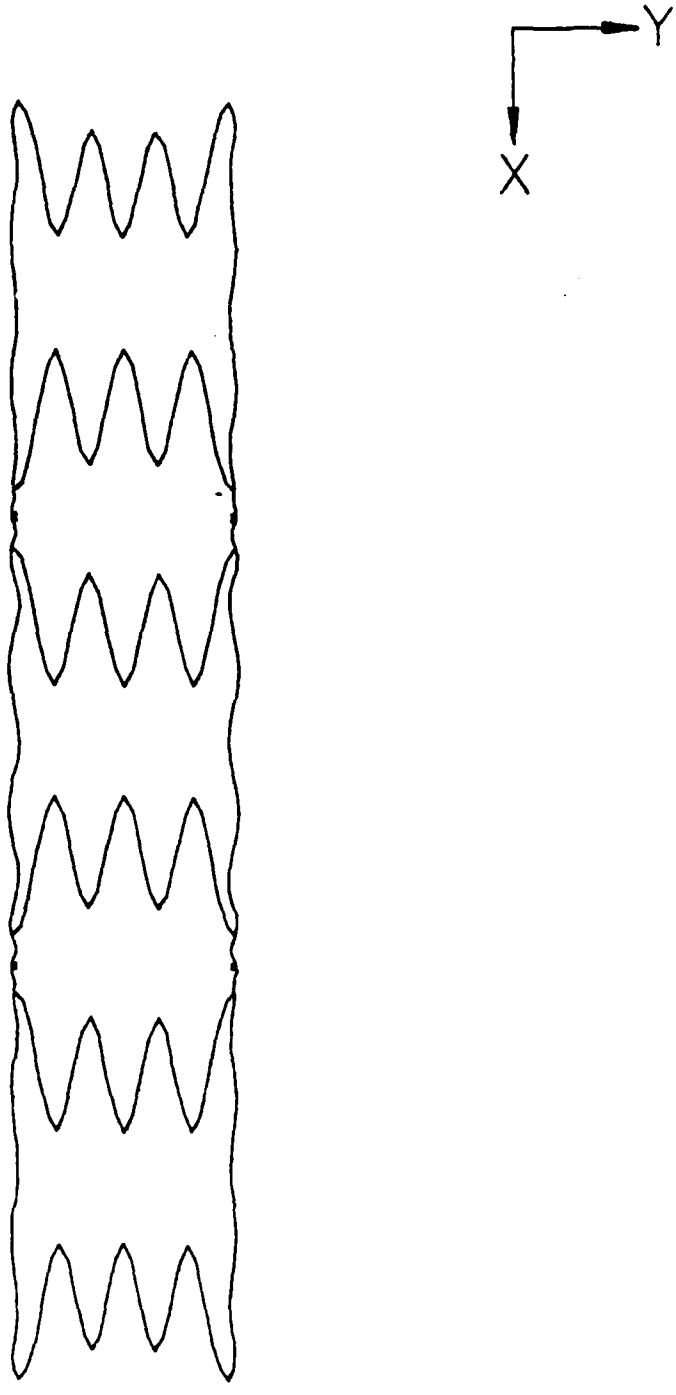

Fig. A17 Mode 107 (frequency = 9467.47 Hz).

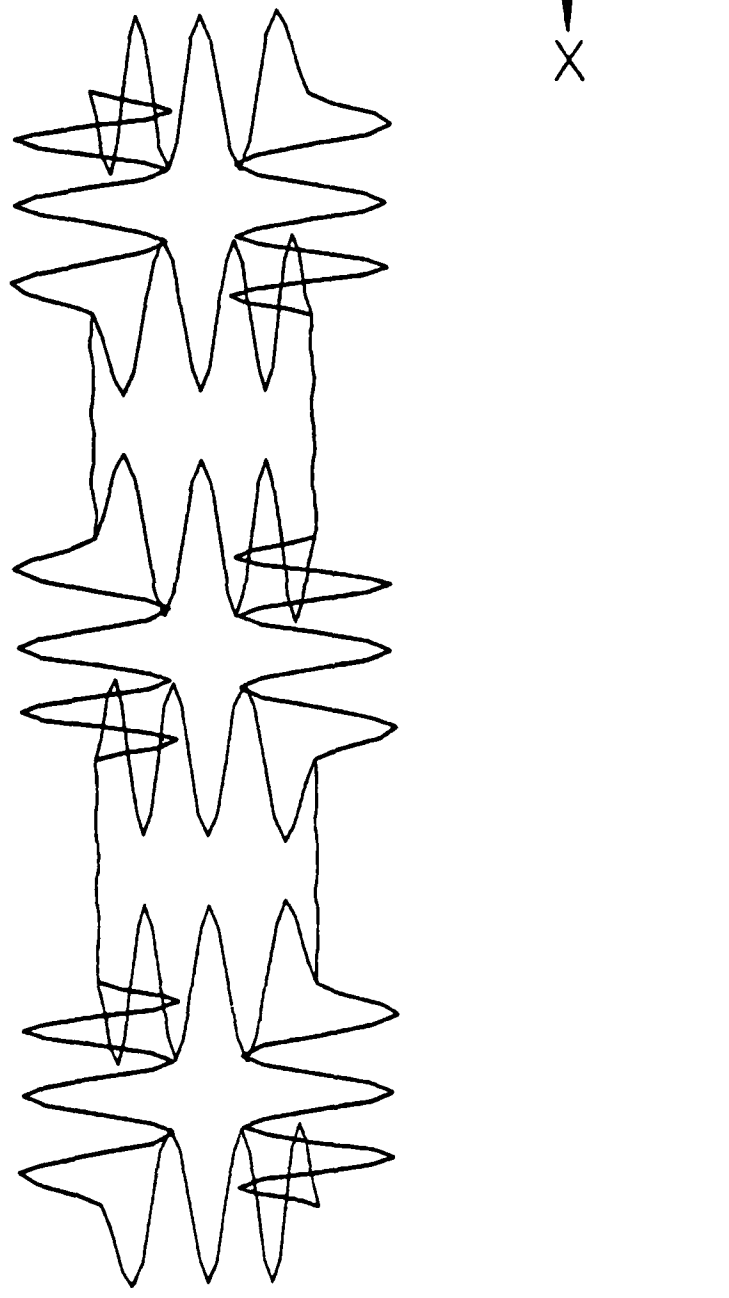

Fig. A18 Mode 111 (frequency = 9708.54 Hz).

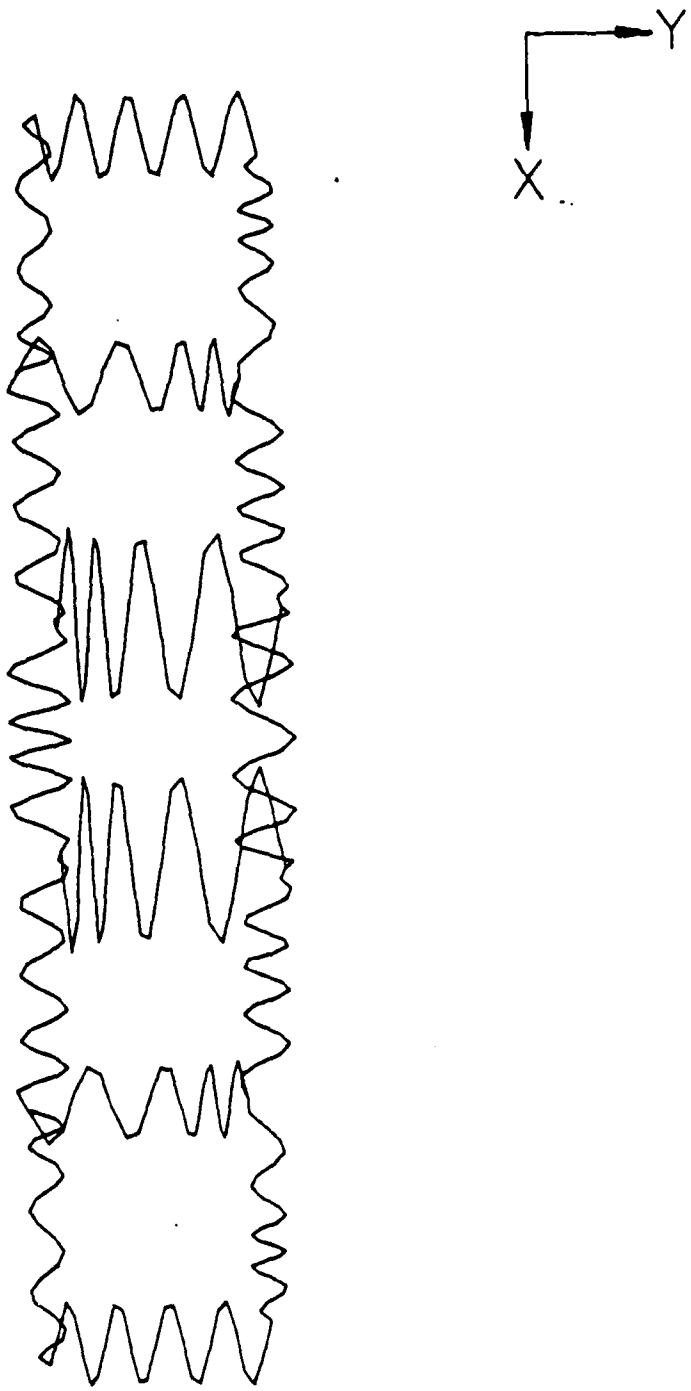

Fig. A19 Mode 137 (frequency = 16231.09 Hz).

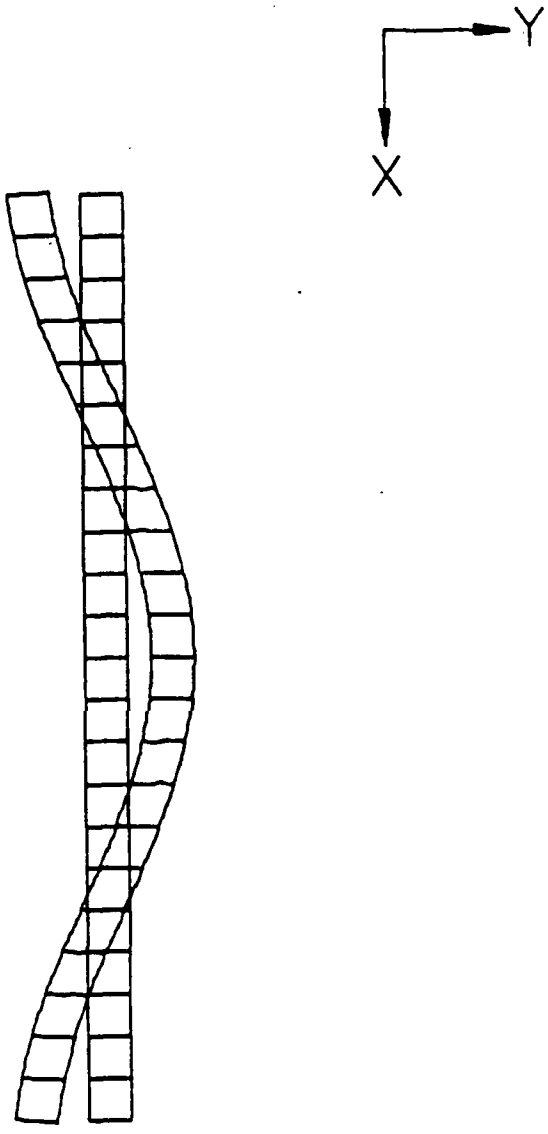

Fig. A20 Mode 1 (frequency = 94.94 Hz).

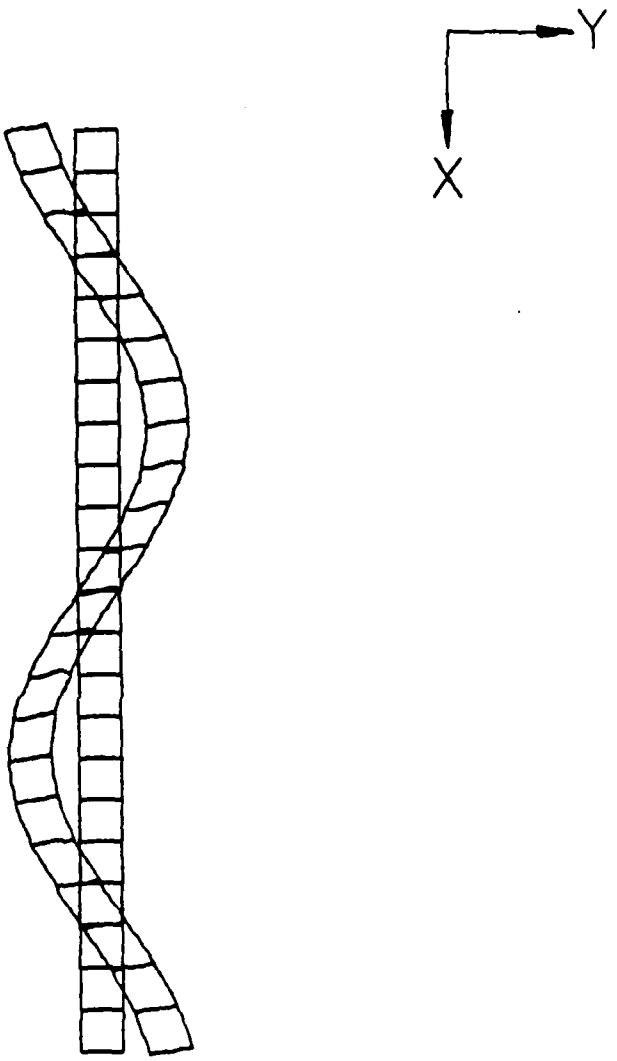

Fig. A21 Mode 2 (frequency = 145.46 Hz).

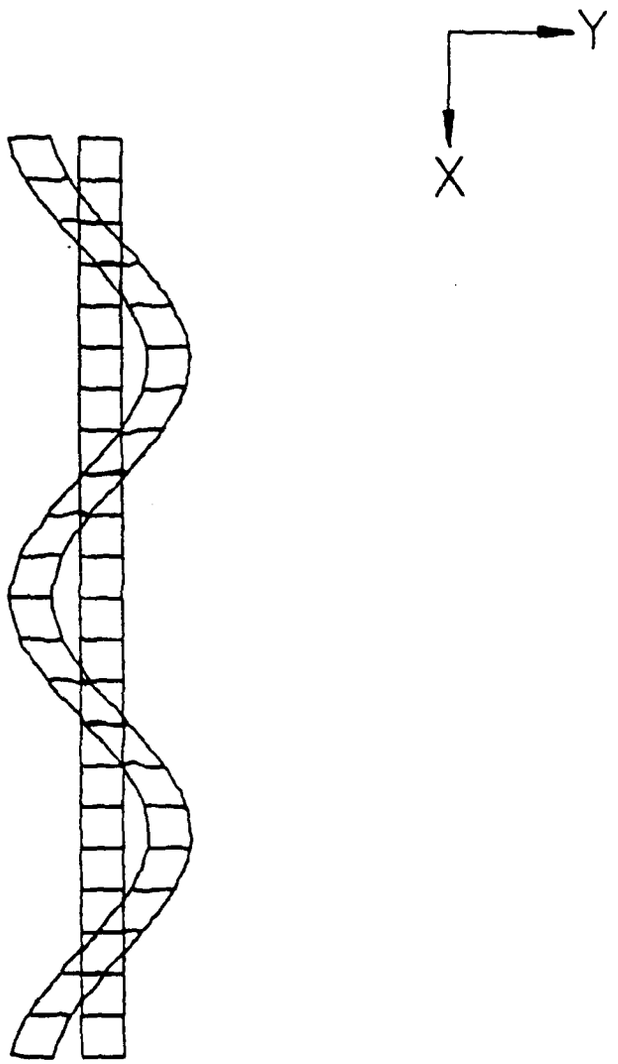

Fig. A22 Mode 3 (frequency = 207.53 Hz).

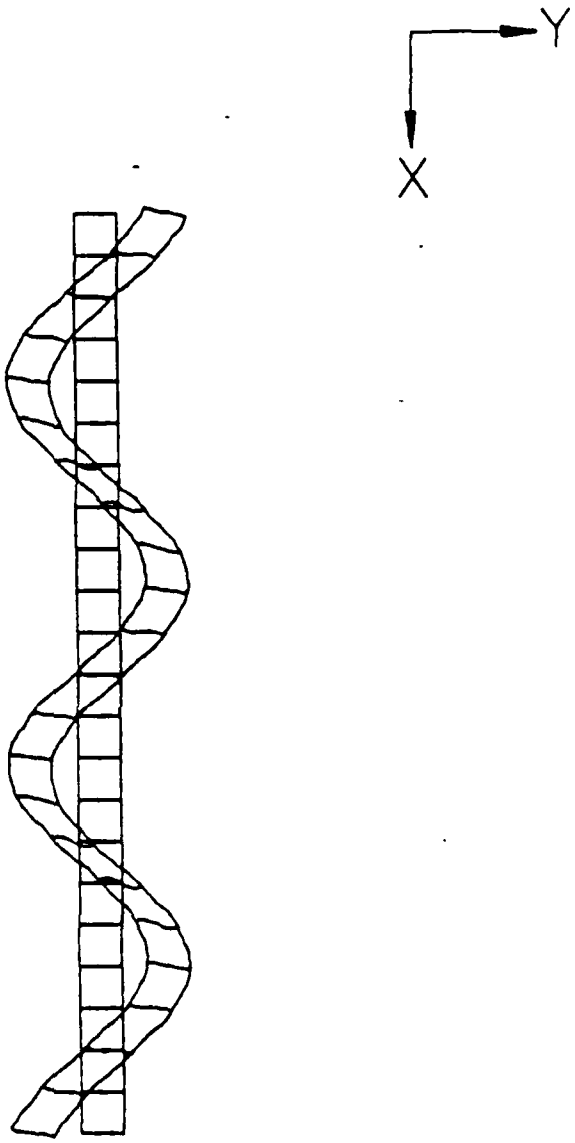

Fig. A23 Mode 4 (frequency = 261.92 Hz).

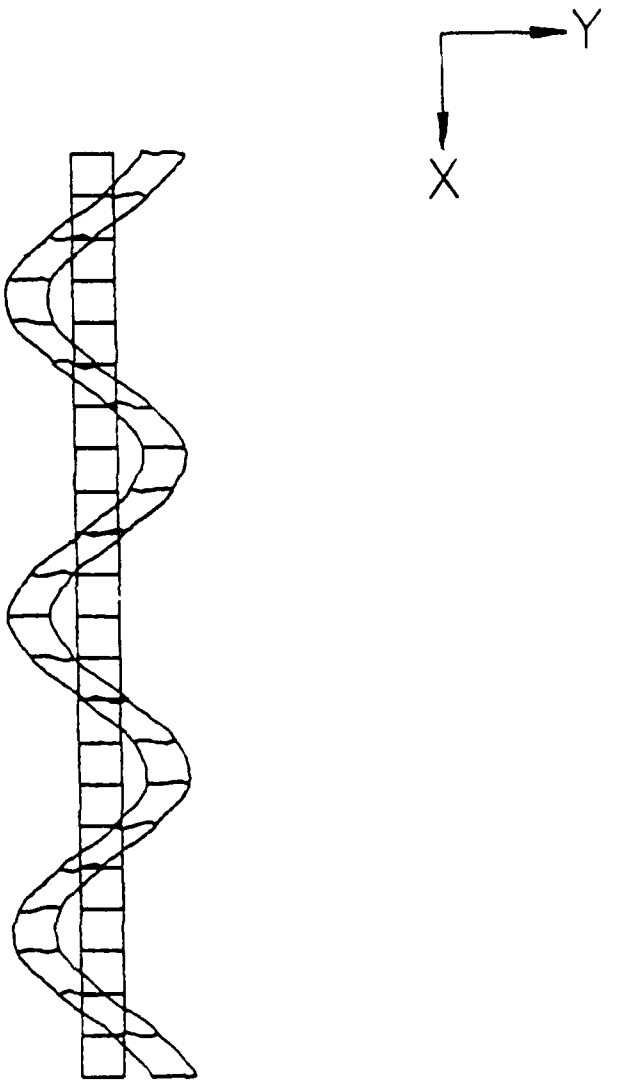

Fig. A24 Mode 5 (frequency = 326.50 Hz).

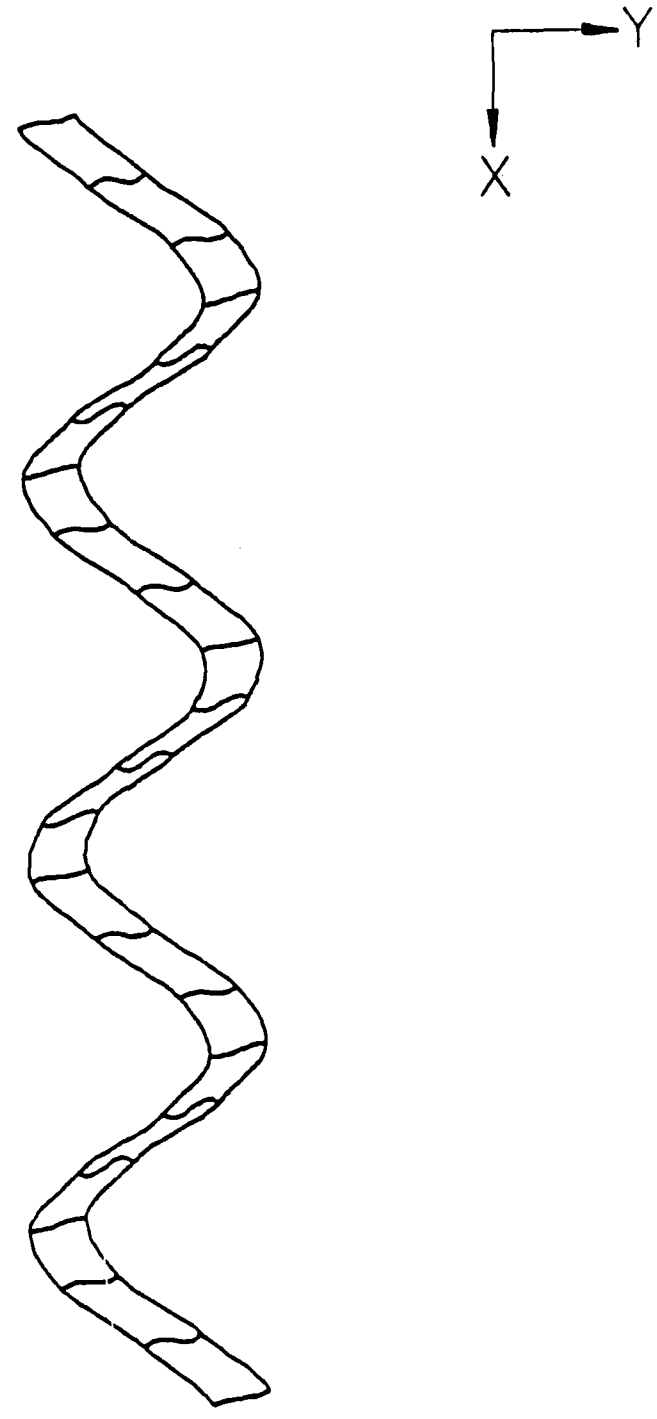

Fig. A25 Mode 6 (frequency = 386.57 Hz).

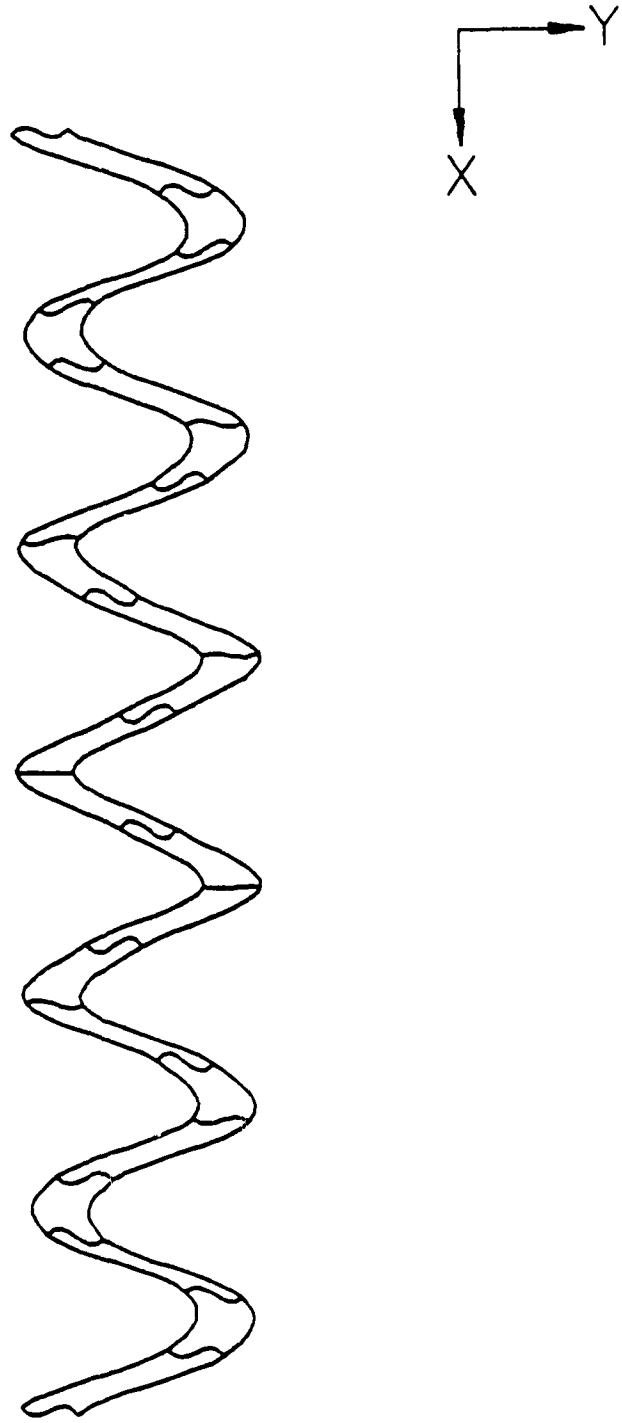

Fig. A26 Mode 7 (frequency = 762.07 Hz).

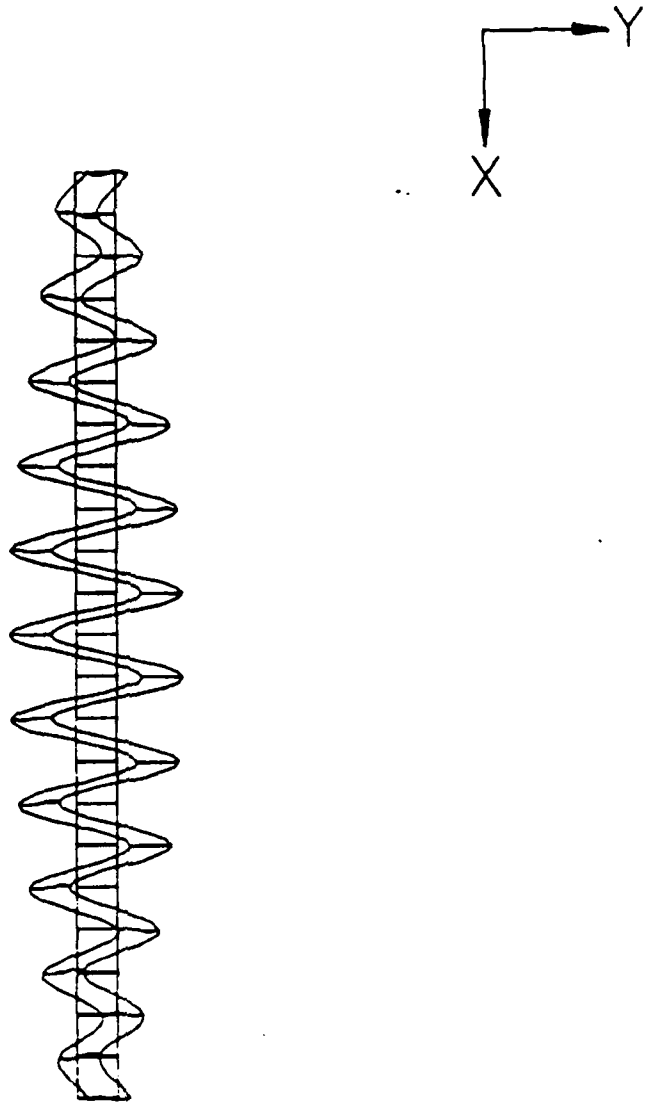

Fig. A27 Mode 23 (frequency = 1544.77 Hz).

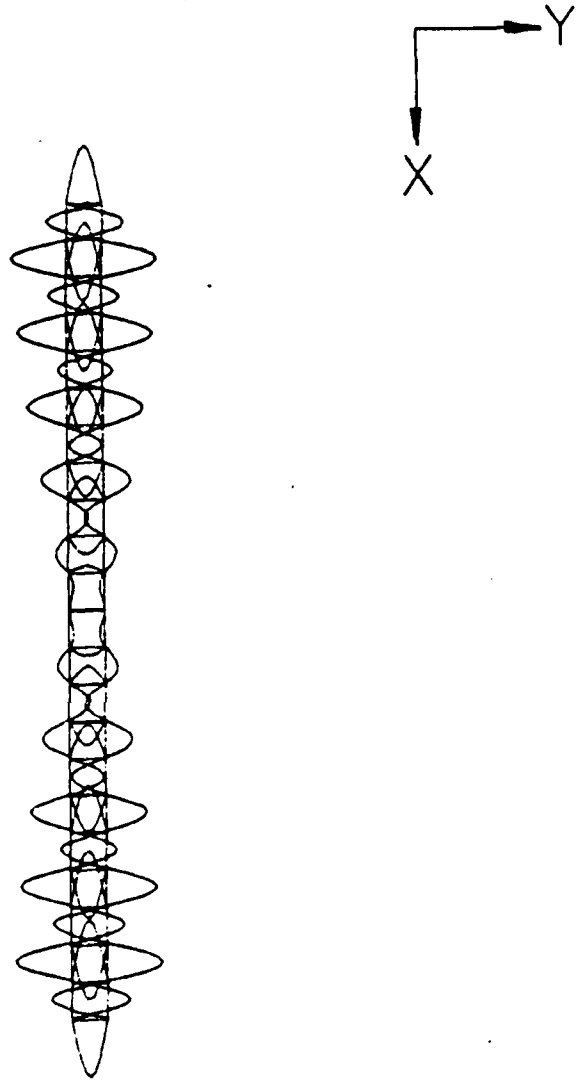

Fig. A28 Mode 26 (frequency = 2215.13 Hz).

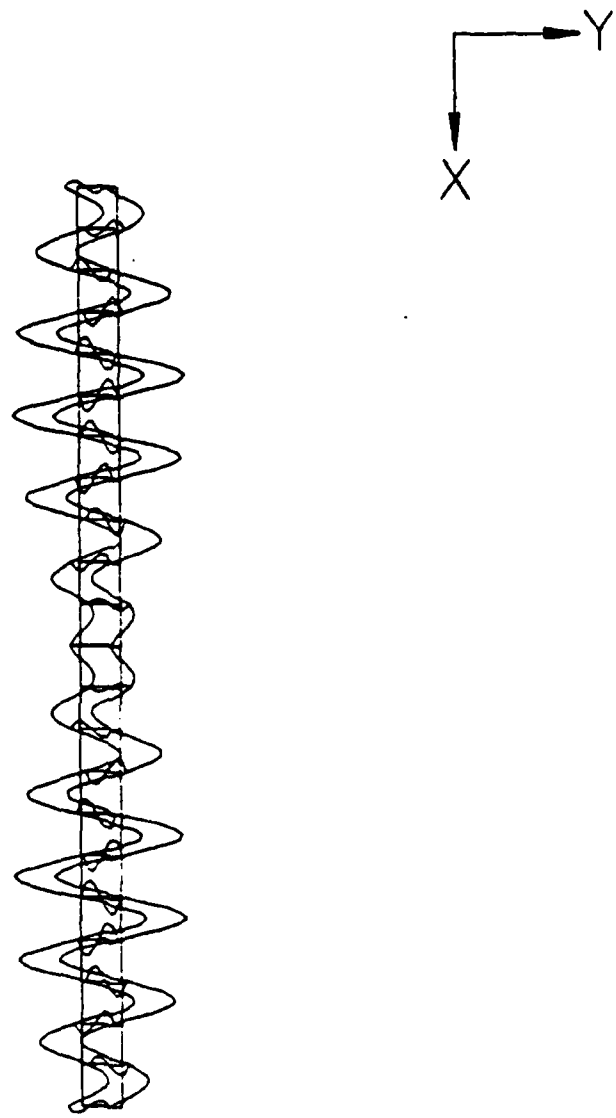

Fig. A29 Mode 40 (frequency = 3106.11 Hz).

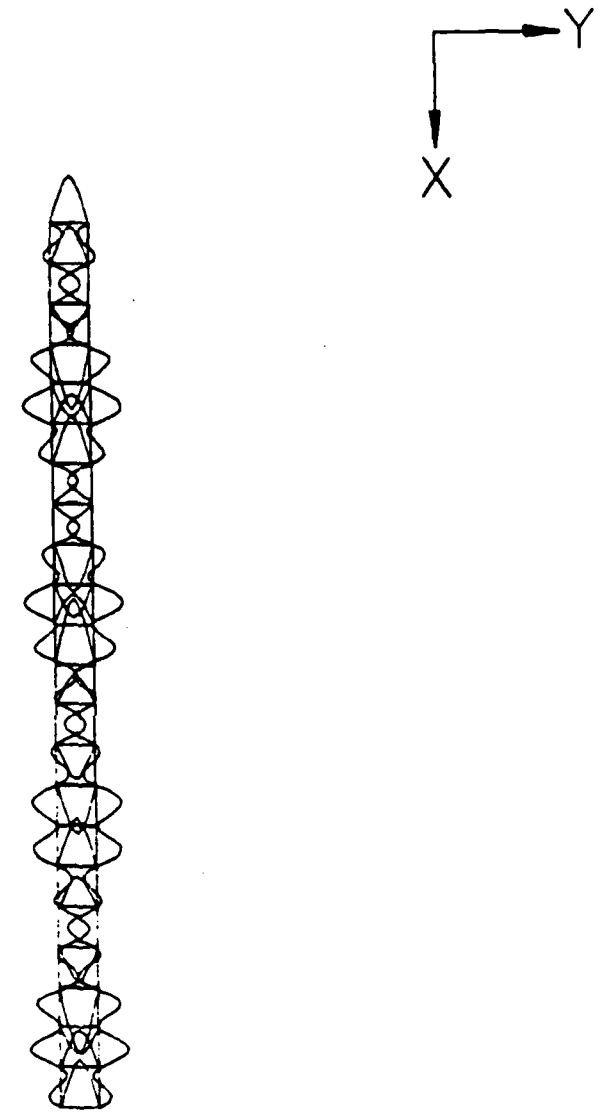

Fig. A30 Mode 44 (frequency = 3304.94 Hz).

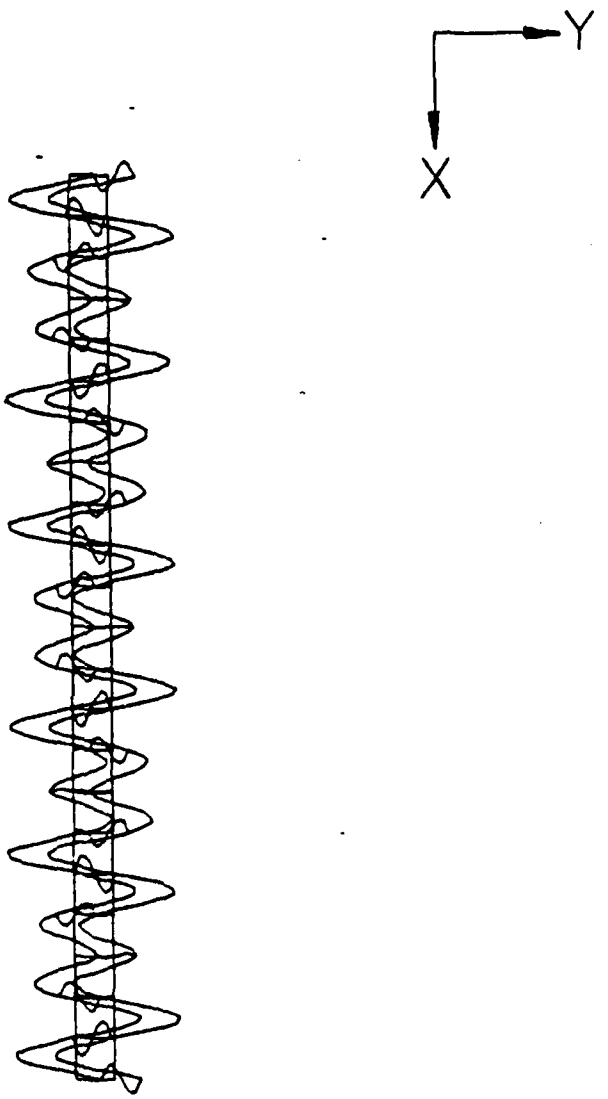

Fig. A31 Mode 52 (frequency = 3594.39 Hz).

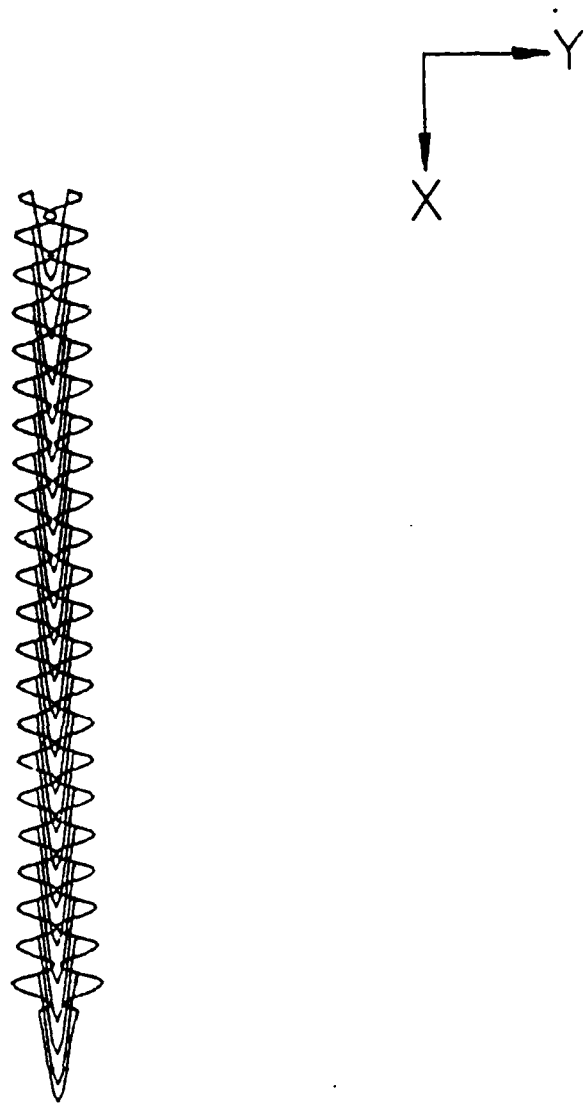

Fig. A32 Mode 57 (frequency = 4437.96 Hz).

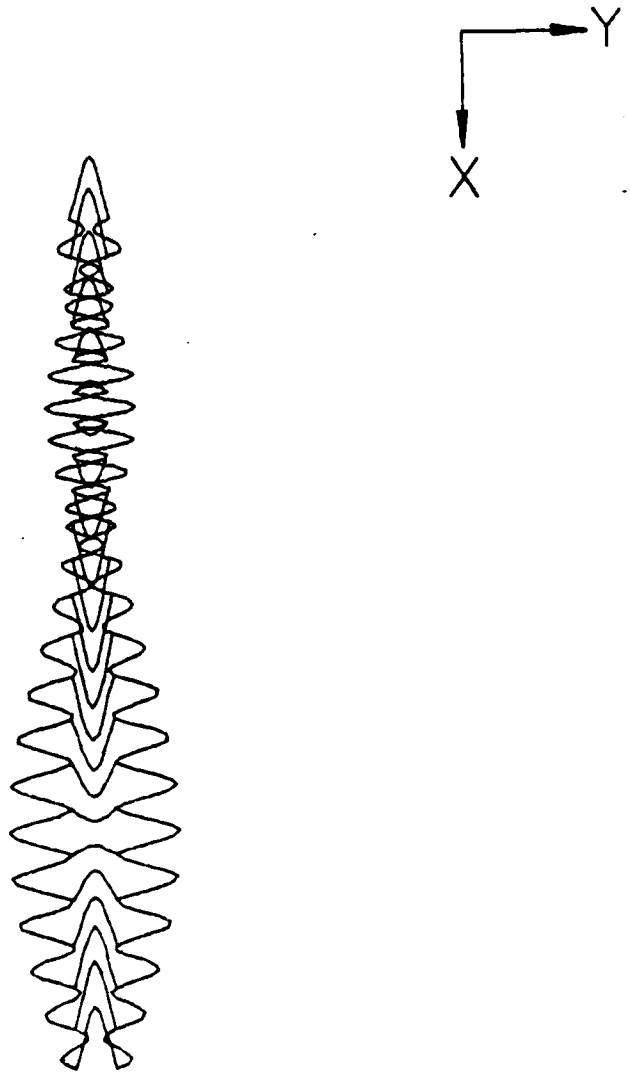

Fig. A33 Mode 60 (frequency = 4659.72 Hz).

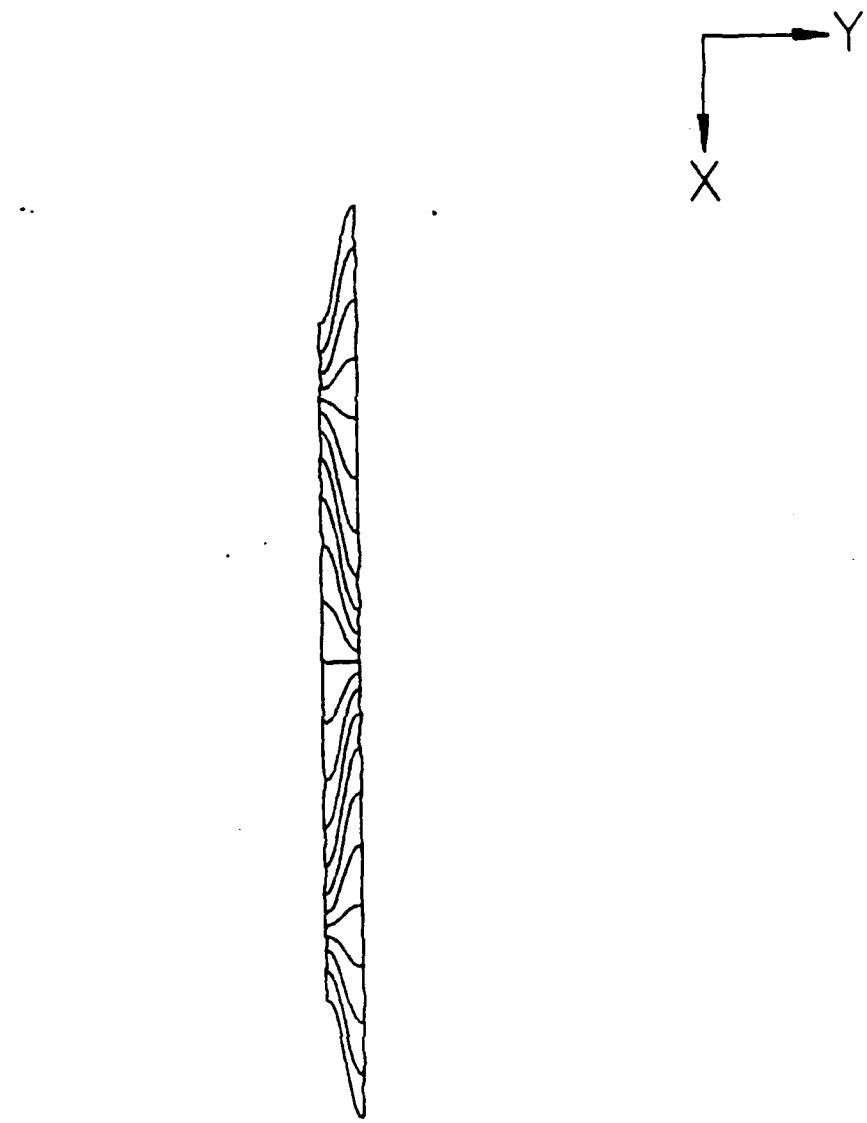

Fig. A34 Mode 69 (frequency = 4904.92 Hz).

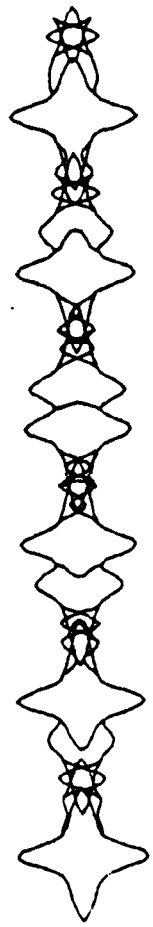

Fig. A35 Mode 74 (frequency = 4948.36 Hz).

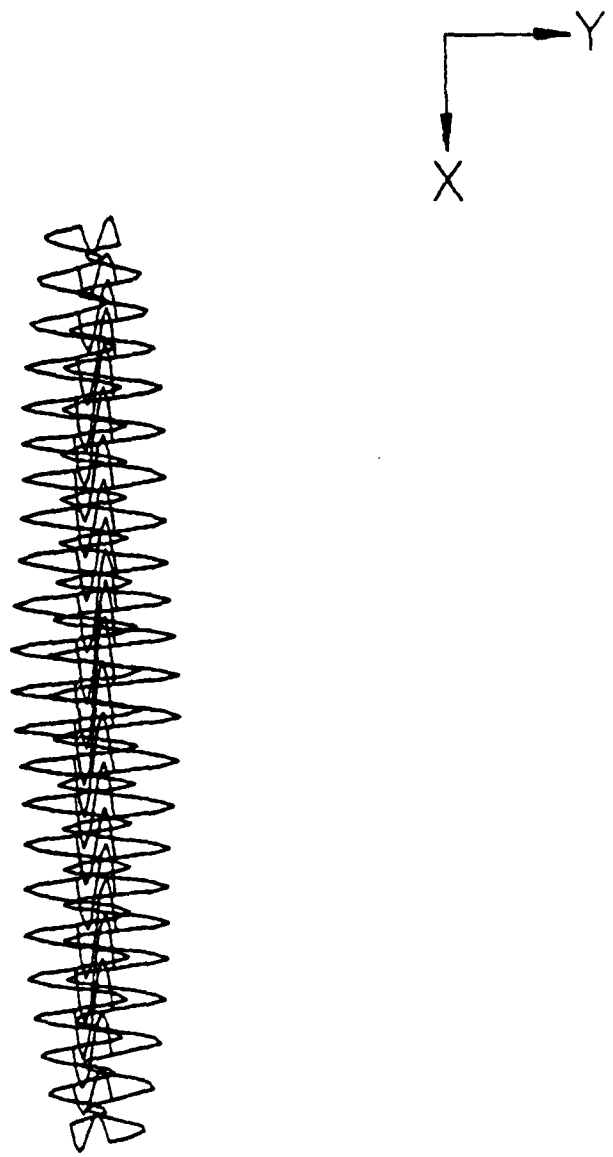

Fig. A36 Mode 109 (frequency = 8954.04 Hz).

APPENDIX B

REPRESENTATIVE FREQUENCY RESPONSE FUNCTIONS OF THE 5-BAY BEAM

Figs. B1 and B2 show the real and imaginary parts of a typical transfer function of the 5-bay beam. This transfer function was obtained by exciting the structure near the response accelerometer using the impact hammer. The load cell attached to the hammer's head recorded the input to the structure in units of N(lb). The response to the impacts was measured by an accelerometer fixed to the structure at the response location. The response was measured in units of g ($1g = 9.8\ N/sec^2$ ($386.4\ in/sec^2$)). Thus the vertical scale of the transfer function is given in units of output/input or g/N (g/lb).

The frequency response function of Figs. B1 and B2 contains frequencies from 0Hz to 500Hz. Frequency response functions whose lowest frequency is 0Hz are called "base band" frequency response functions. The spikes in Figs. B1 and B2 indicate natural frequencies. Figs. B3 and B4 show the real and imaginary parts, respectively, of a frequency response function obtained by impacting the 5-bay structure at location 1 and measuring the response at the fixed response location. The frequency range (bandwidth) of Figs. B3 and B4 extends from 450Hz to 1000Hz. This frequency response was obtained using band selectable Fourier analysis (BSFA). In order to obtain better resolution, all frequency response functions above 500Hz were obtained using BSFA.

Notice, in Figs. B3 and B4, the small group of spikes near 550Hz. From Figs. B3 and B4 it was impossible to determine exactly the number

of spikes in this group. Fig. B5 shows an expanded view of Fig. B3 obtained using BSFA. Fig. B5 shows frequencies ranging from 500Hz to 600Hz. From the frequency response function of Fig. B5, the Fourier analyzer was able to identify four distinct spikes in the region near 550Hz.

BSFA proved to be an invaluable tool for measuring frequency response functions at higher frequencies.

AD-A174 602 DYNAMIC ANALYSES OF TWO-DIMENSIONAL LATTICES(U) MEA 2/2
CAMBRIDGE MA J H WILLIAMS ET AL 01 AUG 84
AFOSR-TR-86-2070 F49620-83-C-0092

UNCLASSIFIED F/G 22/2 NL

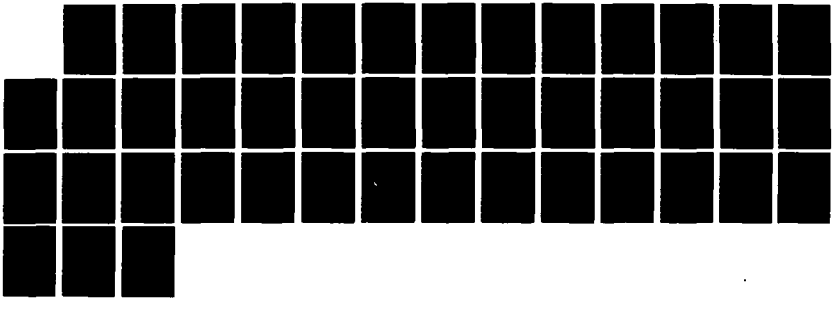

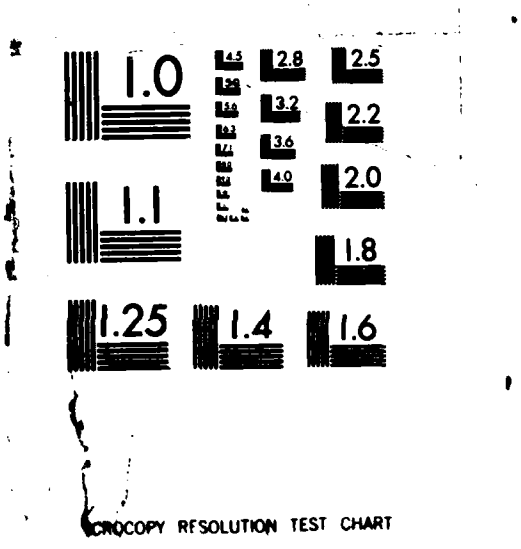
1.0
1.1
1.25
1.4
1.6
2.8
3.2
3.6
4.0
2.5
2.2
2.0
1.8
CROCOPY RESOLUTION TEST CHART

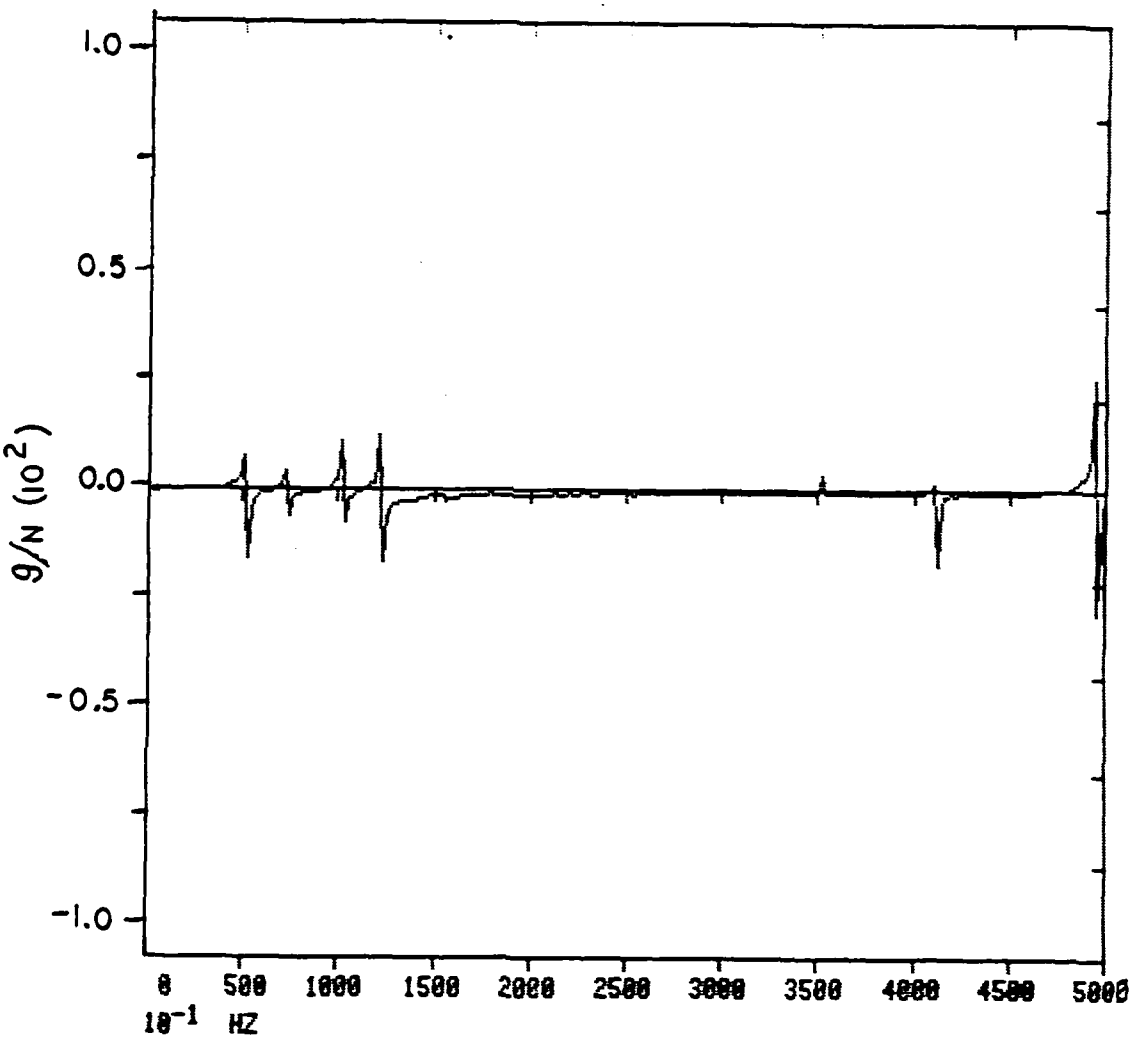

Fig. B1 Real part of the baseband frequency response function obtained by impacting the 5-bay lattice structure near the response accelerometer.

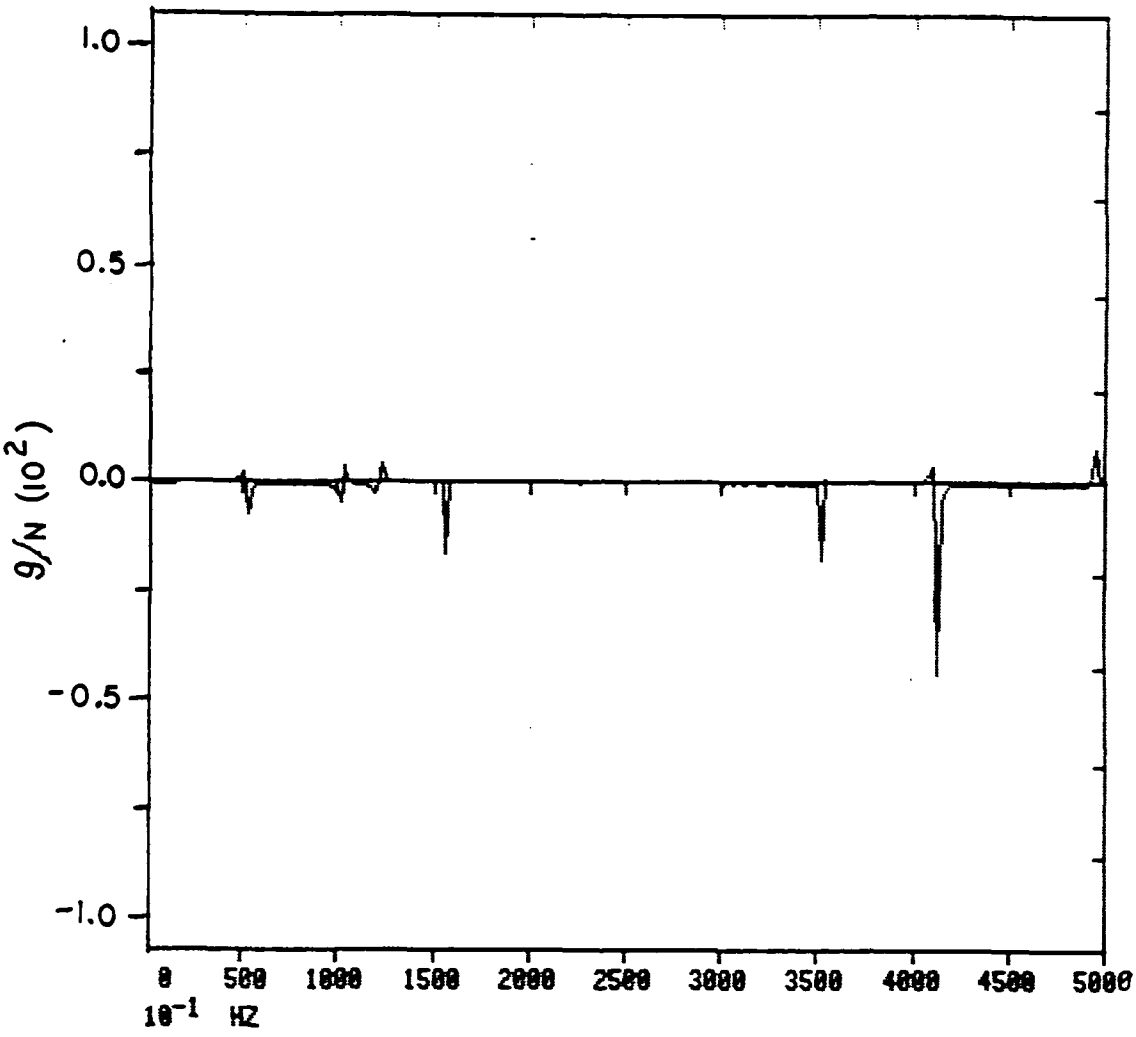

Fig. B2 Imaginary part of the baseband frequency response function obtained by impacting the 5-bay lattice structure near the response accelerometer.

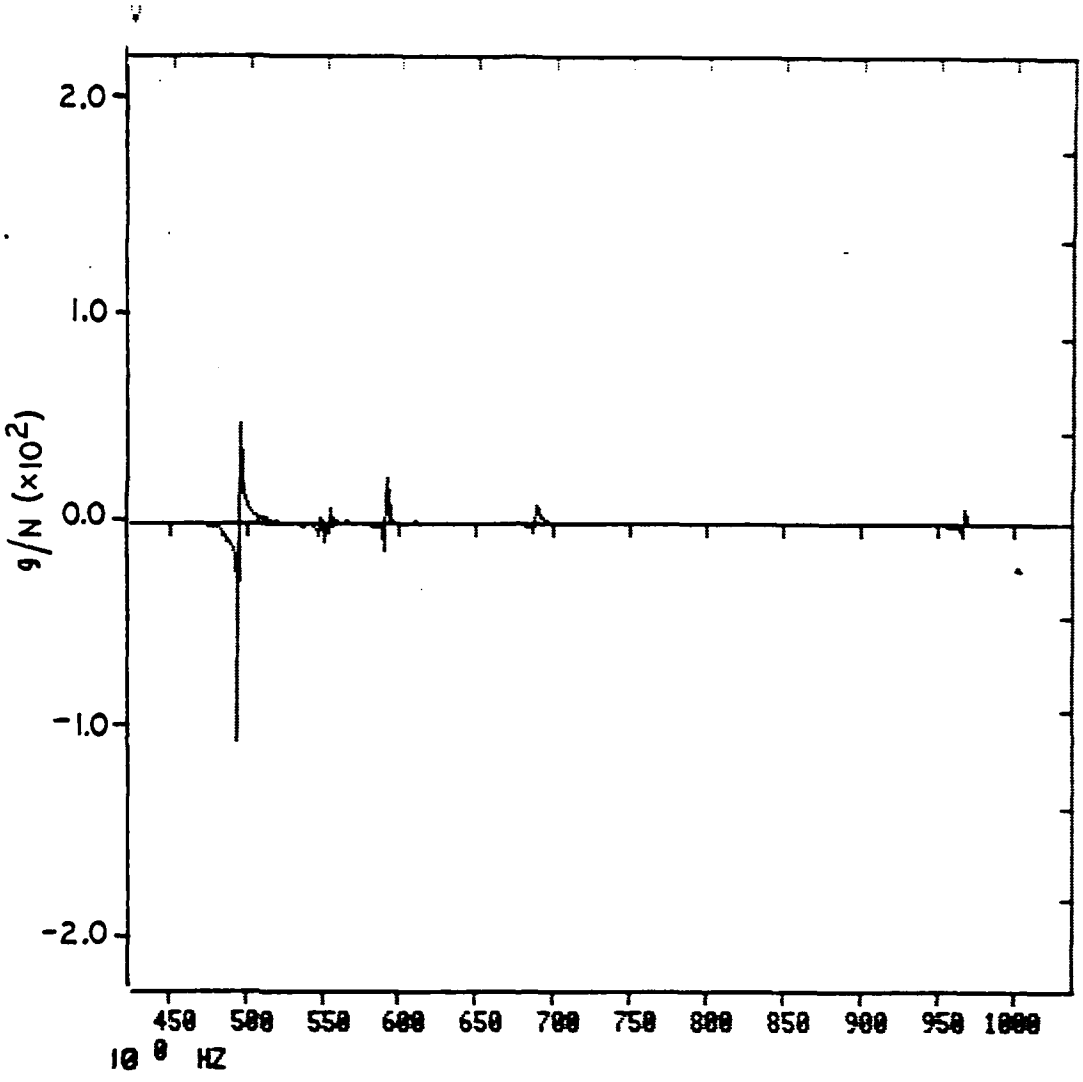

Fig. B3 Real part of a BSFA-measured frequency response function obtained by impacting the 5-bay lattice structure at location 1.

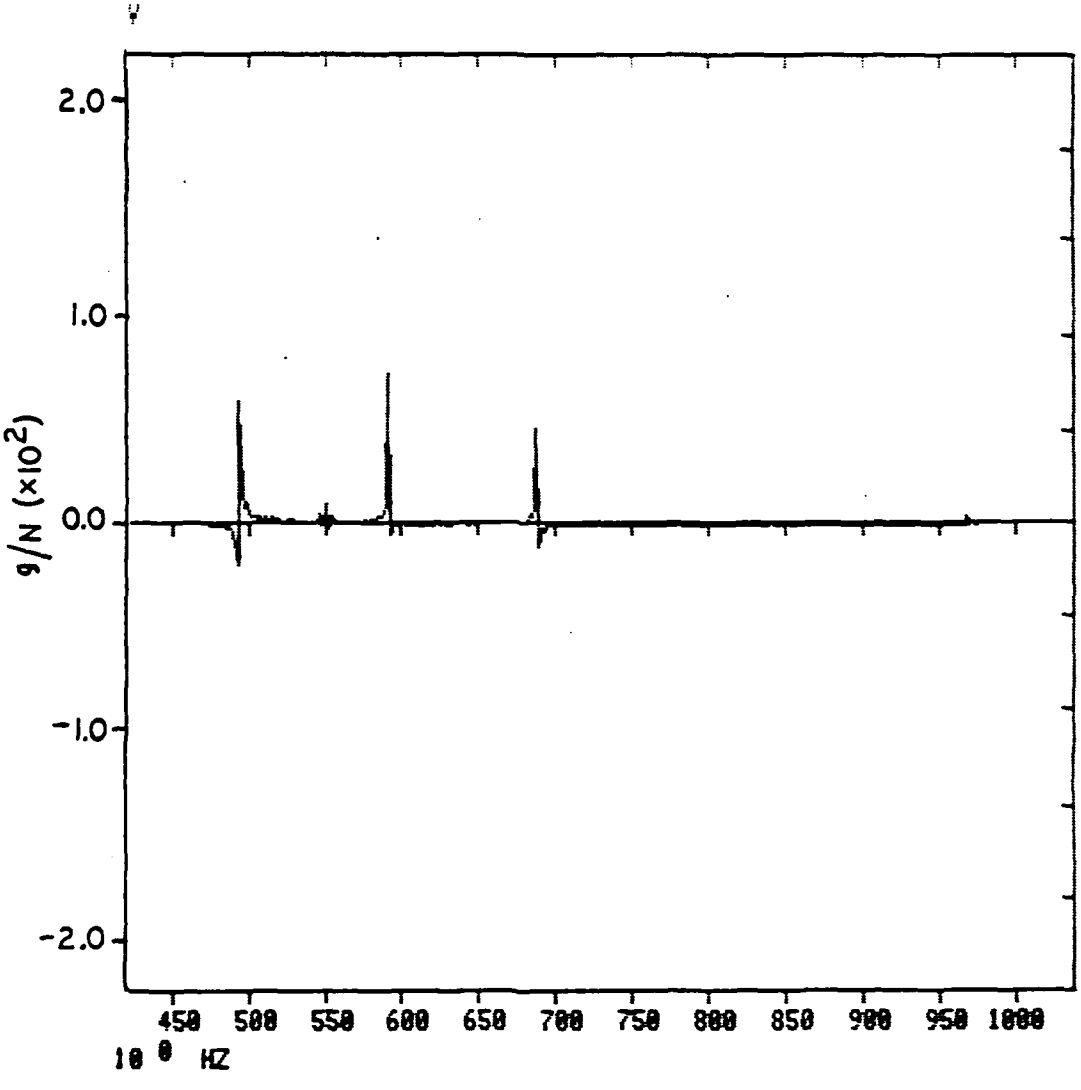

Fig. B4 Imaginary part of a BSFA-measured frequency response function obtained by impacting the 5-bay lattice structure at location 1.

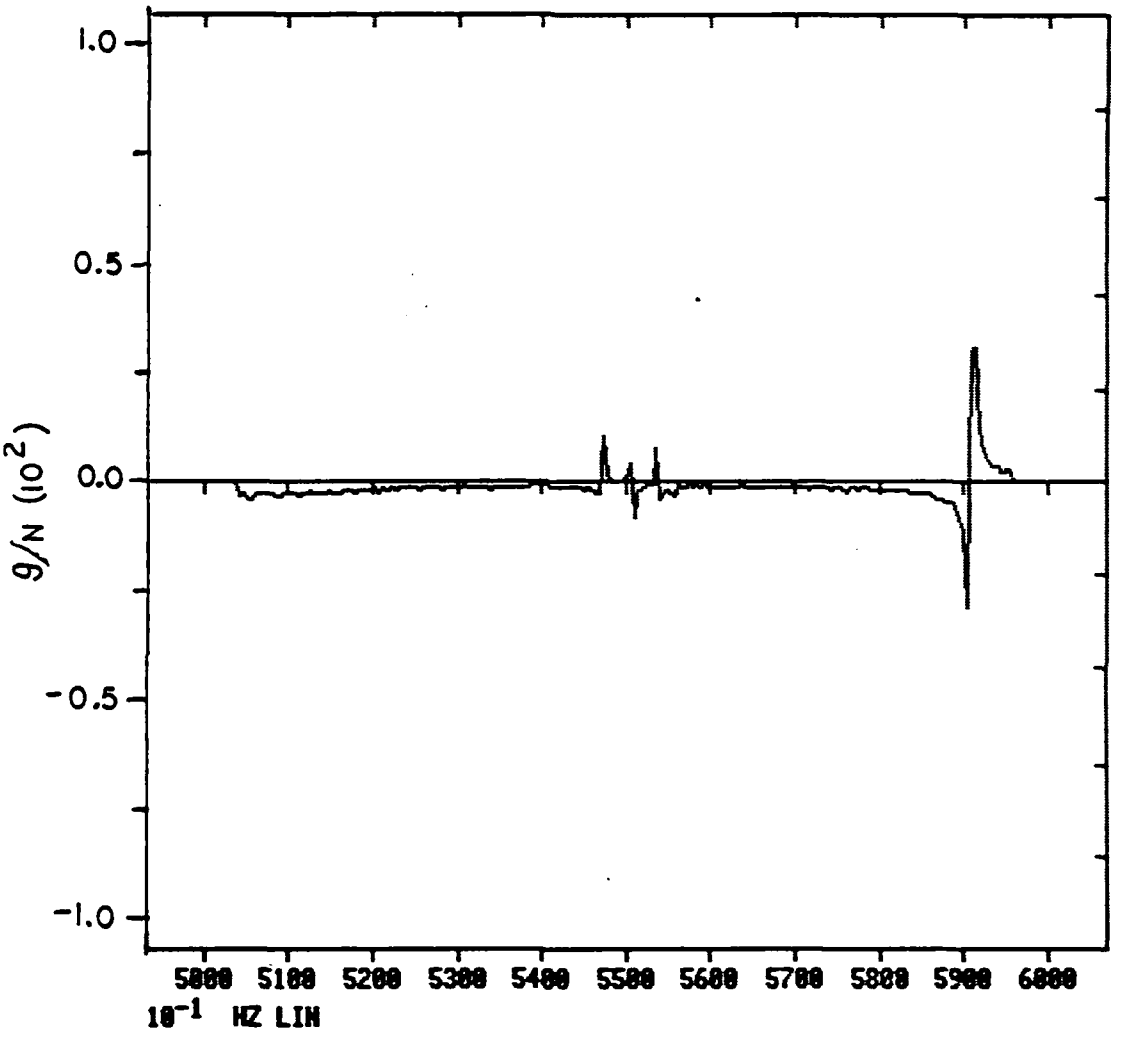

Fig. B5 BSFA-measured expanded view of Fig. B3.

APPENDIX C

SIGNIFICANCE OF MODAL PARAMETERS

Introduction

The following is an explanation of the theoretical and physical significance of the modal parameters (natural frequencies, damping, and complex residues) that constitute the numerical output of an experimental modal analysis.

Analytic Description of a Single Degree of Freedom System

The single degree of freedom (SDOF) system shown in Fig. C1 can be represented mathematically by the equation

$$m\ddot{x}(t) + c\dot{x}(t) + kx(t) = f(t) \qquad \text{(C1)}$$

where

m = mass in kg ($lb\text{-}s^2/in$)

c = damping coefficient in N-s/m (lb-s/in)

k = spring stiffness in N/m (lb/in)

$x(t)$ = time history displacement in m (in)

$\dot{x}(t)$ = time history velocity in m/s (in/sec)

$\ddot{x}(t)$ = time history acceleration in m/sec^2 (in/sec^2)

$f(t)$ = time history force applied to mass in N (lb) .

Eqn. (C1) can be written in the Laplace domain as [12]

$$H(s) = \frac{R}{s-p} + \frac{R^*}{s-p^*} \qquad \text{(C2)}$$

where

$H(s)$ = complex frequency response

R = complex residue

p = complex pole = $-\sigma + i\omega$

i = $\sqrt{-1}$

The asterisks in eqn. (C2) denote complex conjugates. The complex pole (p) can best be visualized in the s plane as in Fig. C2. The system pole determines the natural frequency ω(rad/sec) and the damping ratio σ(rad/sec). The complex residue (R) contains all the magnitude and phase information necessary for describing the system's mode shape [14].

The inverse Laplace transform of the system transfer function, eqn. (C2) gives [4]

$$h(t) = |R|e^{-\sigma t} \sin(\omega t + \alpha) \qquad (C3)$$

where

$h(t)$ = impulse time history response

$|R|$ = magnitude of complex residue

α = phase angle of complex residue

σ = damping ratio

ω = natural frequency .

Thus the four parameters (R , α, σ, ω) which constitute the numerical output of the experimental modal analysis are sufficient to completely

describe the dynamic behavior of the SDOF system, both in the Laplace domain and in the time domain. See [14] for an analytic derivation of the complex residues.

Mass-Spring System Investigation

The following investigation was carried out to verify that the parameters generated by the Fourier analyzer could be used in eqn. (C3) to predict the impulse response of a SDOF system.

Experimental Setup --

Fig. C3 shows the experimental setup used in this investigation. The hammer was equipped with a PCB SN1377 force sensor attached to its head. The force sensor measured the force applied to the mass. An Endevco 2222B piezoelectric accelerometer was fixed to the mass and recorded the response acceleration of the mass. Damping in the system was provided by the damping in the spring. Thus, the mass-spring system of Fig. C3 was idealized to a mass-spring-damper SDOF system such as that shown schematically in Fig. C1.

Calculation of Impulse Response of Mass-Spring System --

The spring stiffness, k, was measured using a tensile test machine. The average spring stiffness (between tension and compression) was about 4027.89N/m(23 lb/in). The mass weighed 0.4463 kg(0.002548 lb-s^2/in). The weight of the spring, 0.0181 kg (0.0001 lb-s^2/in), was neglected in all calculations. The damping of the spring was calculated using [15]

$$C = 2m\sigma \qquad (C4)$$

$$= 0.3838 \text{ N-s/m}(.0022 \text{ lb-s/in})$$

where the value of σ (.43 rad/s) was taken from the output of modal analysis (to be described later).

The response of the mass was measured as an acceleration, thus eqn. (C3) will give the acceleration impulse response h(t). The analytic expression for the impulse response of a single degree of freedom system is given as [15]

$$h(t) = \frac{1}{m\omega_d} e^{-\zeta\omega nt} \sin \omega_d t \qquad (C5)$$

where

m = mass = 0.4463 kg

ω_n = natural frequency = $\sqrt{k/m}$

= 95.05 rad/s

ζ = damping ratio = $c/2m\omega n$

= .00011

ω_d = damped natural frequency

= $\omega_n\sqrt{1 - \zeta^2} \approx \omega_n$.

The impulse response acceleration was obtained by taking the second time derivative of eqn. (C5) which gave

$$h(t) = e^{-\zeta\omega_n t}\left[\left(\frac{\zeta^2\omega_n}{m} - \frac{\omega_d}{m}\right)\sin(\omega_d t) - \frac{2\zeta\omega_n}{m}\cos(\omega_d t)\right]. \qquad (C6)$$

Note that the units of h(t) are m/N-s^3 (in/lb-s^3). Substituting the appropriate values into eqn. (C6) gives

$$h(t) = e^{-.01t}\left(-21.72 \sin 95(t) - .0091 \cos 95(t)\right) \qquad (C7)$$

where a factor of 1/9.8 m/sec^2 has been introduced into eqn. (C7) to obtain acceleration in units of g's, where 1g = 9.8 m/sec^2 (386.4 in/sec^2). Eqn. (C7) actually gives the impulse response acceleration due to a unit impulse. The units of impulse are N-sec (lb-sec). Thus, the units of eqn. (C7) are g/N-sec (g/lb-sec). Fig. C4 shows a plot of eqn. (C7) from t = 0.0 to t = 1.0 seconds.

Calculation of Impulse Response Using Modal Analysis Parameters --

An experimental modal analysis was then performed on the mass spring system. The real part of the resultant frequency response function of this system is shown in Fig. C5.

As shown in Fig. C3, the mass was free to move in any direction, not just vertically. The largest spike ($\sim$16 Hz) of Fig. C5 corresponds to the natural mode of vibration of the mass moving vertically - ideally the only mode of the single degree of freedom system. The mass, when hit with the hammer, would not only move vertically, but would also sway laterally. The small spike ($\sim$20 Hz) corresponds to the non-vertical motion of the mass.

The Fourier analyzer then fit an equation of the form of eqn. (C2) to the measured data. (See [3, 7] for an explanation of the curve fitting techniques used by the analyzer.) The modal parameters

(complex poles and residues) that were output from the analyzer were the parameters that corresponded to the curve fit frequency response function data. The data in Table C1 corresponded to the first spike of the frequency response function of Fig. C5 (vertical motion of the mass). (As will be shown later, the Fourier analyzer's curve fit data also included the effects of lateral mass motion, but these contributions are neglected here.) The value of σ in Table C1 was used in obtaining a value for the damping in the spring (eqn. (C4)).

Fig. C6 shows a plot of eqn. (C3) evaluated using the parameters of Table C1. Note that because the response was measured as an acceleration, eqn. (C3) actually gives the impulse response acceleration per unit impulse not the impulse response displacement per unit impulse.

A comparison of Figs. C4 and C6 shows the similarity between the analytical prediction of the impulse response acceleration and the modal analysis parameter prediction of the impulse response. The natural frequency ω_n, predicted analytically was about 95 rad/sec while that measured using the Fourier analyzer and modal analysis was 100.5 rad/sec. The maximum acceleration per unit impulse predicted analytically was about -22g/N-sec (-95g/lb-sec) and that predicted using eqn. (C3) and the measured modal parameters was approximately -20g/N-sec (-9g/lb-sec). The phase angles between Figs. C4 and C6 appear to be quite close. Note, the response accelerometer was oriented so that upward acceleration of the mass was a positive acceleration. The above negative values indicate that the peak

response acceleration per unit impulse of the mass-spring system corresponds to a downward acceleration of the mass.

Conclusions --

Thus the use of the experimentally determined modal parameters along with eqn. (C3) seemed to be an effective way of predicting the impulse response acceleration of a SDOF system. This technique is particularly well suited for systems who's spring constant, damping factor and mass may be difficult to measure.

Analysis of the Mass-Spring System as a Two Degree of Freedom System

Introduction --

It is evident from the frequency response function of Fig. C5 that the mass-spring system used in this investigation was not a true single degree of freedom system. The second smaller spike of Fig. C5 indicates that the impulse response acceleration should have been similar to that of a two degree of freedom (2DOF) system. The Fourier analyzer was capable of identifying many modes of vibration of a structure and could fit a multiple degree of freedom system equation of the form [4]

$$H(s) = \sum_{k=1}^{n} \frac{R_k}{s-p_k} - \frac{R_k^*}{s-p_k^*} \qquad (C8)$$

to a measured frequency response function with n natural frequencies (spikes). The p_k and R_k of eqn. (C8) were the complex poles and

residues, respectively, that corresponded to the $k^{\underline{th}}$ natural mode of vibration.

Modal Analysis Results --

The Fourier analyzer identified two modes of vibration in the frequency response function of Fig. C5 and fit a 2DOF system equation of the form of eqn. (C8) (with n = 2) to this frequency response function. The 2DOF modal analysis resulted in the modal parameters shown in Table C2.

Modal Parameter Prediction of 2DOF System Impulse Response --

The two sets of modal parameters in Table C2 were substituted into the following equation [4]

$$h(t) = \sum_{k=1}^{2} R_k \, e^{-\sigma_k t} \sin(\omega_k t + \alpha_k) \qquad (C9)$$

which is the inverse Laplace transform if eqn. (C8). Eqn. (C9) includes the contributions of the two modes of vibration of the impulse response acceleration. Fig. C7 shows the results of substituting the parameters of Table C2 into eqn. (C9).

Experimental Verificaton of 2DOF System Impulse Response --

An actual time history impulse response acceleration was measured by hitting the mass with the impact hammer and then recording the response accelerometer signal. This recorded response signal is shown in Fig. C8.

Comparison of Results --

A comparison of Figs. C7 and C8 reveals that the shapes of the two curves are nearly identical, the vertical scale being the only major difference.

The time history acceleration impulse response curve predicted using the modal parameters had the units of the residues, or g/N-sec, while the response accelerometer signal (Fig. C8) had units of g's (where 10 mV = 1g). The vertical scales of Figs. C7 and C8 differ by the units N-sec, which were the units corresponding to the area under the impulse excitation curve. Thus, multiplying the modal parameter generated impulse response acceleration curve (Fig. C7) by the area under an arbitrary impulse curve should give the actual impulse response acceleration due to the particular impulse.

Validity of Using Modal Parameters to Predict Peak Impulse Response Acceleration

The validity of using Fig. C7 to predict the impulse response acceleration of the mass due to any impact is examined in the following investigation.

Experimental Procedure and Results --

The previously described mass spring system was excited using the impact hammer equipped with tips made of different materials. A rubber-tipped hammer caused the pulse shown in Fig. C9. The area under this pulse had units of N-sec and determined the amount of momentum

imparted to the mass, and hence determined the magnitude of the impulse response acceleration. Fig. C10 shows the peak acceleration response of the mass due to the impulse of Fig. C9. Figs. C11 and C12 show the impulse and acceleration response of the mass, respectively, obtained using a plastic-tipped hammer. Figs. C13 and C14 show the corresponding results obtained using an aluminum-tipped hammer. The peak accelerations of Figs. C10, C12 and C14 are given in Table C3.

Modal Analysis-Predicted Results —

Fig. C7 shows that the peak impulse response acceleration per unit impulse of the mass is about -24 g/N-s (111 g/lb-s, where 1 lb = 4.4482N). So the maximum acceleration of the mass due to an arbitrary impulse should have been equal to

$$\ddot{x}_{max} = -24 \text{ g/N-s} \times A \text{ N-s} \qquad \text{(C10)}$$

where A was the area under the arbitrary impulse curve.

The area under the impulse in Fig. C9 was approximately 7.71×10^{-2} N-s, so the peak acceleration of the mass, according to eqn. (C10) should have been

$$-24 \text{ g/N-s} \times 7.7 \times 10^{-4} \text{ N-s} = -1.85 \text{ g}$$

The predicted peak response accelerations due to the other two impulses (plastic-tipped and aluminum-tipped hammers) were calculated in a similar fashion and are summarized in Table C3.

Comparison of Results --

An examination of the results of Table C3 indicates that the modal parameters can indeed be used to predict the response acceleration of the mass due to an arbitrary impulse.

Conclusions

As shown above, the usefulness of a modal analysis extends beyond the frequency domain, where natural frequencies and mode shapes are obtained, and into the time domain where the modal parameters can be used to predict impulse response behavior. In addition, the impulse response acceleration curves predicted using the modal parameters could easily be integrated to give impulse response velocity or displacement time histories.

TABLE C1 Modal Parameters Associated With the First Spike of Figure C5

ω	σ	R	α
100.5 rad/sec	0.43 rad/sec	20.4622 g/N-sec	2.6 rad

TABLE C2 Modal Parameters Associated With the 2DOF Frequency Response Function of Figure C5

Mode	ω (rad/sec)	σ (rad/sec)	$\lvert R \rvert$ (g/N-sec)	α (rad)
1	100.5	0.43	20.46	2.6
2	125.2	0.71	5.5348	3.03

TABLE C3 Measured and Predicted Peak Impulse Response Accelerations Caused By Hammer Impacts Using Different Tip Materials

Tip Material	Measured Peak Acceleration Response (g)	Predicted Peak Acceleration Response (g)
Rubber	-2.0	-1.9
Plastic	-1.2	-1.0
Aluminum	-1.3	-1.2

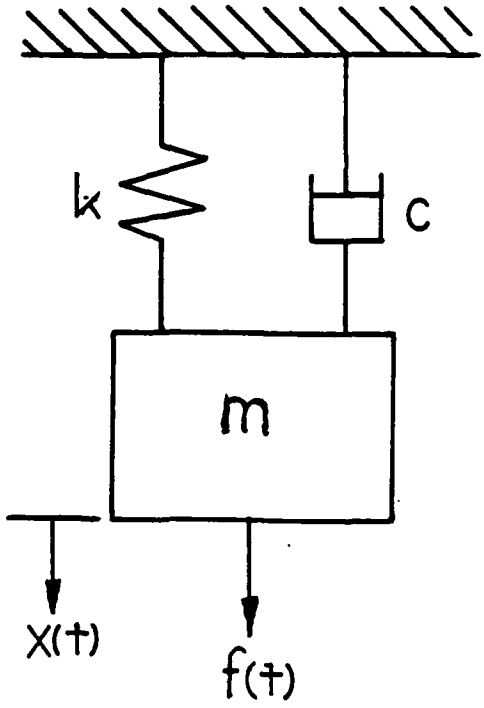

Fig. C1 Schematic representation of a single degree of freedom system.

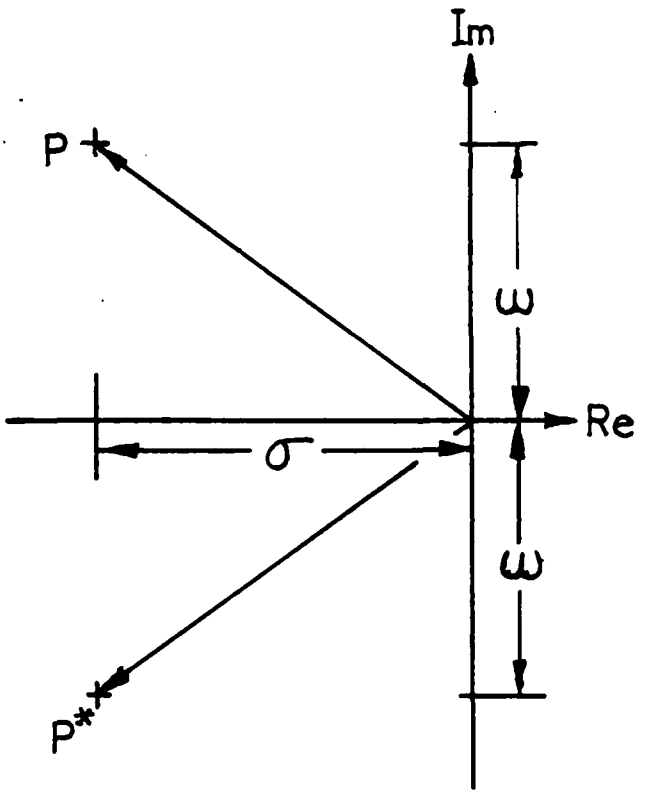

Fig. C2 S-plane representation of a complex pole.

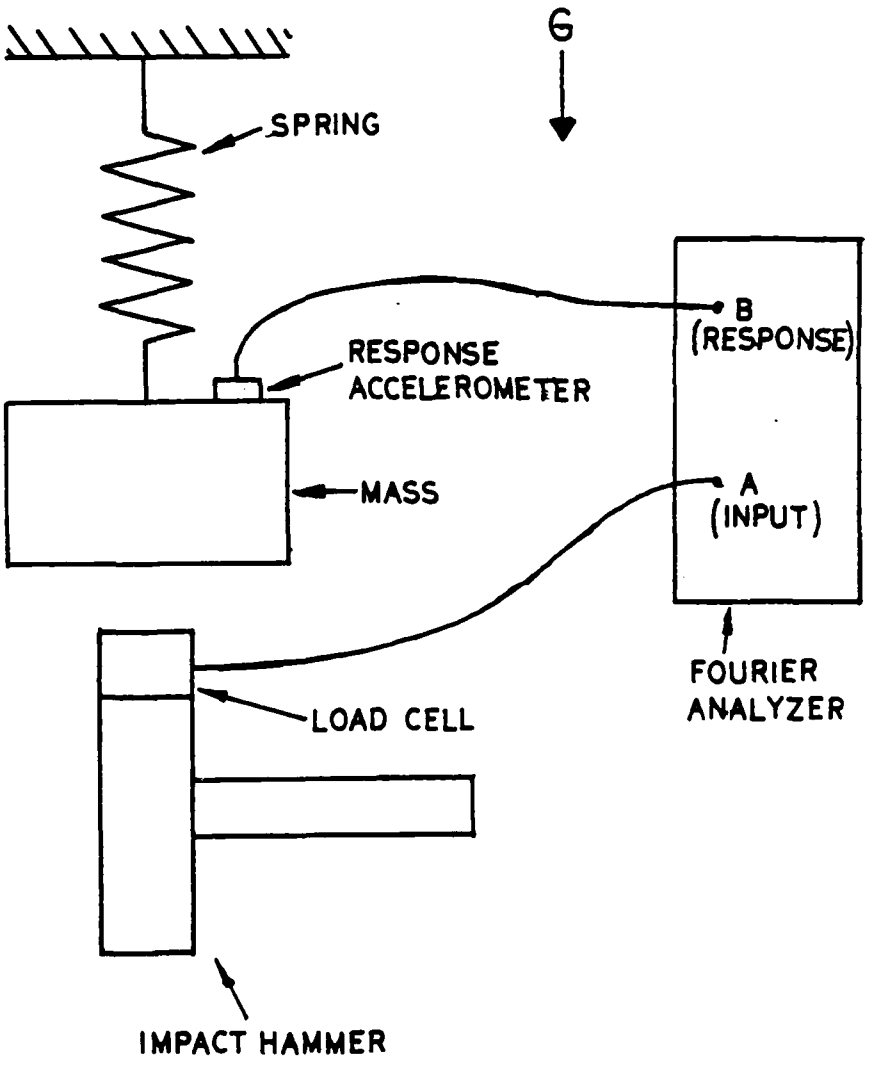

Fig. C3 Mass-spring system setup.

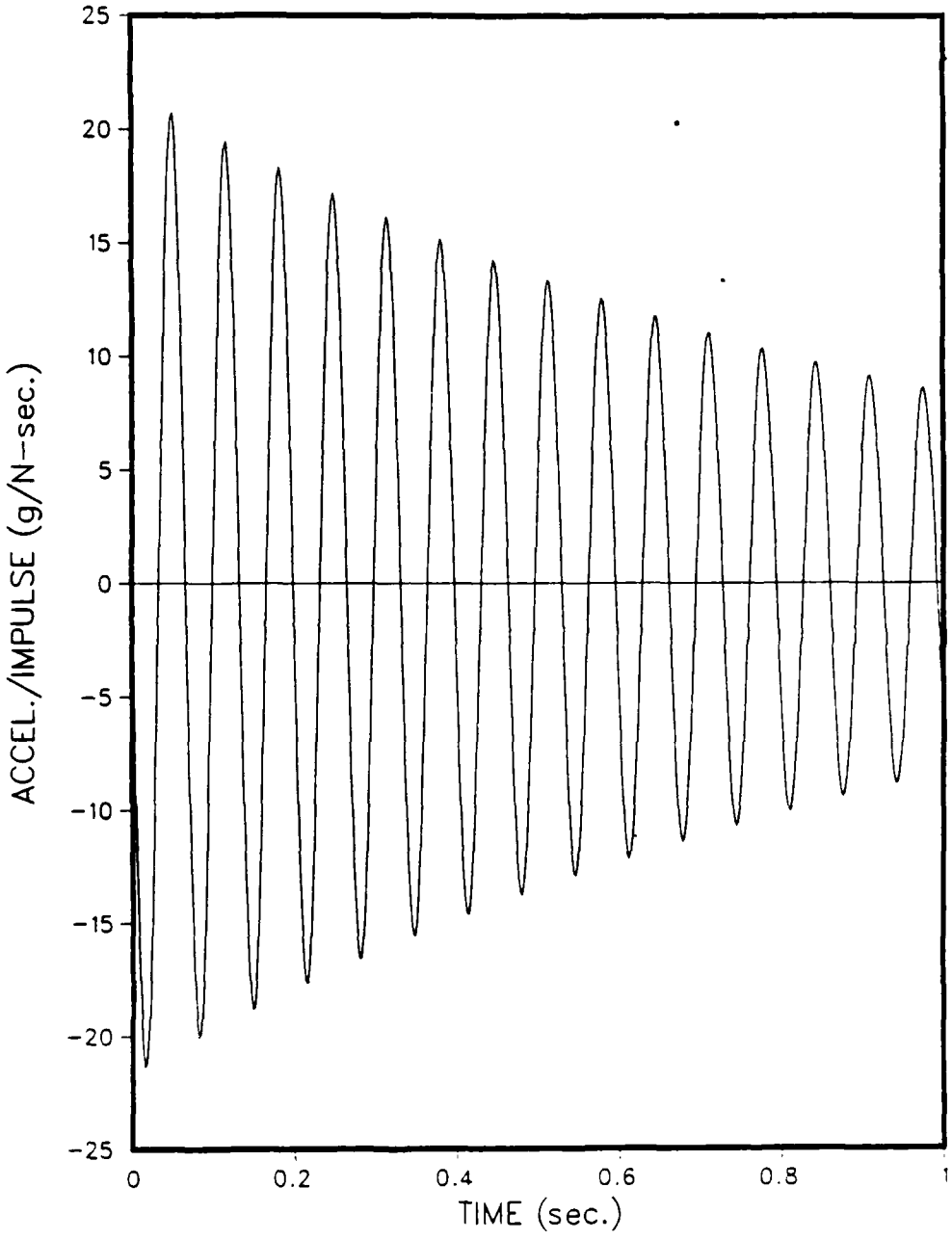

Fig. C4 Plot of eqn. (C7).

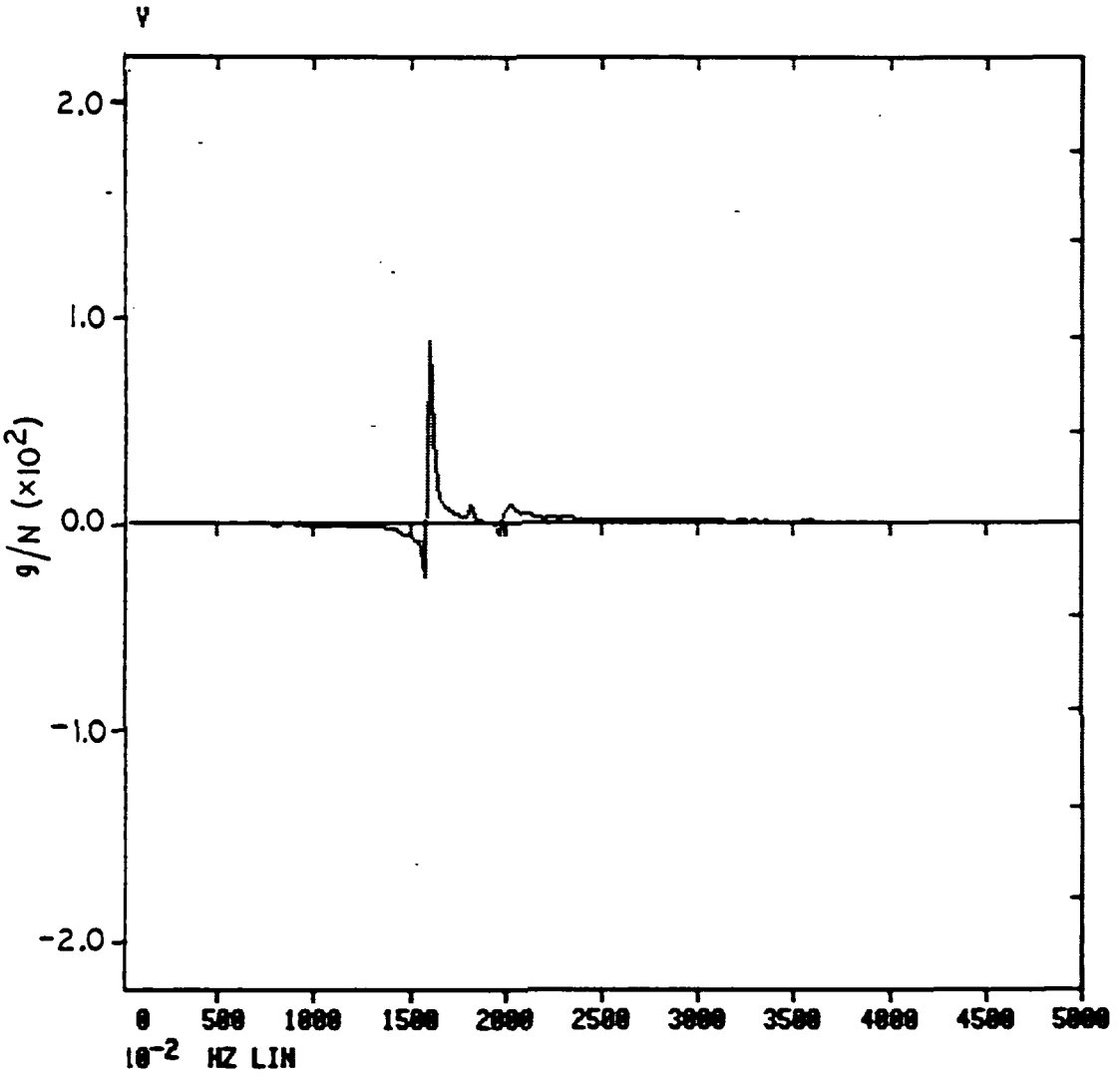

Fig. C5 Real part of the frequency response of the mass-spring system.

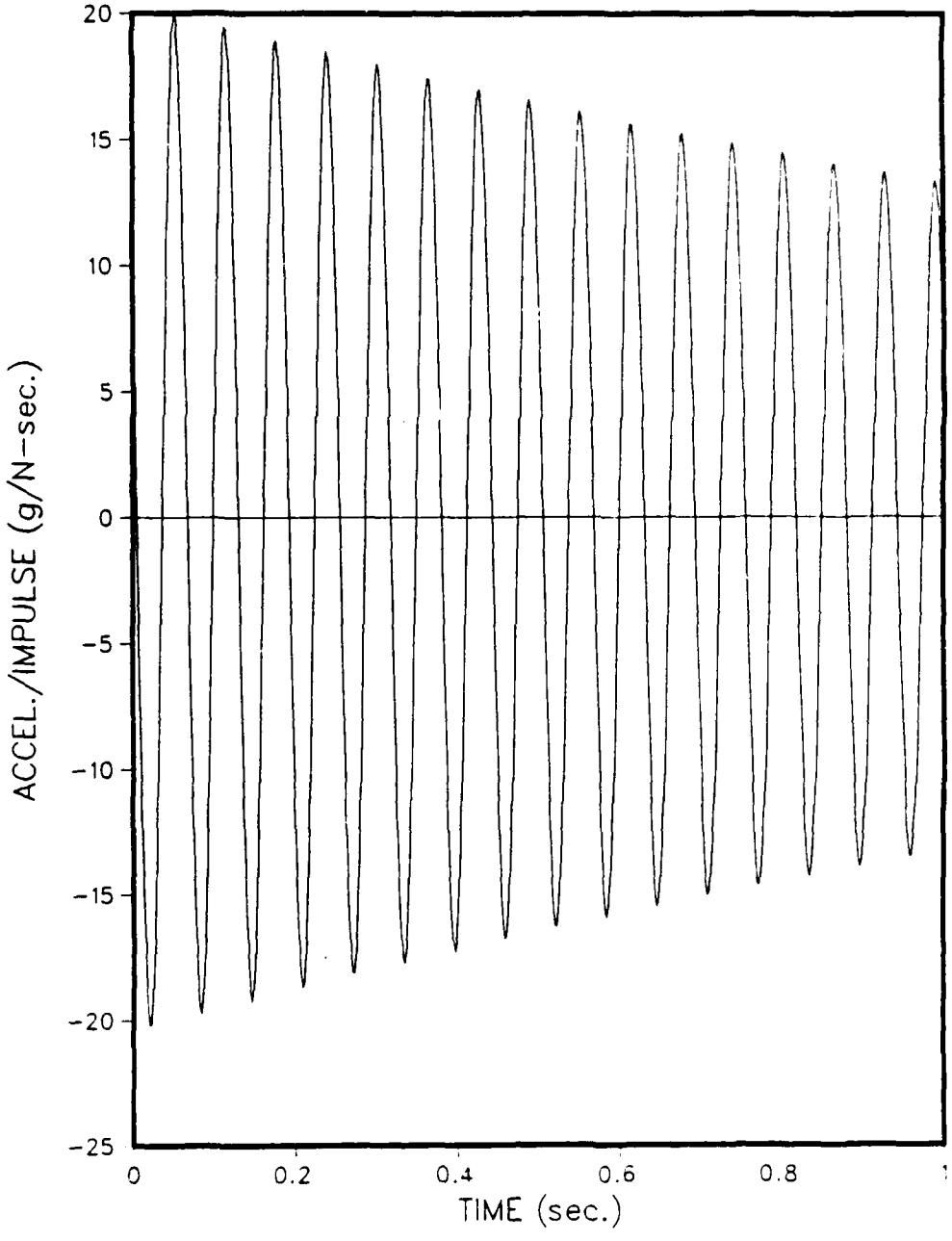

Fig. C6 Plot of eqn. (C3) using parameters of Table C1.

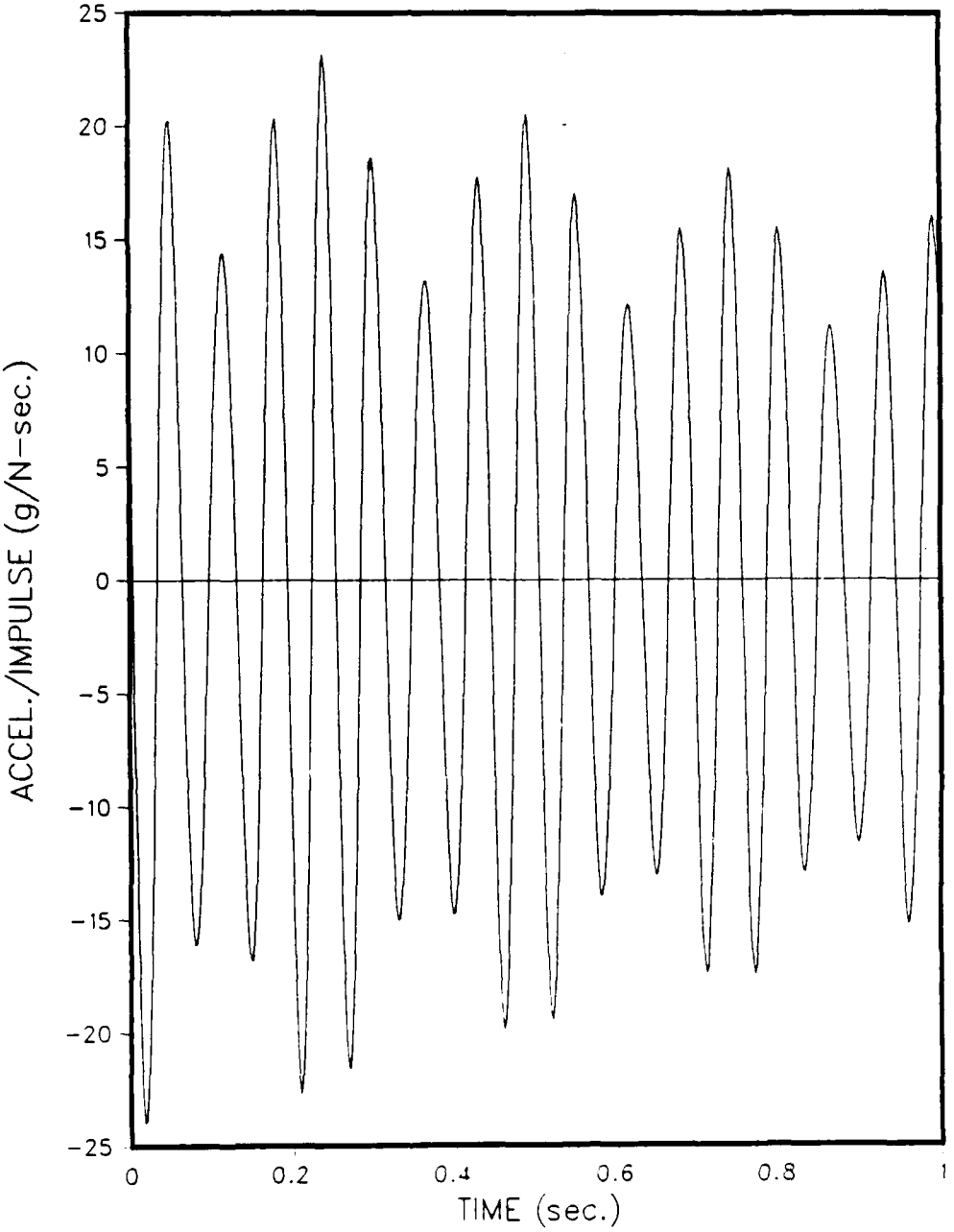

Fig. C7 Plot of eqn. (C9) using parameters of Table C2.

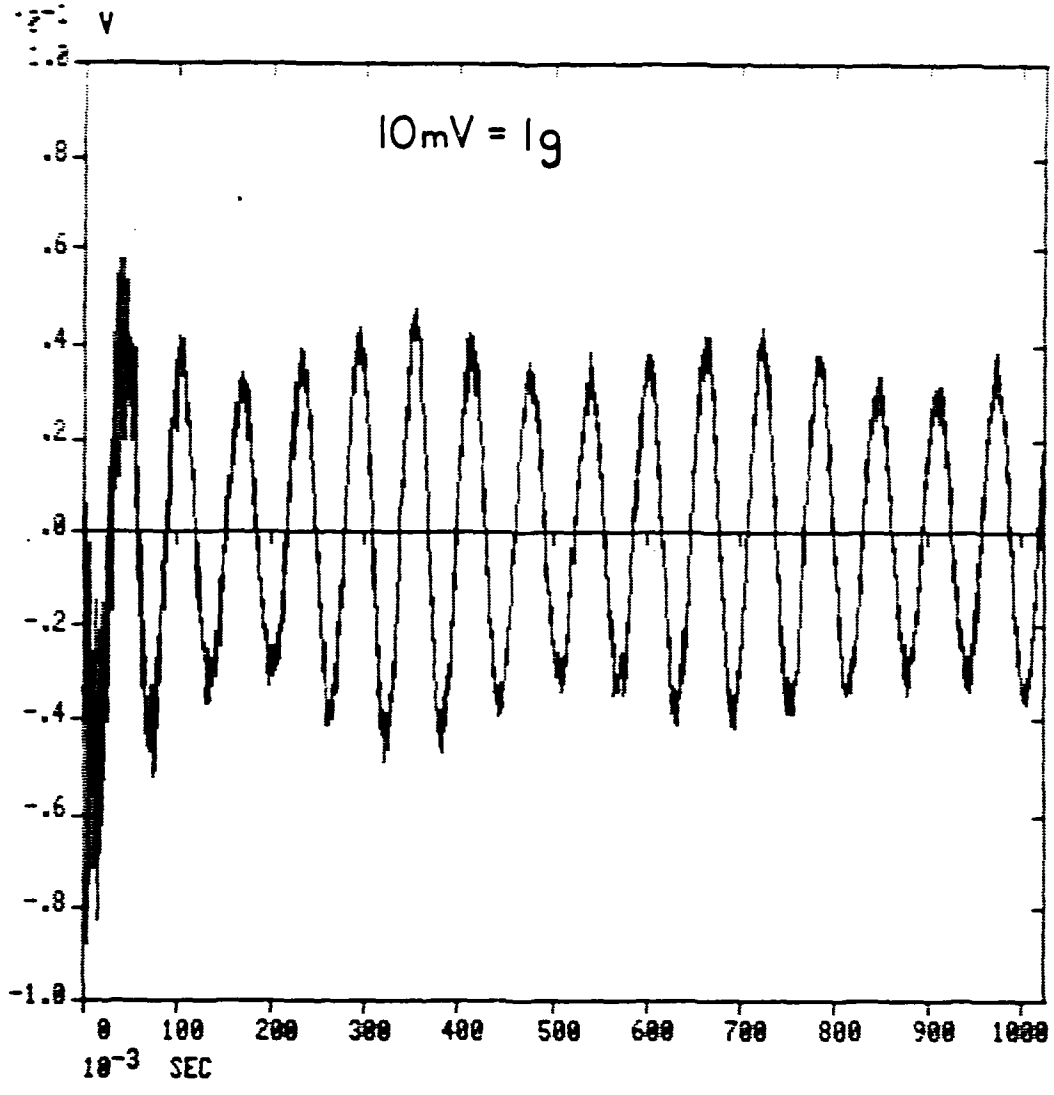

Fig. C8 Measured impulse response acceleration of the mass-spring system.

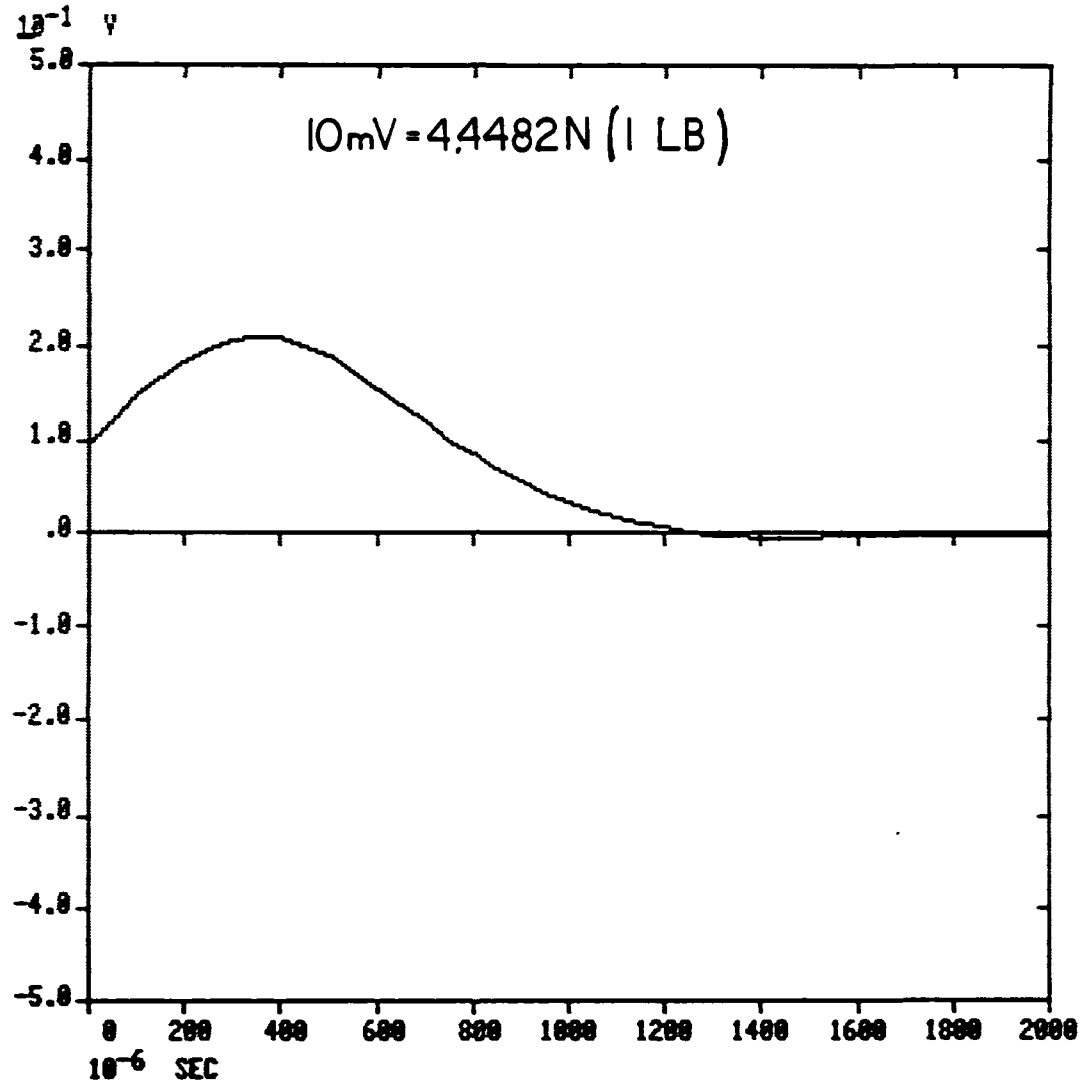

Fig. C9 Rubber-tipped hammer impulse curve.

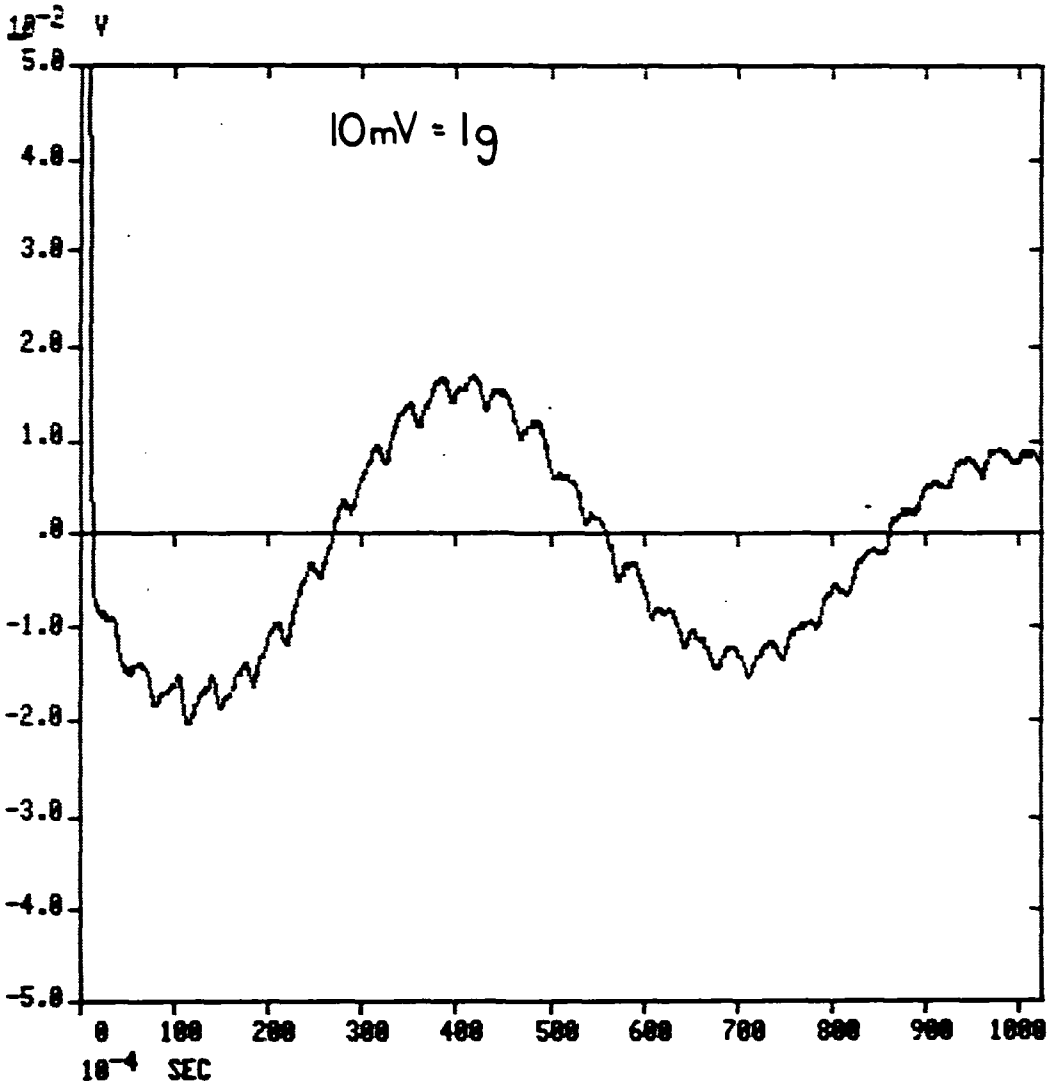

Fig. C10 Response acceleration of the mass due to rubber-tipped hammer impulse of Fig. C9.

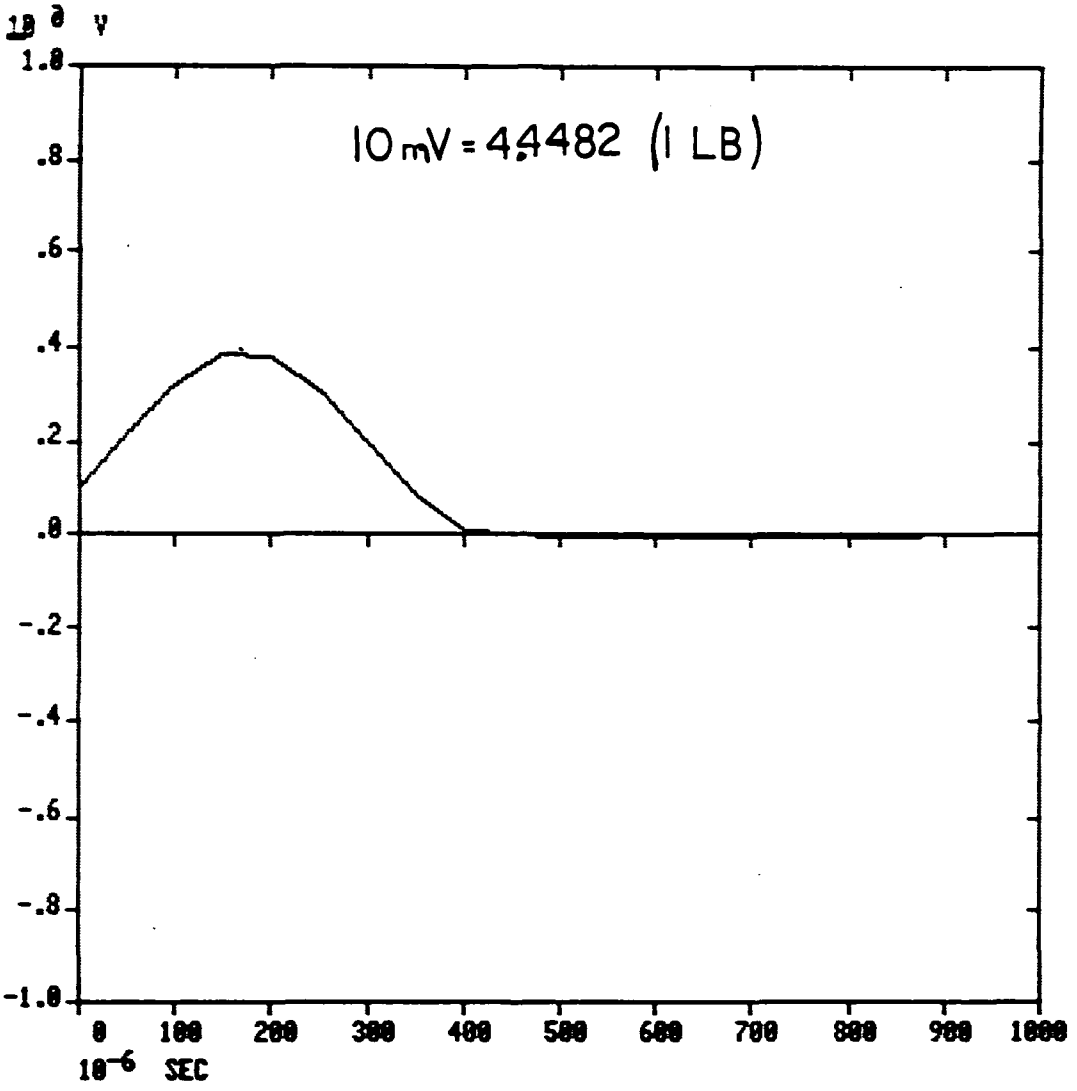

Fig. C11 Plastic-tipped hammer impulse curve.

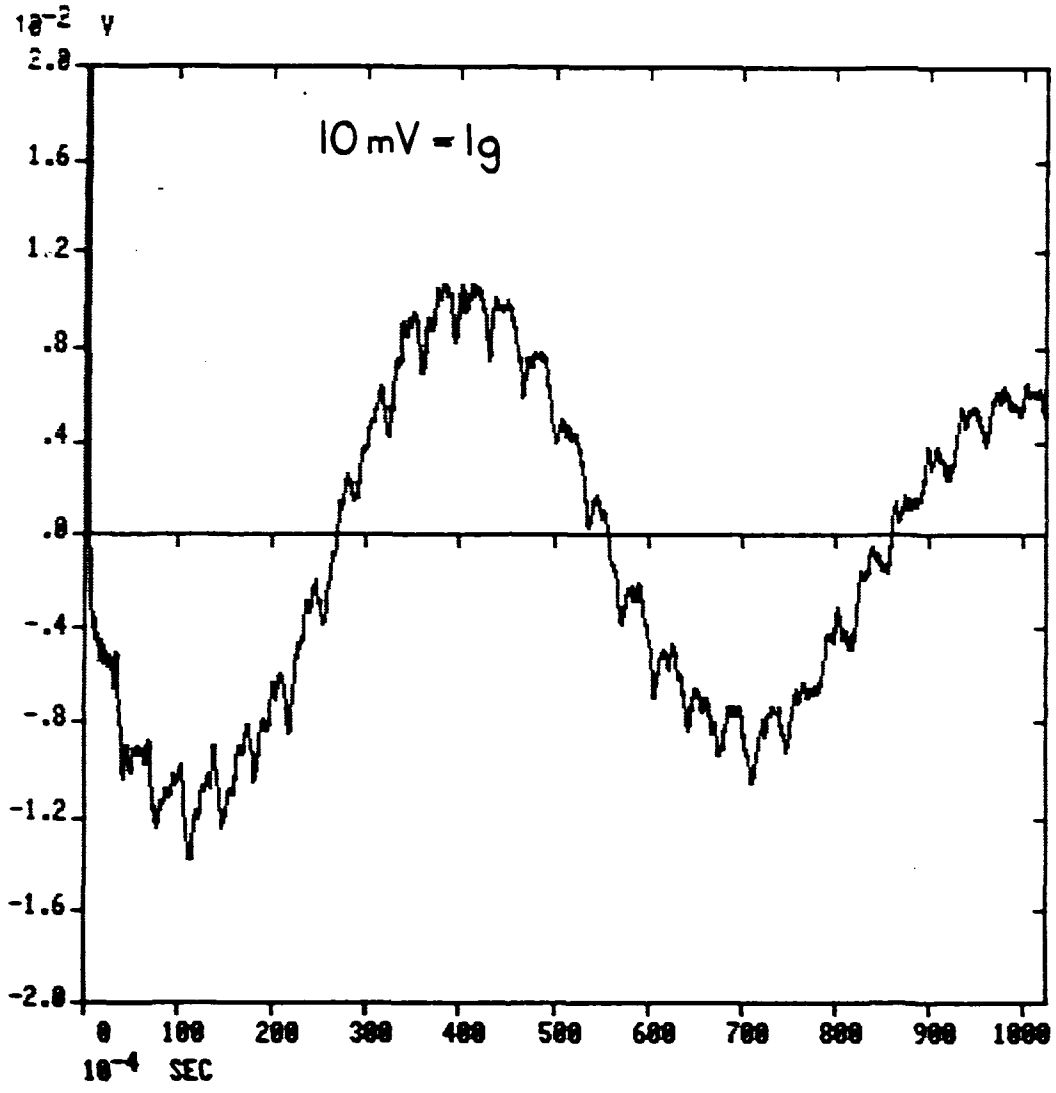

Fig. C12 Response acceleration of the mass due to the plastic-tipped hammer impulse of Fig. C11.

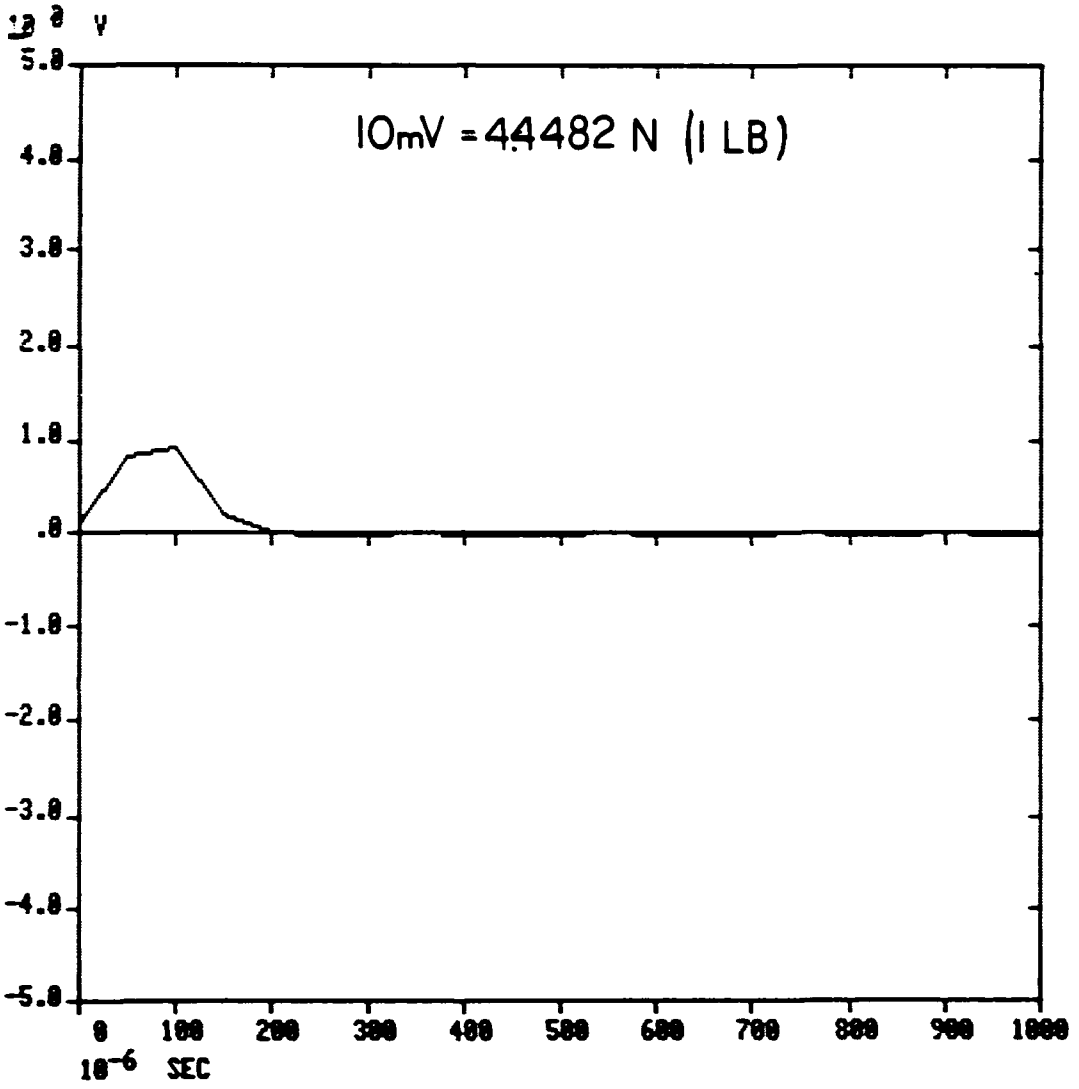

Fig. C13 Aluminum-tipped hammer impulse curve.

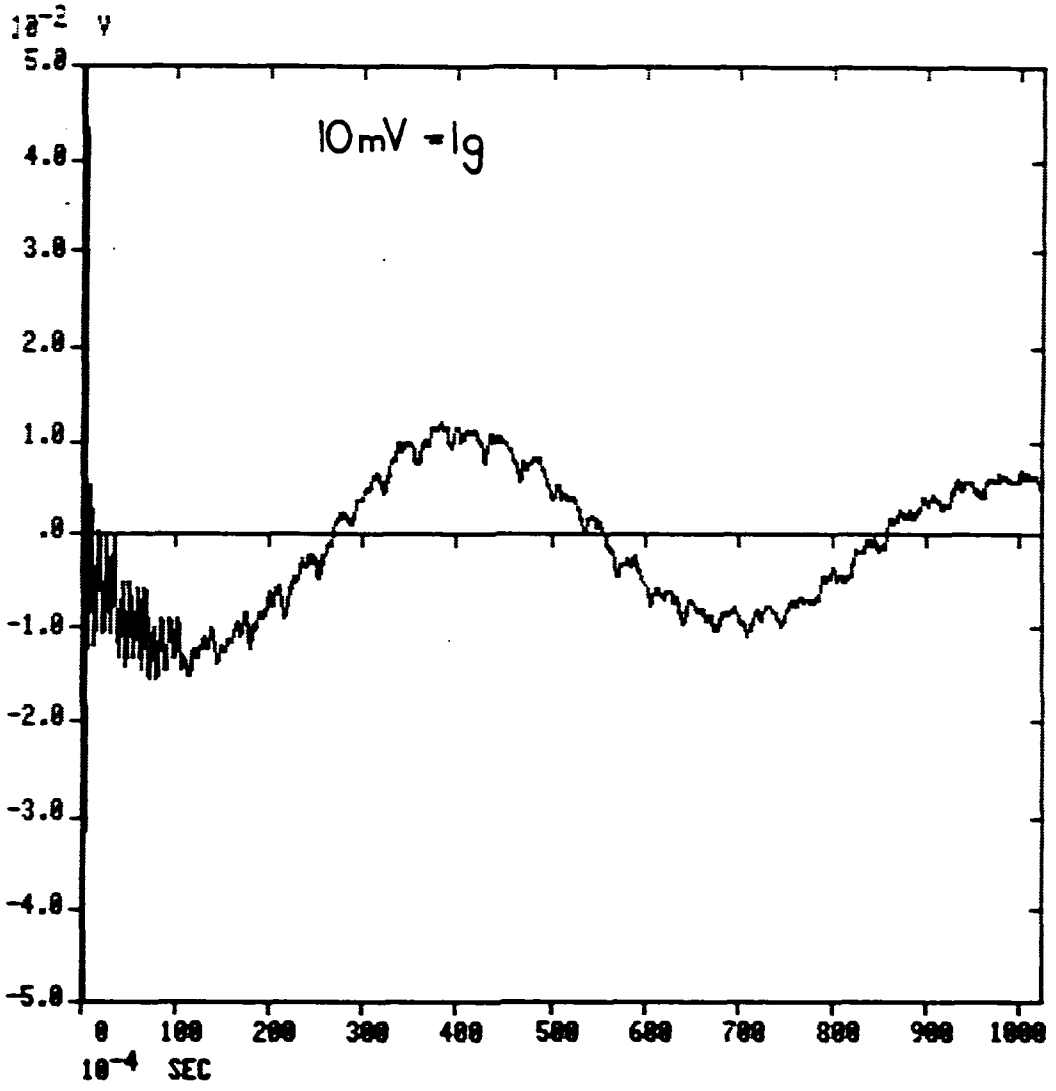

Fig. C14 Response acceleration of the mass due to the aluminum-tipped hammer impulse of Fig. C13.

APPENDIX D

IMPULSE RESPONSE OF LATTICE STRUCTURES

Introduction

The following investigation was performed in an attempt to use model parameters to predict the impulse response characteristics of the two-dimensional lattice structures.

Experimental Procedure

The only location on either of the two structures where a clean impulse (single spike) could be imparted was at location 2 of the 5-bay beam structure. Only responses due to impluses at location 2 were predicted because responses due to impulses at other locations could not be generated experimentally, hence there would be nothing with which to compare the predicted results. The 5-bay structure was impacted in the negative Y-direction using a hammer with an aluminum-tipped PCB SN1377 load cell attached to its head. The Y-direction response acceleration was measured at the fixed output location via an Endevco 2222B piezoelectric accelerometer.

Results of Modal Analysis

Fig. D1 is the real part of the frequency response function that was obtained by exciting the structure at location 2 via the impact hammer and measuring its response acceleration at the fixed output location. Fig. D1 indicates that the most prominent natural modes of vibration of the 5-bay structure occurred in the regions near 9 kHz and 20 kHz. These natural frequencies had the greatest influence on the

response of the 5-bay beam due to an impact at location 2.

The Fourier analyzer then fit an analytical expression for the frequency response function of the form

$$H(s) = \sum_{k=1}^{n} \frac{R_k}{s - p_k} - \frac{R^*_k}{s - p^*_k} \qquad (D1)$$

to the frequency response curve of Fig. D1. R_k of eqn. (D1) corresponds to the complex residue at the complex pole, p_k. The superscript asterisks indicate complex conjugates. The n of eqn. (D1) corresponds to the number of natural frequencies, or spikes, in the frequency response function.

The Fourier analyzer indentified n = 17 natural frequencies in the frequency response function of Fig. D1 and generated the four modal parameters (natural frequency (ω), damping ratio (σ), residue amplitude (|R|), and residue phase (α)) for each mode. Table D1 contains the 17 sets of modal parameters generated by the Fourier analyzer.

Modal Parameter-Predicted Impulse Response

The inverse Fourier transform of the analytical expression of the frequency response function (eqn. (D1)) gives

$$h(t) = \sum_{k=1}^{n} R_k \, e^{-\sigma_k t} \sin(\omega_k t + \alpha_k) \qquad (D2)$$

which is the time history response due to an impulse. Eqn. (D2) has the same units as the residue magnitude which are g/N-sec (g/lb-sec). Thus, eqn. (D2) gives the response acceleration per unit impulse. The modal parameters in Table D1 were substituted into eqn. (D2) and the

results are plotted in Fig. D2. Fig. D2 predicts the time history response acceleration per unit impulse due to an arbitrary impulse at location 2.

The maximum value of the curve in Fig. D2 is approximately 76,000 g/N-sec (338,000 g/lb-sec). The equation

$$\ddot{x}(t)_{max} = 76{,}000 \text{ g/N-sec} \times A \qquad \text{(D3)}$$

predicts the peak response acceleration due to an impulse at location 2. The variable A in eqn. (D3) corresponds to the value of the impulse (area under the impulse curve) and has units N-sec (lb-sec).

Evaluation of Results

The following investigation was performed to determine the validity of using eqn. (D3) to predict the peak response acceleration of the 5-bay beam due to an impact at location 2. Fig. D3 shows an impulse curve that was obtained by impacting the 5-bay structure at location 2. Fig. D4 shows the measured response acceleration of the 5-bay lattice structure due to the impulse of Fig. D3.

At first glance, the similarity of shapes between the curves in Figs. D2 and D3 seemed to indicate that the modal parameters were able to predict impulse response acceleration. Further investigation, however, revealed that this was not the case.

The area under the impulse of Fig. D3 is about 5.17×10^{-4} N-sec (.0023 lb-sec). Therefore, according to eqn. (D3), the maximum response acceleration should have been 782 g. The actual peak

response acceleration of Fig. D4 was approximately 150 g, Clearly, the modal parameters did not accurately predict the impulse response acceleration of the 5-bay lattice structure.

Conclusions

The discrepancies between the modal parameter-predicted peak response acceleration and the measured peak response acceleration probably arose from the limited range of frequencies present in the impulse signals used to generate the frequency response curve of Fig. D1. The 6 dB down cut-off frequency for an impact at location 2 was about 5,000 Hz. There were frequencies above 5,000 Hz present in the impulse signal, however, their amplitudes may have been insufficient to adequately excite these frequencies in the structure. The result was spurrious frequency responses above 5,000 Hz. Thus, the frequency response function information above 5,000 Hz should be ignored, and the impulse response of the 5-bay structure cannot be predicted using modal parameters.

Another cause of errors could have been the poor frequency resolution that was required in order to measure frequencies as high as 25 kHz. Using 2048 sampling points resulted in a frequency resolution of about 50 Hz [5]. Thus a great deal of information may have been lost due to the sampling limitations of the analyzer.

TABLE D1 Modal Parameters Corresponding to the Frequency Response of Figure D1

k	R (g/N-sec)	σ (rad/sec)	ω (rad/sec)	α (rad)
1	8544.8008	36.3000	49291.6016	4.4800
2	9793.1992	42.4000	50469.0000	4.2400
3	2547.1001	22.7000	51326.1016	1.8800
4	8904.6992	49.5000	51788.5000	1.0600
5	6896.3984	25.3000	53060.1992	1.4000
6	4332.8984	28.5000	54539.3008	4.4600
7	13654.6992	39.7000	57666.3984	4.0100
8	4703.6016	64.5000	59110.8984	4.3000
9	22303.8008	83.8000	60959.5000	0.7000
10	10545.5000	111.0000	62987.6992	0.6000
11	8339.6016	104.6000	65141.6016	3.3500
12	6658.5000	106.2000	67162.1875	3.7000
13	3938.2000	33.1000	108503.687	2.7800
14	3347.2000	56.1000	111983.312	5.4000
15	6723.3984	45.1000	114007.812	5.6000
16	4158.6016	42.0000	119957.312	2.2700
17	7414.6016	68.0000	124649.625	5.1400

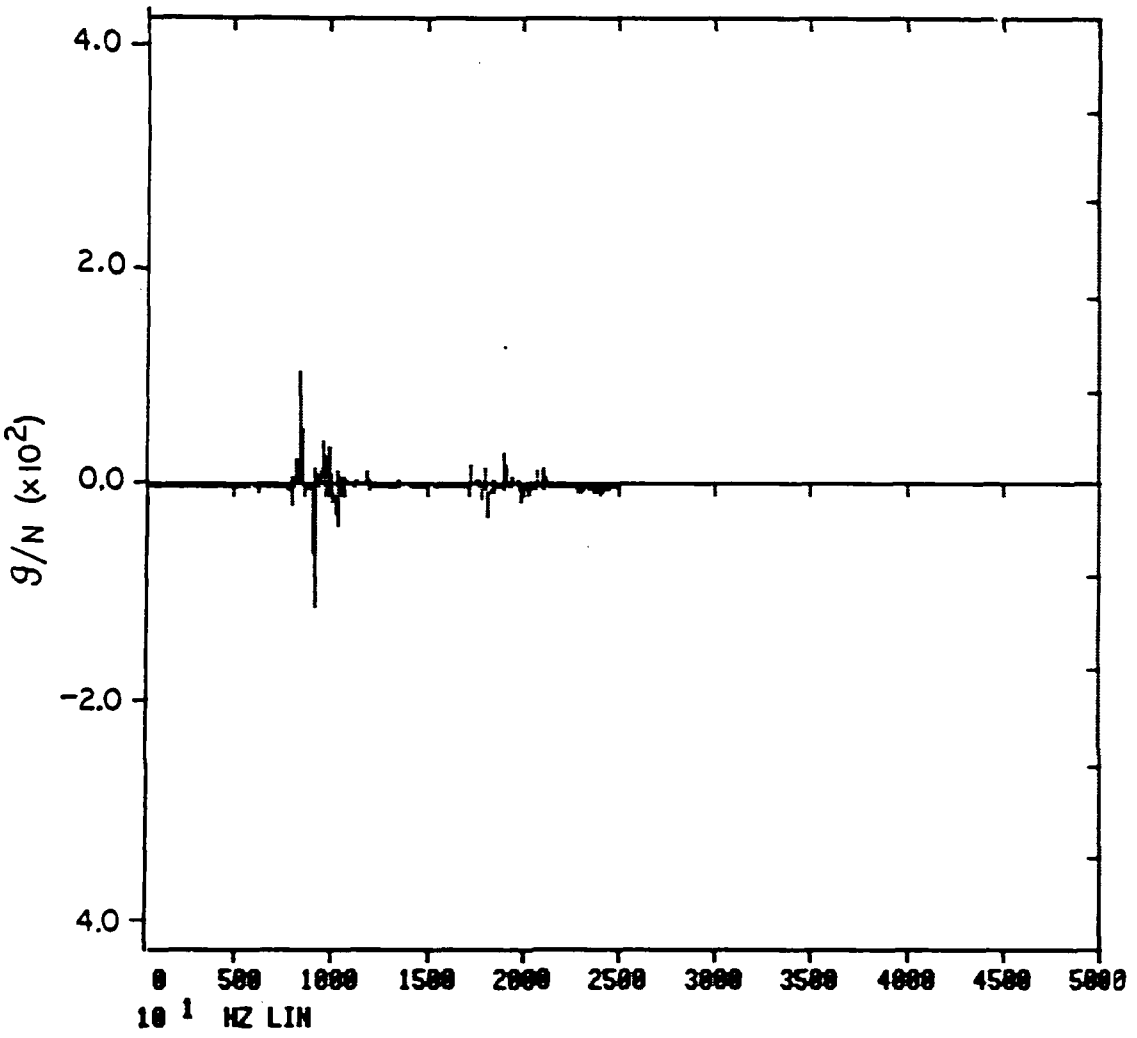

Fig. D1 Real part of the frequency response functions obtained by impacting the 5-bay lattice at location 2.

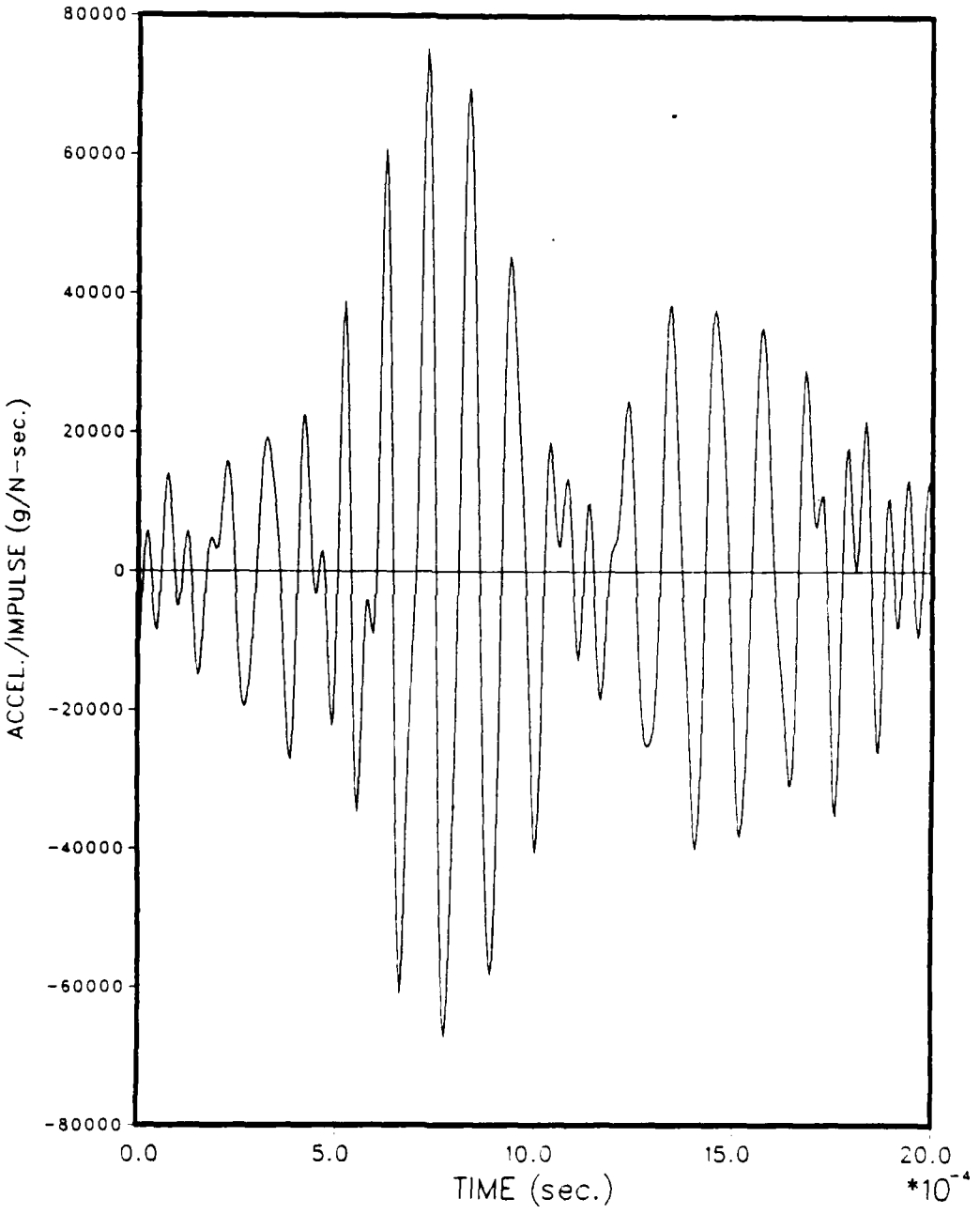

Fig. D2 Modal parameter-predicted response acceleration per unit impulse at fixed response location due to an arbitrary impulse at location 2.

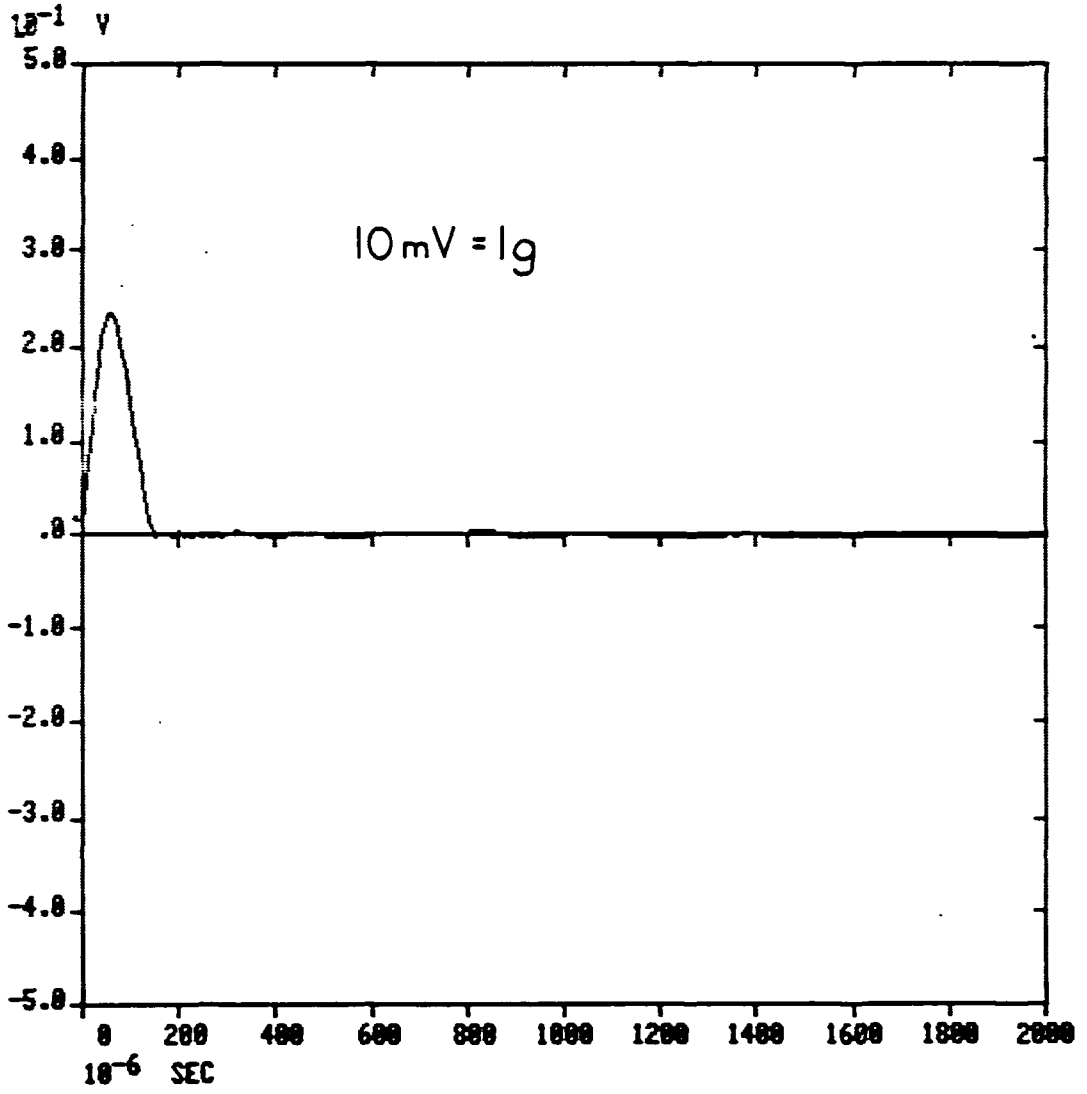

Fig. D3 Impulse obtained by impacting the 5-bay lattice at location 2.

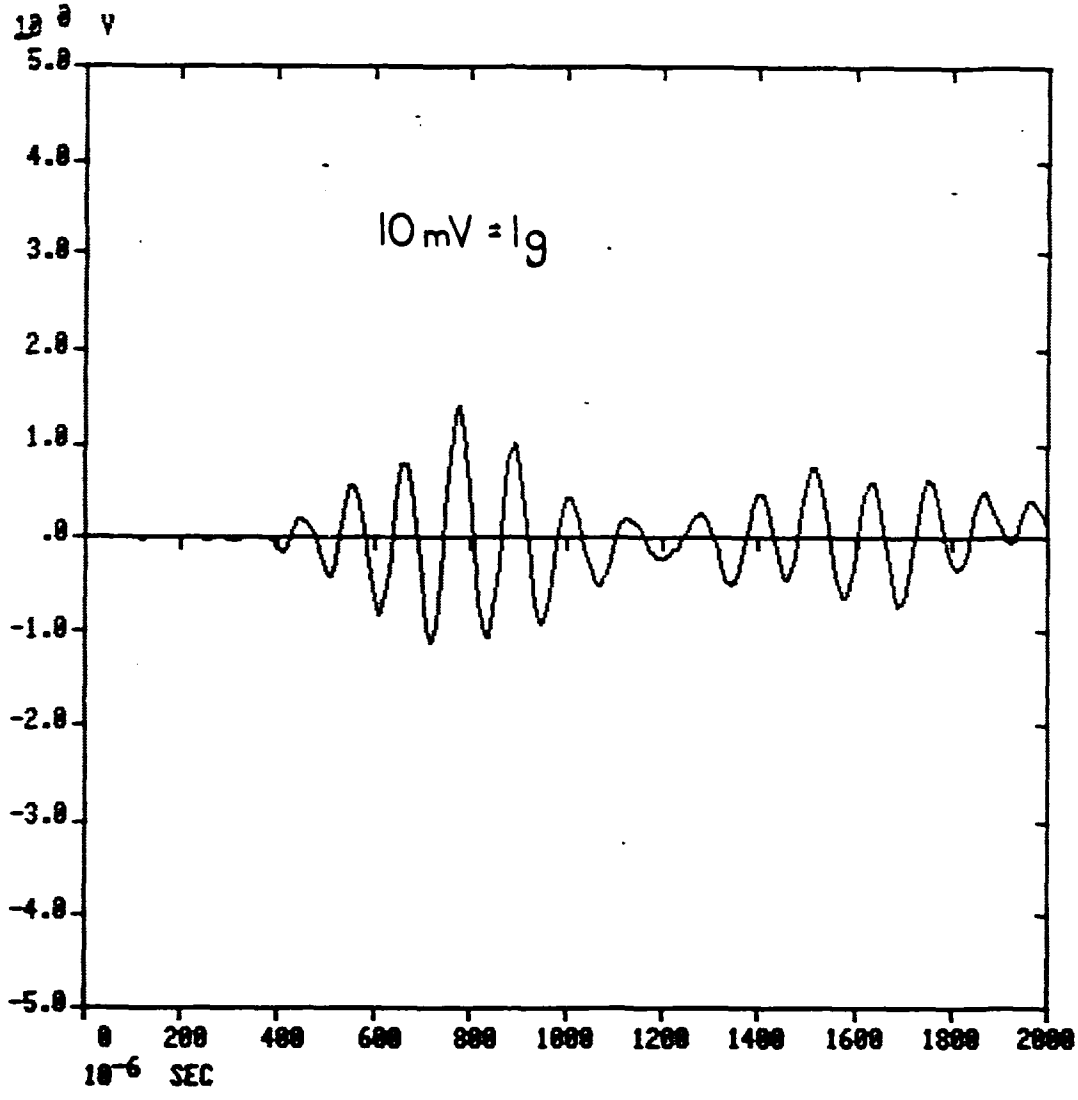

Fig. D4 Measured response location acceleration due to the impulse of Fig. D3.

END

1-87

DTIC